Doctoral Dissertation
Doctoral Program in Metrology (32th Cycle)

Improved PPP for time and frequency transfer and real-time detection of GNSS satellite clock frequency anomalies

Wei Huang
* * * * * *

Supervisors
Ilaria Sesia,Supervisor
Pascale Defraigne, Co-Supervisor
Patrizia Tavella, Co-Supervisor

Doctoral Examination Committee:
Dr. Héctor Esteban, Referee, Royal Institute and Observatory of the Navy, Spain
Dr. Gérard Petit, Referee, Bureau International des Poids et Mesures, France

Politecnico di Torino
June 28, 2020

I hereby declare that, the contents and organisation of this dissertation constitute my own original work and does not compromise in any way the rights of third parties, including those relating to the security of personal data.

Huang Wei

……

Wei Huang

Turin, June 28, 2020

Summary

The aims of this PhD work were 1) to improve the performance of time and frequency transfer using upgraded GNSS PPP algorithms, and 2) to enable the real-time detection of GNSS satellite clock frequency anomalies for positioning and timing applications.

PPP is a state-of-the-art GNSS technique for precise time and frequency transfer, and its time solution has a statistical uncertainty of 100 ps over one day. In recent years, this classic PPP technique has shown some limitations when used to compare atomic clocks of the highest quality. The main limiting factor of PPP time transfer is the time discontinuity at the boundary of the computation batch, which could be more than 1 ns in extreme cases. During the PhD work, the Atomium PPP, which was originally developed by the Observatoire royal de Belgique, has been upgraded in order to improve its performance on time and frequency transfer. In the first part of the dissertation, three main updates to the current Atomium PPP are introduced: 1. adding Galileo signals to the PPP computation; 2. adding a constraint to the receiver clock; 3. new PPP algorithms with integer ambiguity resolution. The experiments carried out demonstrate that the Galileo + GPS PPP improves the short-term stability of the time transfer (in general by 20%-10% from 5 min to 2.5 hours interval) in the daily batch; the constrained PPP can be used to measure the H-maser with very good short-term stability, while it also shows its advantages in providing continuous time solution and retrieving clock measurements in extremely noisy environments; the integer ambiguity PPP shows improved time transfer frequency stabilities at mid and long-term (reaching 10^{-16} at 2 to 10 days averaging), and it also provides more accurate frequency transfer with monthly frequency offset within $\pm 2 \cdot 10^{-16}$.

The second part of the work focuses on developing the methods for producing real-time GNSS satellite clock frequency measurements, which are used for frequency anomaly detection. It has been reported in the experiment that a

frequency jump of size $7.5 \cdot 10^{-13}$ in a GNSS satellite clock could cause accumulated errors of some meters to the calculated position or tens of ns divergence in the time solution if it is not detected within several hours. Current studies into these satellite clock frequency jump detections are based on post-processed measurements, which can not be used for real-time applications. The new method that we propose in this work can provide the frequency measurements of the GPS and Galileo satellite clocks in real-time using the carrier phase observations from a global ground station network. The test results show that the precision of the frequency measurements obtained by the new method is comparable to the post-processed measurements, and that a satellite clock frequency jump as small as 5×10^{-13} could be detected within 30 min by the frequency jump detector using the related frequency measurements. In addition, in order to keep the measurement redundancy and to double check the detected jump, alternative methods are also proposed to provide the same kind of real-time frequency measurements.

Furthermore, it is currently in progress the integration of all the software developed into the DEMETRA project, which is a European project designed to provide time services to the specific users. The DEMETRA time monitoring service has been providing improved daily time solutions with the upgraded Atomium PPP software, while the GPS + Galileo PPP will soon be used instead of the GPS-only PPP to provide an hourly solution. The function of the real-time GNSS satellite clock frequency anomaly detections will be added to the DEMETRA time integrity service in future work.

Acknowledgment

Firstly, I would like to thank my supervisor, Dr. Ilaria Sesia, for the continuous support and guidance through each stage of my PhD activities. I would also like to thank my co-supervisor, Dr. Patrizia Tavella, for her patience in planning and guiding my PhD research and the kind help during my academic visit in Paris.

I am especially grateful to Dr. Pascale Defraigne, not just as my PhD co-supervisor, but also as my tutor during my work in the Royal Observatory of Belgium before the start of the PhD program. She is the one who leads me to this research field and keeps inspiring me.

Many thanks to my colleague Giovanna Signorile, for the discussion and the valuable suggestions during my research at INRIM, and I sincerely wish her new-born daughter, Elisa, health and happiness! My thanks also to my colleague Valerio Formichella for providing me a lot of valuable data, which were very helpful for validating my research.

I wish to thank all the other colleagues and friends that I met in Turin, Paris and Brussels for bringing joys to my life over the past three years. A special thanks to my friend and colleague, Tung Thanh Thai, who offered me a lot of technical help at work and shared nice Asian food with me after work.

Last but not least, I would like to express my sincere gratitude to Dr. Gérard Petit and Dr. Héctor Esteban for their genuine help in providing insightful comments and suggestions for the completion of this dissertation.

I would like to dedicate this thesis to my loving girlfriend and parents

Contents

List of Tables

List of Figures

Abbreviations

SI	International System of Units
CGPM	General Conference on Weights and Measures
SRS	Secondary Representations of the Second
CCTF	Consultative Committee for Time and Frequency
BIPM	Bureau International des Poids et Mesures
TAI	International Atomic Time
UTC	Coordinated Universal Time
IERS	International Earth Rotation and Reference Systems Service
INRIM	Istituto Nazionale di Ricerca Metrologica
AVAR	Allan Variance
ADEV	Allan Deviation
GNSS	Global Navigation Satellite System
QZSS	Quasi-Zenith Satellite System
NavIC	Navigation with Indian Constellation
PNT	Positioning, Navigation and Timing
PRN	Pseudo-Random Noise
C/A	Coarse/Acquisition
P code	Precision code
PRS	Public Regulated Service
CS	Commercial Service
OS	Open Service
AltBOC	Alternate Binary Offset Carrier
PPP	Precise Point Positioning
NTP	Network Time Protocol
TWSTFT	Two-Way Satellite Time and Frequency Transfer
CGGTTS	Common GNSS Generic Time Transfer Standard
CV	Common-View
AV	All-in-View
IGS	International GNSS Service
ORB	Observatoire royal de Belgique
DEMETRA	DEMonstrator of EGNSS services based on Time Reference Architecture
RINEX	Receiver Independent Exchange Format
CCD	Common Clock Difference
MGEX	IGS Multi-GNSS Experiment
ISB	Inter System Bias
ERP	Earth Rotation Parameters
WL	Wide Lane
NL	Narrow Lane
WRB	WL receiver bias
WSB	WL satellite bias
MJD	Modified Julian Date

Chapter 1

Time and GNSS

1.1 Time and frequency metrology

1.1.1 Definition

Time is a physical quantity, and its measurement unit is one of the seven which form the International System of Units (SI), which was first defined by the 11th General Conference on Weights and Measures (CGPM) [1]. The most recent revision of the SI was made during the 26th CGPM in 2018 [2], and the new SI came into effect on 20 May 2019 (World Metrology Day). To facilitate measurements of time, the standard unit of time interval was also defined by the CGPM. The current definition of the SI unit of time is [2]:

The second, symbol s, is the SI unit of time. It is defined by taking the fixed numerical value of the caesium frequency $\Delta\nu_{Cs}$*, the unperturbed ground-state hyperfine transition frequency of the caesium 133 atom, to be 9 192 631 770 when expressed in the unit Hz, which is equal to* s^{-1}.

In this definition, the hyperfine transition frequency of Cs ($\Delta\nu_{Cs}$) is fixed to a constant value of 9 192 631 770, with the unit Hz. A simpler explanation of this definition is that the duration of one second is equal to 9 192 631 770 periods of the radiation corresponding to the transition between the two hyperfine levels of the unperturbed ground-state of the caesium 133 atom [3].

1.1.2 Timekeeping

To measure the flow of time, a device that can produce a periodic signal at a constant rate (in other words, signal of certain frequency) is needed, and this device is called an oscillator. To construct a clock with an oscillator, a counter is added to record the periodic signal in the oscillator and convert it into the time information. For example, when a pendulum in a mechanical clock swings forward and back, 1 second is recorded. Furthermore, this pendulum clock offers a practical method of the realization of second.

1.1.2.1 Realization of second

As they are the most accurate time and frequency standards, atomic clocks are currently the first choice for time laboratories/metrology institutes to realize the definition of second. Among them, the primary frequency standards are the best realization of the SI second, although they are only operated in a few laboratories, for example, the caesium fountain ITCsF2 at the Istituto Nazionale di Ricerca Metrologica (INRIM) in Italy [4]. The accuracy of the best primary frequency standards can reach a few parts in 10^{-16} [3]. Besides the primary frequency standards, secondary representations of the second (SRS) were also proposed by the Consultative Committee for Time and Frequency (CCTF) of the CGPM in 2001 [5], based on the transition frequencies of other atoms [6]. The recommended values of the standard frequencies for the SRS are listed on the website of the Bureau International des Poids et Mesures (BIPM) [7]. In fact, the most advanced optical frequency standards, which are secondary frequency standards, have even higher accuracy than the current primary standards [8], being able to reach almost 10^{-18} [9], which may lead to a new definition of the second in the future.

1.1.2.2 International reference time scale

Coordinated Universal Time (UTC) is an international reference time scale that is generated at the BIPM, and it is based on International Atomic Time (TAI). TAI is generated in two steps: first, a weighted average of the measurements from more than 400 atomic clocks in about 80 time laboratories worldwide is calculated; Secondly, the frequency of the results from the first step is steered by the primary standards to let TAI realize the SI second as closely as possible.

TAI is a continuous time scale that is not distributed for public usage, while UTC is a global distributed time standard that is commonly used by the public. UTC keeps the same frequency as TAI, but it differs from TAI by an integer number of seconds. These integral seconds (called leap seconds) are applied to ensure that the UTC agrees with the UT1 (the astronomical time scale defined by the rotation of the Earth) within 0.9s. Due to the decrease of the rotation rate of the earth, the number of leap seconds is still increasing. On average, leap seconds have been inserted at a rate of once every 2-3 years since 1972, when they were introduced, and the insertion is decided by the International Earth Rotation and Reference Systems Service (IERS). By 2019, the difference between UTC and TAI has been increased to 37 seconds.

It should be noted that UTC is not a real-time distributed time scale. Most of the national metrology institutes or time laboratories keep steering their own atomic clocks using the monthly UTC dissemination report (circular T) from the BIPM to generate their own real-time local realization of UTC, which is called UTC(k) for laboratory k. For example, UTC(IT), which is the Italian national time standard, is generated at INRIM in Italy. It is recommended to maintain these local realizations within ±100 ns of UTC [10], while in practice the best

laboratories can keep these offsets to tens of ns. In Figure 1-1, the behaviour of UTC(IT) with respect to UTC is recorded for the period from April to August in 2019 with the data taken from the BIPM circular T [11].

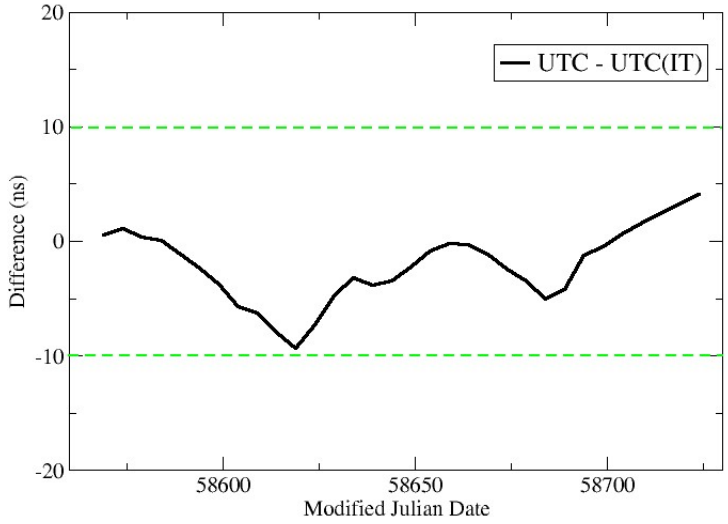

Figure 1- 1. UTC(IT) compared to UTC

1.1.3 Time and frequency measurement

To carry out any time and frequency measurement on the source under test, a higher quality reference is always needed. The details of the processes are introduced in the next sections. In this dissertation, the source under test could be any device (for example, a clock), any time scale and any medium/method that is used to transmit time and frequency information. Time and frequency measurements are closely related, since the signal frequency can be known by counting the number of cycles in one second. The time measurement quantity is usually the time offset (also called time deviation) compared to the reference, while the measured quantity for the frequency is normally the frequency offset (also called frequency deviation), and their relationships can be expressed as

$$\mathrm{f} = \frac{\Delta t}{T} \tag{1}$$

where f is the frequency deviation, and Δt is the change of time deviation over the measurement period T. The unit of time deviation is the second, while the frequency deviation is dimensionless. It is known from equation (1) that the frequency measurements can be obtained from the corresponding time measurements; however, from the frequency measurements only the relative change of the time deviation can be retrieved, and the initial value of the time measurements is lost.

Time and frequency measurements can be made by instruments such as time interval or frequency counters in the local laboratories, while for remote time and frequency measurement, techniques called time and frequency transfer are needed. More details of time and frequency transfer can be found in section 1.3.

Moreover, the following two features are those mainly used to describe the quality of the aforementioned time and frequency measurements:

Accuracy: the degree of the correctness of the measurements according to the real values.

Stability: the degree of the similarity of the measurements within a given time interval.

The accuracy describes how "correct" the time/frequency of the source or the method itself to transmit the time/frequency is, while the stability indicates how "stable" the quantity is. A classic example that shows the relationship between the accuracy and the stability in frequency measurements is given in Figure 1-2 [12].

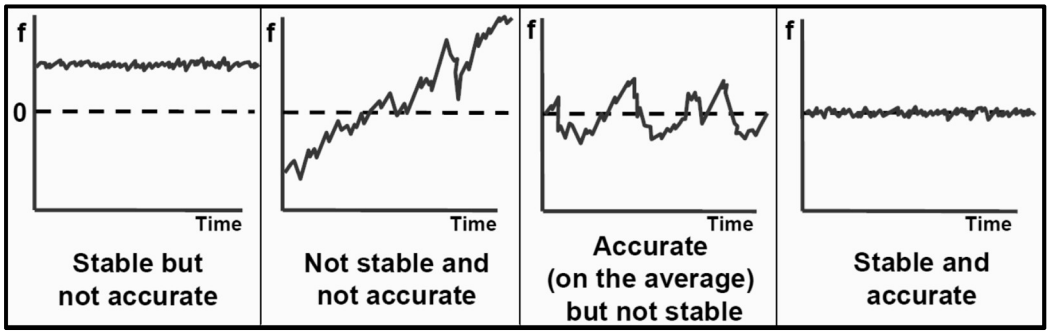

Figure 1- 2. An example of accuracy and stability in frequency measurements

Traditional stability analysis with standard deviation is not suitable for time and frequency measurements in some situations, since the data from the atomic frequency standard is normally nonstationary, which means the standard deviation and mean of the measurements will never converge as more data are added [13]. For stability analysis in the time and frequency domain, another tool called Allan Variance (AVAR) is introduced, together with its square root Allan Deviation (ADEV) [14]. AVAR indicates the stability of clocks at each observation time interval: the smaller the value of AVAR or ADEV at an observation time interval, the better the corresponding stability. The slope of the ADEV can be used to identify the dominating noise type of a clock at a certain time interval. An example of a plotted ADEV is given in Figure 1-3, which is taken from [13].

From the ADEV plot, we can also obtain further important information, namely how long we need to average the data to reduce the noise (which could be from the measurement or the reference) and meet the required measurement precision.

Good quality atomic clocks and accurate time and frequency measurements give the opportunity to improve many industrial or scientific applications, which include the Global Navigation Satellite System (GNSS). The principle of the GNSS and how time plays as a vital role in the whole system is introduced in the next section.

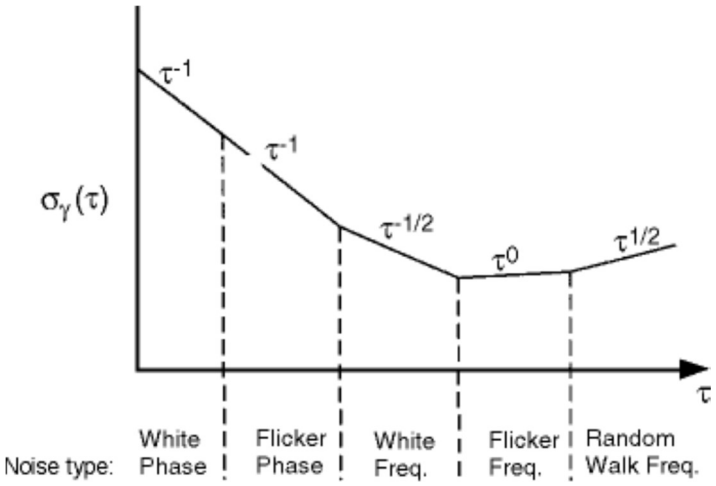

Figure 1- 3. An example of ADEV (with the notation $\sigma_y(\tau)$)

1.2 GNSS

A satellite navigation system generally refers to a system with a constellation of satellites, which transmit signals from space that could be used by the users on or near ground for the Positioning, Navigation and Timing services (PNT). GNSS is a generic term for all the satellite navigation systems with global coverage, it includes USA's Global Positioning System (GPS), Russian's Global Navigation Satellite system (GLONASS), Europe's Galileo and China's BeiDou Navigation Satellite System, among which the GPS and GLONASS have been fully operational for many years, while the Galileo and BeiDou will have their full constellations in the very near future (The last BeiDou satellite has been successfully launched on 23 June 2020).

Additionally, there are currently two regional navigation satellite systems in operation, they are Japan's Quasi-Zenith Satellite System (QZSS) and India's Navigation with Indian Constellation (NavIC). These reginal systems provide GNSS-like and/or additional services to the users within a limited area. For example, the four-satellite constellation QZSS (will be increased to seven satellites) has been operated since 2018 to provide improved PNT services to the users in the Asia-Oceania regions by transmitting the extra GPS-compatible signals, meanwhile it provides additional services such as the GPS augmentation service and the Public Regulated Service (PRS) [15][16].

1.2.1 GNSS signals

On modernized GNSS satellites, signals are transmitted on three carrier frequency in the L band. Figure 1-4, which is taken from the ESA GNSS book [17], summarises the allocation of the GNSS frequency bands.

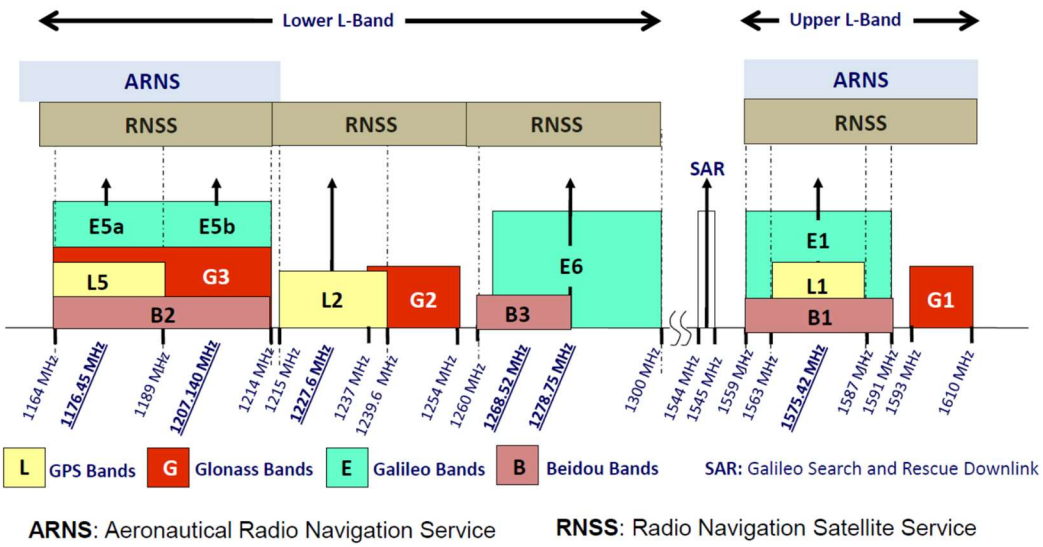

Figure 1- 4. the distribution of the GNSS bands

There are three main components in the GNSS satellite signals: carrier, PRN code and navigation message. Carrier is a sinusoidal microwave at a given frequency; PRN code is a "pseudo-random noise" sequence, which is unique for each satellite, this sequence can be used for a GNSS receiver to identify a satellite, and estimate the travelling time of the GNSS signal from the satellite to the receiver; navigation message includes important information for the user positioning, such as satellite ephemeris (satellite position) and satellite clock offset with respect to the system time, and it also includes other information like prediction of UTC, satellite health status and so on.

The legacy GPS signals are on the L1 and L2 channels, with two types of PRN codes: Coarse/Acquisition (C/A) code and Precision (P) code. The C/A code is only modulated on L1, which is a civilian code for the standard positioning services, while the signal with the P code can be used for more precise positioning, but it only serves military or authorized users. The encrypted P code is called P(Y) code. The Galileo E6 band is dedicated for the Public Regulated Service (PRS) and Commercial Service (CS), while the E1 and E5 signals are freely available for the Open Service (OS). The Galileo E5 signal employs the Alternate Binary Offset Carrier (AltBOC) modulation to form a large-bandwidth signal, which could mitigate the multipath and tracking noise in the solution [17]. The E5 signals can be further divided into two signals E5a and E5b, both of the signals can be used independently for positioning and timing. GLONASS and BeiDou have their own signal structures, all the details could be found in their Interface Control Documents [18][19].

1.2.2 GNSS positioning and timing

All GNSS satellites are equipped with atomic clocks of high quality to provide precise time tag for their transmitted signals, such as the rubidium or

caesium atomic clocks on the GPS satellites [20] and the passive hydrogen maser (H-maser) master clocks on the Galileo satellites [21].

The fundamental GNSS observables are the GNSS signal travelling time (Δt) from a satellite to a receiver and the estimated satellite-receiver range (ρ), which can be expressed as $\rho = \Delta t \times$ (speed of light). This signal travelling time Δt is estimated in the receiver by looking at the shifted time after the peak of the autocorrelation between the received PRN code from the satellite and its local replica of the same code is reached [22]. Since the received code and its local replica are driven by the satellite clock and receiver clock separately, this satellite-receiver range can be further expressed as $\rho = (T_r - T_t) \times$ (speed of light), where: T_r is the signal receiving time, measured by the receiver clock; and T_t is the signal transmitting time, measured by the satellite clock. Normally the receiver clock and the satellite clock are not synchronized; moreover, the signal suffers from additional delays and noises when it passes through the atmosphere and the instrument hardware. Therefore, the estimated ρ is a sum of the true range, the synchronization errors between the satellite and receiver clocks, the atmosphere delays and other noises, and thus this range ρ is called the pseudorange.

By receiving GNSS signals, the position of the satellite and the synchronization errors of the satellite clock referring to their system time (for example, GPS system time for GPS satellites) can be calculated from the received navigation message. Thus, in each equation built from a single observable ρ of one satellite, there are four unknowns: the receiver three-dimensional position (x,y,z) and the receiver clock offset with respect to the GNSS system time. In order to solve the GNSS equations and calculate the four unknowns simultaneously, at least four independent observables from four different satellites are needed at a single epoch in a single GNSS system.

Besides the GNSS measurements using the PRN code (hereafter called code measurements), the carrier phase in the GNSS signal also can be used to contribute to the range measurement by measuring the cycles of the carrier signals that have passed during the transmission. Carrier phase measurement is much more precise than code measurement, but it is biased by an unknown integer number of carrier wavelength (called integer ambiguity); moreover, this ambiguity may change to another integer number (called cycle slip) when a receiver loses the lock of the signal. The process to fix these integer numbers is called carrier phase integer ambiguity resolution [23].

The GNSS receivers in the mass market normally use single-frequency code measurements for positioning or navigation (for example, within the GNSS-enabled smartphone), and it has an accuracy of several meters [24]. A (sub-)centimetre level accuracy can be reached by combining carrier phase measurement with code measurement, a classical example is the approach called the Precise Point Positioning (PPP) [25], which will be introduced in the following sections.

In addition, combing the estimated receiver clock offsets (referring to GNSS system time) and the predicted time offsets between the GNSS system time and UTC which are provided in the navigation message, the user can keep its receiver

clock synchronized to UTC. Each GNSS system broadcasts its own prediction of UTC, such as UTC(USNO) for GPS. The GPS time is usually within 20 ns with respect to the UTC (USNO) besides the integer leap seconds [26]. However, to reach the same level of synchronization accuracy, the GNSS signal delays in the receiving system at the user side need to be well calibrated. If no calibration is performed, only sub-microsecond time synchronization accuracy can be achieved using the GNSS timing service.

1.3 Time and frequency transfer with GNSS

With atomic clocks of high quality, the very accurate and precise local time scale can be built, but it's far from enough. Many applications require to set the local clocks at different sites to the same time or frequency, time and frequency transfer techniques thus have emerged as demanded, for the time and frequency comparison/distribution remotely.

The most popular time and frequency distribution application in the mass market is the synchronization of user's clock to UTC. By receiving the time and frequency signals distributing UTC (in practice it's a UTC(k), since UTC is not distributed in real-time), any device can steer its clock to UTC, for example, a radio watch synchronizes its clock by receiving the signals from the longwave time and frequency radio station in Germany which is called DCF77, another example might be synchronizing the clock of a personal PC to UTC through the internet from a Network Time Protocol (NTP) server . Due to the quality of the devices and the uncorrected errors along the signal propagation path, these kinds of synchronization methods can only have millisecond to microsecond accuracy [27][28].

1.3.1 Time and frequency transfer at the BIPM

For some industrial and scientific applications, it's necessary to apply a more reliable time/frequency transfer method to make sure that the method itself does not contaminate the accuracy and the stability of the compared clocks [29]. The state-of-the-art time/frequency transfer techniques are used at the BIPM to generate the international time scale TAI and UTC. The two clock-comparison techniques that are currently adopted by the BIPM for the calculation of TAI are GNSS time and frequency transfer and Two-Way Satellite Time and Frequency Transfer (TWSTFT), and a new method of time and frequency transfer using optical fibres is also under study at the BIPM.

To carry out the Two-Way Satellite Time and Frequency Transfer, the two stations who need to compare their clocks transmit signals to each other simultaneously via a geostationary satellite. Each station receives signal from the other side and measures the signal delay through the path with its own clock. Due to the similarity of the two signal paths, most of the signal delay can be cancelled out, combining the two measurements from the two stations, and the remaining

path delay that is not cancelled out can be corrected or calibrated, for example, the delay due to the satellite motion and the internal signal delay within each station [30], then the time differences of the clocks at the two stations can be determined with an uncertainty of 0.5 ns over one day. TWSTFT is a very accurate way for quasi-real-time international clock comparisons with relatively higher expense compared to the GNSS time and frequency transfer (i.e. expense to rent a satellite and maintain the ground station).

Currently, the most stable way for frequency transfer reported by the BIPM is to use the optical fibre link, the related optical transfer allows a frequency stability of 10^{-15} at 1 s and 10^{-19} at 1 day [31][32]; meanwhile, the current time transfer through optical fibre link shows a sub-ns accuracy [33][34]. The high potential of the optic fibre link time and frequency transfer makes it the optimal choice for future optical clock comparison. However, the optical fibre link has its drawbacks, for example, high cost for the installation and operation, and its confined comparison region which is limited by the distribution of the fibre network (mainly for continental comparison).

Among these three clock comparison techniques, the GNSS time and frequency transfer is the most economic and pervasive method. [35] and [36] showed that almost all the established time links at the BIPM for the generation of TAI use GNSS either as the primary method or as the backup of TWSTFT for the remote clock comparison. The GNSS time and frequency transfer methods are introduced in the following two subsections.

1.3.2 GNSS code measurements

GPS has been used since the 1980s for accurate time and frequency transfer with single-channel C/A code receivers [37]. As described previously, the GNSS solution includes the 3D position and the receiver clock offset with respect to the reference time of the GNSS (for example, the GPS system time). By connecting the atomic clock in a laboratory to a GNSS receiver to drive the receiver internal clock, the time difference of the atomic clock and the GNSS reference time also can be obtained once the time delay between the atomic clock and the receiver internal clock is well calibrated. To compare two remote atomic clocks in two different time laboratories, the clock difference of each atomic clock to the same GNSS reference time is estimated separately and simultaneously from the GNSS solution, then the difference of these two clock measurements are computed, in order to cancel out the same GNSS reference time and finally obtain the time difference of the two remote clocks at that specific epoch.

For the sake of simplicity, the term “receiver clock” is used in this dissertation, and it always refers to the clock that need to be measured: it could be a receiver internal clock when a user needs to synchronize this internal clock (as in the mobile phone) to UTC using GNSS timing, or it could be an external atomic clock which is connected to a receiver to drive its internal clock (as in the atomic clock comparison at the BIPM).

To facilitate the GNSS time transfer, the clock estimations at each laboratory can be recorded in a standard format called CGGTTS (Common GNSS Generic Time Transfer Standard), which was proposed for standardizing the GPS time transfer [38], then it was updated to include GLONASS [39], and the newest version is CGGTTS-V2E [40], which also includes Galileo and BeiDou measurements. In a standard process, the antenna of the receiving station is fixed, and its coordinates are already well known, so the receiver clock offset can be estimated from the measurements of each visible GNSS satellite after knowing the satellite position and clock offset from the navigation message and compensating the remaining propagation delays along the path. Figure 1-5 gives an example of the CGGTTS file that was generated at INRIM from the GNSS station GR01. The data in the column "REFSYS" as shown in Figure 1-5 are the estimated receiver clock offsets referring to the GPS system time, and each raw is corresponding to the estimation based on a 13 minutes long observation of a single GPS satellite.

```
CGGTTS     GENERIC DATA FORMAT VERSION = 2E
REV DATE = 2014-04-10
RCVR = POLARX4-TR-PRO                R2CGGTTS v8.0
CH = 12
IMS = POLARX4-TR-PRO
LAB = IT
X = +4476537.76 m
Y =  +600441.66 m
Z = +4488754.80 m
FRAME = ITRF
COMMENTS =           GR01 after moving
INT DLY =   54.2 ns (GPS P1),   50.4 ns (GPS P2)     CAL_ID = -
CAB DLY =  298.6 ns
REF DLY =  483.2 ns
REF = UTC((IT)
CKSUM = DE

PRN CL   MJD   STTIME TRKL ELV AZTH   REFSV      SRSV     REFSYS    SRSYS  DSG IOE MDTR SMDT MDIO SMDI MSIO SMSI ISG FR HC FRC CK
            hhmmss  s  .ldg .ldg    .lns     .lps/s     .lns    .lps/s .lns     .lns.lps/s.lns.lps/s.lns.lps/s.lns
G01 FF 58584 000600  780 640 1237    +1991484    +92          53    +11    7  67   88   +6   84   -1   84   -1    6  0  0 L3P C6
G03 FF 58584 000600  780 780 3529    -1881021     +2          15     +5    6  25   81   +0   66   +2   66    2    4  0  0 L3P 7B
G09 FF 58584 000600  780 121 2093    -4309098    +25          18    -38   24   4  374 -206  139  +49  139   49   15  0  0 L3P 53
G11 FF 58584 000600  780 427 1607    +6288615    -79          28     -7   12   7  116  +17   92   +1   92    1    8  0  0 L3P CC
G14 FF 58584 000600  780 208  445     +849728    +39          52    +53   19  83  220  +61   75  -46   75  -46   12  0  0 L3P 17
G17 FF 58584 000600  780 417 2911     -371542    -78          51    -20   11   2  118   -5   65  +13   65   13   10  0  0 L3P D4
G18 FF 58584 000600  780 342 1292     -430313    -48          53    -12   13  67  140  +25   98  +10   98   10   11  0  0 L3P FA
G19 FF 58584 000600  780 272 3124    +3321184   -104          68    -60   22  28  172  -29   62  +57   62   57   18  0  0 L3P 34
G22 FF 58584 000600  780 633  609    +6813588    +74          80     +3    6  39   88   +5   49   -3   49   -3    6  0  0 L3P B4
G23 FF 58584 000600  780 458 1949    +1906879     -1          41    +14   10  75  110  -15   93  -16   93  -16    7  0  0 L3P 11
G31 FF 58584 000600  780 207  734     -459344     -6          26    -32   30   6  222  -17  103  +35  103   35   22  0  0 L3P E2
G01 FF 58584 002200  780 568 1307    +1991563    +78          55     -3    7  67   94   +8   86   -2   86   -2    7  0  0 L3P C8
G03 FF 58584 002200  780 752  234    -1881014     -9          24     -6    6  25   82   +2   60   +4   60    4    6  0  0 L3P 69
G09 FF 58584 002200  780 189 2111    -4309018    +40          38    -24   24   4  244  -88  115   -3  115   -3   19  0  0 L3P 0F
G11 FF 58584 002200  780 351 1614    +6288567    -70          48     +2   15   7  137  +26   72   -1   72   -1   13  0  0 L3P D9
G14 FF 58584 002200  780 148  431     +849695    -89          34    -75   31  83  304 +121   84  +56   84   56   20  0  0 L3P 1F
G17 FF 58584 002200  780 428 2815     -371608    -58          41     +0   19   2  116   -1   75   +5   75    5   15  0  0 L3P AE
```

Figure 1- 5. An Example of CGGTTS version 2E file with measurements from the station GR01 at INRIM

Since all the stations in need record their clock estimations in a common time schedule in the CGGTTS files, it's easy to process time transfer following the same schedule for any pair of stations. There are mainly two techniques that are used for the time transfer based on the CGGTTS files, which are called Common-View (CV) and All-in-View (AV). The principle of the CV time transfer is illustrated in Figure 1-6. Computing the difference of the two receiver clock offsets from the two stations that are at the same epoch and from the same satellite, all the satellite clock errors and hardware delays are cancelled out, and most of the satellite orbit errors are also removed, the remaining errors are mainly due to the atmosphere signal propagation delay and the multi-path effect. For each visible satellite i at each epoch, a clock difference $(T_1\text{-}T_2)^i$ between the two stations is estimated, then the final time transfer solution $T_1\text{-}T_2$ at each epoch is calculated as a weighted average of the results obtained from these commonly visible satellites

at the same epoch. Considering the measurement from the satellite with low elevation may have larger noise, how much the weight of each satellite measurement is set depends on the current satellite elevation (e.g. the weight is set to $sin^2(elv)$, where elv is the elevation of that satellite).

The quality of the CV time transfer depends on the number of commonly visible satellites for both stations. As the distance between the two stations increases, the number of commonly visible satellites decreases, and the noise in the CV time transfer solution raises. Therefore, this method is not suit for a global clock comparison. AV time transfer is a method without any restriction on the distance, and its principle is described in Figure 1-7. At each epoch, the local receiver clock offset with respect to the GNSS reference time is estimated separately for each station using all the visible satellites, then the clocks of the two stations are compared by computing the difference of these local clock offset estimations.

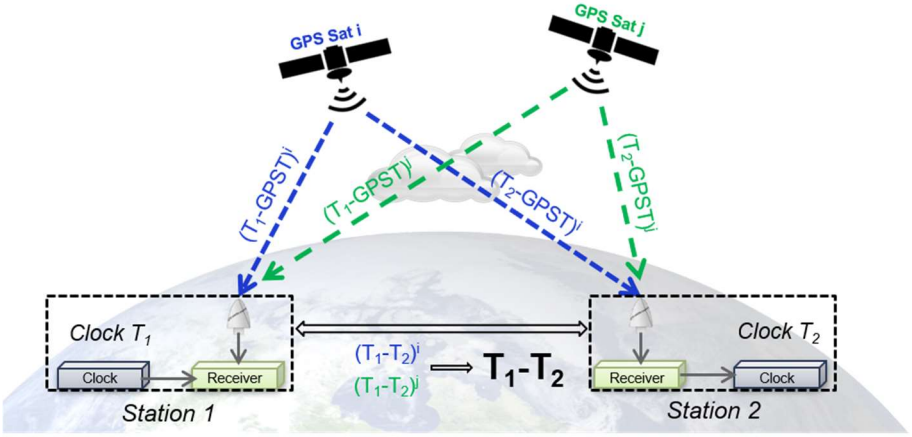

Figure 1- 6. Principle of GNSS Common-View time transfer. GPST means the GPS system time

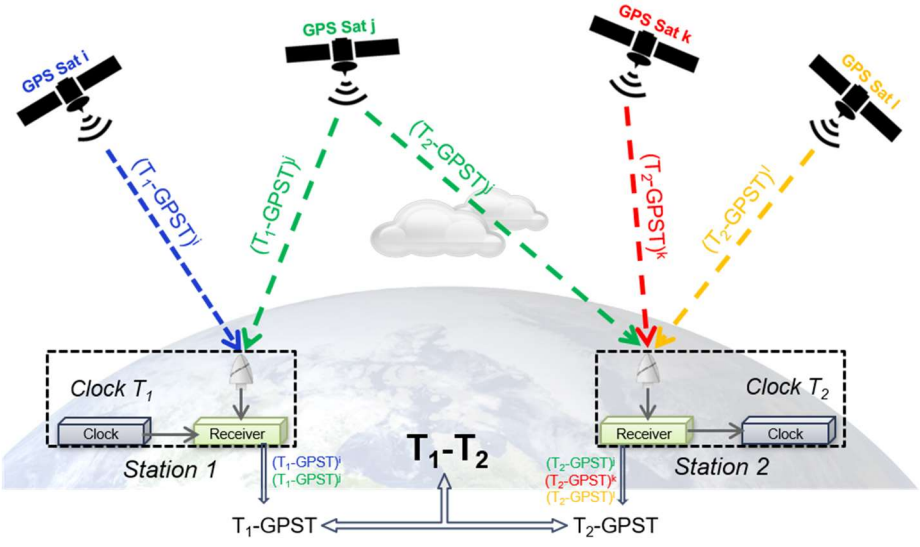

Figure 1- 7. Principle of All-in-View GNSS time transfer

However, the errors from satellites are not cancelled out in the AV time transfer, more accurate satellite orbit and clock products are therefore needed instead of the broadcasted ones to reduce the errors from the satellites. The most common accurate satellite products are provided by the International GNSS Service (IGS). The IGS products are available with different latencies and accuracies for various applications [41][42]. Since IGS estimates satellite clocks with its own reference time in the provided products, the GPST in Figure 1-7 will be substituted by the IGS reference time if the IGS products are used in the AV time transfer.

Meanwhile, many other efforts have also been done to improve the time and frequency transfer performances, which include but not limited to: using two-frequency P code receiver that enables to remove 99% of ionospheric signal propagation delay with ionosphere-free dual-frequency code measurements combination [43]; reducing transfer noise by increasing the number of satellite measurements (from the GPS-only to the multi-GNSS measurements) [44]; combining carrier phase measurement with code measurements to improve frequency transfer stability [45].

1.3.3 GNSS carrier phase measurements

In some cases, clock comparison in the time or frequency domain could be interconverted, since the frequency that is compared here can be simply understood as the changing rate of the time (see section 1.1.3). However, the difference between the time transfer and frequency transfer is worthy of attention. The time information is only included in code measurement, since carrier phase measurement is ambiguous as introduced before. Thus, to perform any accurate GNSS time transfer, the code measurements need to be included, and the signal delay in the receiving system of the station needs to be well calibrated [46]. Meanwhile, the carrier phase measurement is about 100 times more precise than the code measurement [31], the more precise frequency transfer solution could be obtained using the carrier phase measurements even if no calibration is performed in the station. In this dissertation, sometimes the shorter term “time transfer” is used instead of “time and frequency transfer” unless it is specially stated.

PPP is a state of the art GNSS time and frequency transfer technique that includes dual-frequency code and carrier phase measurements. The principle of PPP time and frequency transfer is very similar to the one of the AV, which is to estimate separately the local clock offsets with respect to the reference time at each station. As carrier phases are much more precise than code data, PPP needs to precisely estimate the signal propagation delays from different sources including the ones that are ignored in the code-only time and frequency transfer, and it calculates both the station position and station clock offsets in its final solution. The best performance of the PPP time and frequency transfer can be obtained by using the post-processed satellite orbit and clock products (such as IGS rapid and final products). As reported in [47], the code-only AV time transfer has a statistical uncertainty of several nanosecond over one day; while it is

concluded in [48] that the classic PPP time transfer using the IGS post-processed satellite products can reach the 100 ps level uncertainty, with a 10^{-15} frequency stability over one day.

Currently there are several PPP tools that are available for precise time and frequency transfer, such as, Bernese [49], NRCAN [50] and Atomium [51]. Similar time transfer performance of these PPP tools was shown in [52]. The principle of the Atomium PPP is introduced in what follows.

1.3.3.1 ATOMIUM PPP software

The Atomium PPP was developed by ORB (Observatoire royal de Belgique) since 2006 for geodetic positioning and time transfer using both GPS and GLONASS observations [51][52]. The Atomium estimates very precisely the propagation delays of the signals from the satellite to the receiver to corrects the corresponding pseudorange measurements, which include [52]:

- Satellite positions and clock offsets using precise satellite products (like IGS products)
- Satellite and receiver antenna phase centre offset and variation corrections using data provided by IGS [53]
- Hydrostatic part of tropospheric delay
- Solid Earth tides and ocean loading that effects on the station position.
- Ionospheric delay, which are estimated using ionosphere-free combination of carrier phase and P code measurements on L1 and L2 frequency.
- Wind-up that affects only carrier phase measurements.

Then the weighted least square analysis is performed on the corrected carrier phase and code measurements to determine the receiver clock offsets with respect to the reference time at 5 min interval, the tropospheric zenith wet delay at defined interval, one station position for the whole computational batch and the float carrier phase ambiguities. The computational batch for the Atomium PPP is normally one day, since the used GNSS products are generally generated based on one-day measurements (such as daily IGS products) [52].

Furthermore, in order to have accurate time solution, the calibrated value of the GNSS signal instrumental delay (from the GNSS antenna to the receiver clock) at the user side needs to be additionally removed from the receiver clock offset. If the instrumental delay is not considered, the PPP receiver clock solution can only be used for frequency transfer, because an additional offset will be introduced in the time solution (the instrumental delay is normally determined as a constant from the calibration).

1.3.4 Other time applications with GNSS

GNSS is not just well known for the clock comparison in the computation of TAI at the BIPM, it is also one of the most popular intermediaries for accurate time and frequency dissemination and synchronization in both industrial and scientific domain. In the GNSS market report [54] of the year 2017 from the European GNSS Agency (GSA), the wide usage of the GNSS for timing or synchronization purposes in the industrial domain were introduced, such as the synchronization of the telecommunication network and the precise time stamping in the financial systems. Meanwhile, GNSS has proved its advantages in various specific applications, for example, for the time synchronization of the intelligent transportation systems [55] and the spacecrafts in space [56].

In the scientific domain, GNSS is also the primary choice for many scientific activities, which require highly time synchronized stations in the network to observe the same event, such as, the seismic monitoring [57], deep space tracking [58] and neutrinos speed measurement [59].

In the next section, a European project which is dedicated to the development of different time services based mainly on GNSS is introduced.

1.4 Time services in DEMETRA project

DEMETRA (DEMonstrator of EGNSS services based on Time Reference Architecture) is a project funded by the European Union through the Horizon 2020 programme [60], it was coordinated by INRIM and involved 16 European partners, including ORB. The goal was to develop and provide improved or new time services to the specific users in the industrial and scientific domain, and most of the services were based on the European GNSS. The general concept of the DEMETRA project is demonstrated in Figure 1-8.

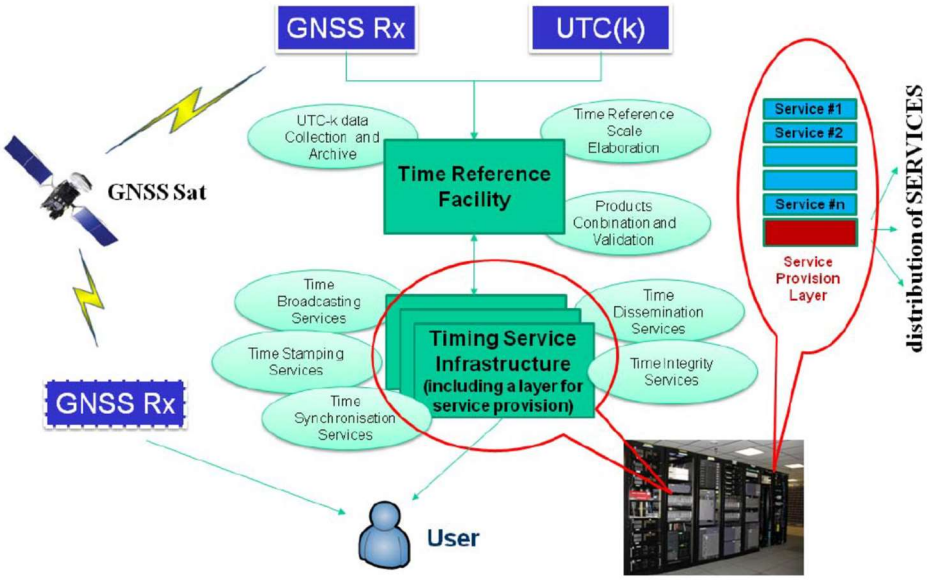

Figure 1- 8. General concept of DEMETRA [61]

DEMETRA provides the “end to end” time services from the generation of an accurate and precise reference time at the time laboratory to the delivery of the time services to the users [61]. During the project, nine different time services have been developed and integrated in the DEMETRA laboratory of INRIM, to meet the needs of different users. These services are briefly introduced below [62]:

Service 1: Time broadcasting over TV/Radio links. It disseminates the local UTC time with one millisecond accuracy to the users through the radio and TV links.

Service 02: Certified Trusted Time Distribution with Audit and Verification using NTP. This service disseminates the UTC time and frequency through the internet using the NTP.

Service 03: Time and Frequency Distribution over Optical link. It provides the time and frequency signals with sub-nanosecond level accuracy over the optical fibre to the users.

Service 04: Time and Frequency Distribution via GEO Satellite. It broadcasts the time and frequency information via a geostationary satellite, being a back-up to the GNSS solution.

Service 05: User GNSS Receiver Calibration. It refers to the calibration service measuring the GNSS signal delays in the receiving system at the user side for the accurate GNSS time transfer.

Service 06: Certified Time Steering. It allows a remote steering and synchronization of the user oscillator by monitoring the user clock with the reference time at INRIM in real-time.

Service 7: Time Monitoring and Steering. Using the GNSS PPP time transfer techniques, DEMETRA monitors the user clock in near real-time and reports any phase or frequency jump that happens on the clock. Meanwhile, the KPIs (Key Performance Indicators) of the user station are also available for check.

Service 8: Time Integrity. By monitoring the GNSS satellite, any anomaly in the GNSS signals will be checked, and a list of unhealthy satellites will be sent to the user to improve its positioning and timing performance.

Service 9: All-in-one Time Synchronization Solution. This service is based on a Thales Alenia Space patented GNSS time and frequency transfer solution for accurate synchronization of a scalable network of clocks.

Currently the whole project has completed its final test in a real user environment, and most of the time services still remain operative through their infrastructures maintained at INRIM premises, for example, INRIM keeps providing the UTC time dissemination service via the fibre link to the financial district in Milan [63]. Meanwhile, some of the services, such as the service 7 and 8, are still undergoing some updates to improve the performances and to add more features.

1.5 The research topics

This section includes some general introductions about the PhD work.

As previously introduced, GNSS provides positioning and timing services based on the accurate measurements of their atomic clocks. Meanwhile, the GNSS signals are often used as the intermediaries for time and frequency transfer. In the following two chapters, some concerns of the related GNSS techniques in these two aspects are introduced, and some new algorithms are proposed accordingly to solve the specific problems or to improve the performances of the current techniques.

Currently, the most precise GNSS time and frequency transfer is carried out in a post-processing way, for example, the BIPM uses both AV and PPP techniques for the international clock comparison in the computation of TAI, taking advantage of the IGS post-processed precise satellite products [64]. In chapter 2, the limitations of the current PPP technique in time and frequency transfer are listed. Then the updated versions of the Atomium PPP software, which have been developed in this PhD work, are introduced, and their performances in time and frequency transfer are measured in the designed experiments. In the last section of chapter 2, the application of the updated PPP software in the DEMETRA project are presented.

On the other side, in real-time GNSS applications, broadcasted satellite ephemeris and clocks from the navigation messages are normally used for positioning and timing. That means any anomaly that happens in a GNSS satellite clock could affect the final GNSS solution if it was not successfully detected. In chapter 3, the effects of the satellite clock frequency anomalies on the GNSS positioning and timing are first demonstrated. Then a real-time method of the GNSS satellite clock frequency monitoring is proposed, and its performances in the real-time satellite clock frequency jump detection are tested. In addition, two alternative methods are also introduced to have redundant measurements. At last, the upgrade of the current DEMETRA time integrity service by applying these methods is investigated.

Chapter 2

Improved Atomium PPP for time and frequency transfer

Some descriptions and results from the journal paper [65] are reused in this chapter. Futhermore, the shorter term "time transfer" is normally used in this chapter instead of the "time and frequency transfer".

Note that, in the previously published paper [65], the PPP clock solution "receiver clock – reference time" was wrongly written as "reference time – receiver clock", but the conclusions remain the same.

Time (and frequency) transfer with PPP technique has been studied for many years [66]. By using carrier phase measurements, PPP can highly increase the short-term stability of its time transfer for the averaging time within several days [67]. Currently, PPP time transfer has been applied to more than half of the laboratories contributing to TAI at BIPM [68][69]. However, as the clock quality improving, the current PPP technique has shown some limitations to compare the best clocks. As part of the PhD work, some new PPP algorithms have been developed based on the Atomium PPP recently, in order to have better PPP time transfer performances.

This chapter consists of seven sections. The first section introduces the limitations of the current PPP time transfer. The second section depicts the two kind of experiments that were designed to test the new PPP time transfer algorithms. The mathematic details of three updates to the current Atomium PPP and their performances in the designed experiments are reported in the sections 3-5. The updates include: 1. Adding Galileo measurements in the PPP computation; 2. Adding a function to constrain the receiver clock; 3. New PPP algorithms for integer ambiguity resolution. In section 6, the frequency accuracy of these new PPP time transfer solutions is studied. And the last section is about the application of these new PPP algorithms in the DEMETRA Horizon 2020 project.

2.1 Current PPP time transfer

As already explained, PPP provides very precise time transfer solution taking advantage of carrier phase measurements. however, the carrier phase measurements include unknown ambiguities that need be determined relying on the code measurements which have much larger noise. Therefore, the carrier phase only determines the precision/stability of the PPP time transfer solution, and the accuracy of the PPP time transfer is given (and limited) by the code measurements.

Combining code and carrier phase measurements can largely increase PPP time transfer stability inside the daily batch boundary, however the problem arises when multiple day solutions are needed: the PPP time solution is not continuous at the daily batch boundaries. Figure 2-1 displays the discontinuity of the multi-day clock comparison between the stations BRUX and ZTB3, which are two stations located at ORB, and both connected to UTC(ORB). The clock comparison results are expected to be around zero since the same clock is compared. The discontinuity at the daily boundaries, as can be discovered in Figure 2-1, is caused by the averaging on the noisy code measurements inside each daily batch, and its size can be more than 1 ns in some extreme cases [70].

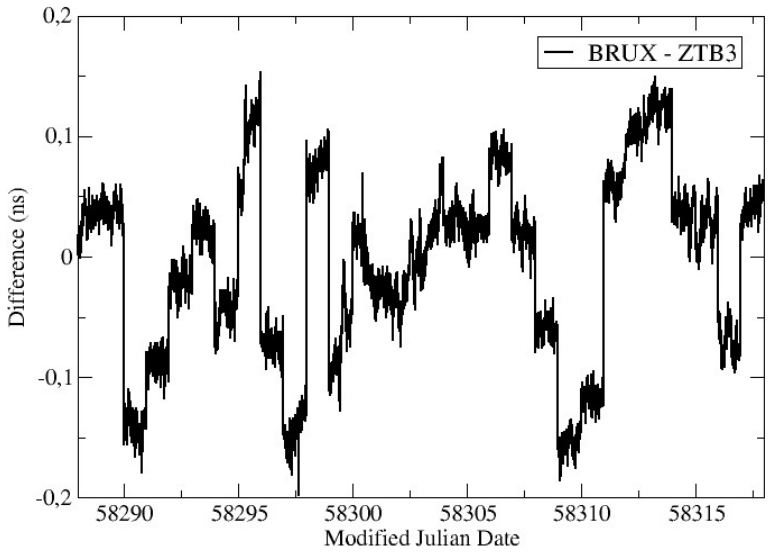

Figure 2- 1. Daily boundary discontinuity from the PPP time solution

A common way to deal with the daily boundary discontinuity is to build a multi-day computational batch to avoid the discontinuity inside the batch (such as the clock comparison within monthly batch at BIPM using NRCAN PPP), however, there are still discontinuities at the boundaries of the multi-day batches; moreover, this method may still include additional random walk noise to the clock estimation inside the batch [66], which affects the long-term stability of the time solution. It was reported in [71] that the introduced random walk noise could be partly due to the fact that in the classic PPP, such as Atomium and NRCAN, one treats carrier phase ambiguities as float values rather than integer values. The use

of PPP for the best frequency standard comparison is therefore limited by the long-term instability of its time transfer technique [69].

In addition, the short-term stabilities of the PPP time transfer are also limited by the thermal noise effect on the carrier phase measurements. Figure 2-2 shows the measurement stability of the carrier phase for the BRUX-ZTB3 comparison and the clock stabilities of CHI-75 active H-maser and 5071A Cs primary frequency standard. It indicates that in order to measure the clock behaviour of the best commercial clock, more precise frequency measurements need to be extracted from the PPP solution in the short term. Note that Figure 2-2 is only made for the sake of comparison, the measurement stability of the carrier phase in Figure 2-2 is better than the actual PPP time transfer performance, since it is only the theoretical performance the carrier phase measurement can reach: the ambiguities of the carrier phase measurements are fixed with respect to the reference zero since it's a common clock comparison.

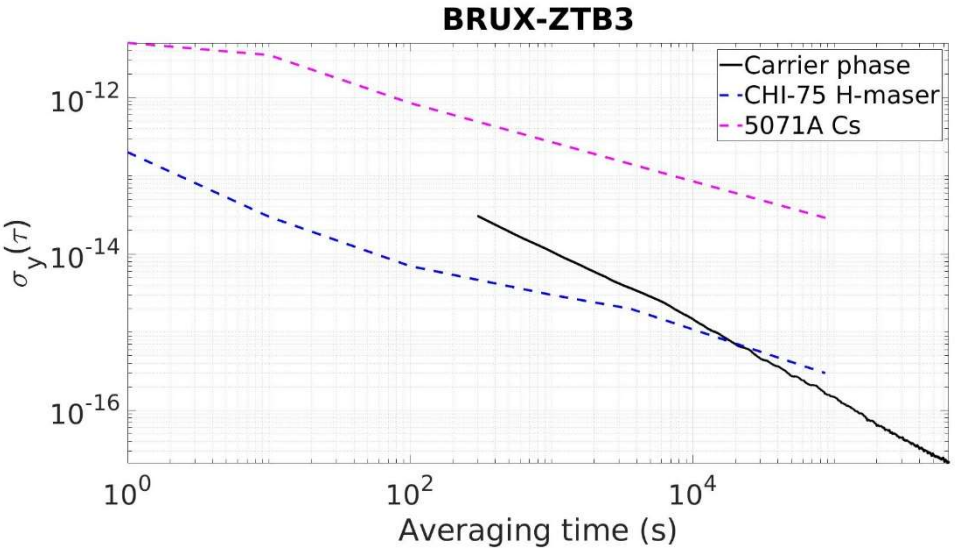

Figure 2- 2. Stabilities of carrier phase measurements and clocks

New versions of Atomium PPP software have been developed in this work aiming at overcoming these limitations. In order to test the performances of these new PPP algorithms, two kinds of experiments were designed, and they are explained in the next section.

2.2 Experiment methods

When we perform a time transfer experiment between two remote stations to evaluate the performance of PPP algorithms, it is difficult to distinguish between the noise generated by the PPP algorithms and the noise from the clocks themselves. In order to minimize the effect of the compared clocks, two kinds of experiments were built: 1. Common Clock Difference (CCD); 2. "PPP - OPT".

The idea of the CCD (which is also called common clock comparison) is illustrated in Figure 2-3. Two GNSS stations are driven by the same atomic clock and they compare their clock difference using the PPP technique, just as the clock comparison between BRUX and ZTB3 that was shown in the previous section (see Figure 2-1). Since they are connected to the same clock, the effect of the clock itself is cancelled out during the comparison, and the CCD result should be always around zero if the hardware delay in both stations are accurately measured. In fact, the calibrated value of the hardware delay at a GNSS station is normally determined as a constant value with ns uncertainty [46] until the next calibration, therefore the CCD result will never be zero in practice even if there is no noise introduced by the PPP algorithms. In any case the CCD result will include the noise introduced by the PPP algorithms and an offset that is caused by the inaccuracy of the hardware delay calibrations in the two stations. Since this experiment is only designed to evaluate the performance of the new PPP time transfer stability, the calibration values will not be applied to the CCD results, therefore the offset will reflect the difference of the hardware delays in the two stations. In the following CCD experiments, the results were shifted parallel towards zero (compensating the offsets) for a better comparison of the PPP time transfer solutions.

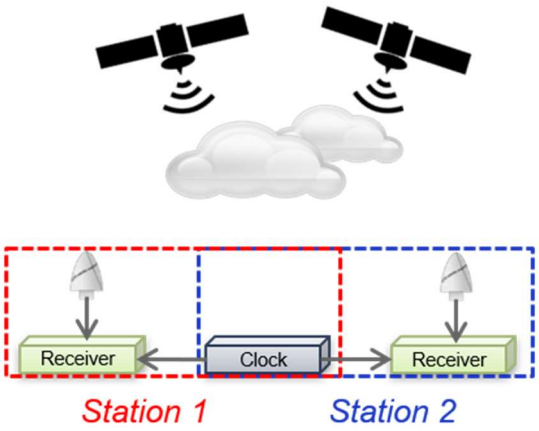

Figure 2- 3. Common clock comparison between station 1 and 2

The other kind of experiment is called “PPP - OPT”, which means the PPP clock comparison result minus the comparison result between the same clocks over the same period using the optical fibre link in order to cancel out the effect of the clocks. As mentioned before, time transfer with optical fibre link is currently much more precise than GNSS time transfer, therefore the result of the subtraction could be used to study the stability of the PPP time transfer solution.

The CCD experiments were built using the pairs of common-clock stations at ORB and INRIM during different periods: MJD 58288-58318 (1 month) and MJD 58663-58848(6 months) for “BRUX – ZTB3” (at ORB); MJD 58591-58636 (1 month) and MJD 58663-58848(6 months) for “GR01 – GR02” (at INRIM).

A continuously operating atomic clock comparison via the optical fibre link has been established since 2013 between the astrogeodynamic observatory of the

space research center (AOS) and the central office of measures (GUM) [72], meanwhile the two clocks are also compared using NRCAN PPP through their GNSS stations AO_4 and GUM4. Both the comparison results and the GNSS observation data of the two stations are available on the BIPM FTP site ftp://tai.bipm.org/ [69]. Hence the following "PPP - OPT" experiments were built based on the link "AO_4 – GUM4", to compare the time transfer solutions of the new Atomium PPP and the NRCAN PPP. A period of 8 months was chosen for this kind of experiment: MJD 58329-58572.

In the following sections, the two kinds of experiments introduced above were carried out for the test of all the new Atomium PPP algorithms. There were two new versions of Atomium PPP that have been developed during the PhD work. The first version is a float ambiguity PPP which includes Galileo measurements and constraint function. The second version is an integer ambiguity PPP which fixes carrier phase ambiguity as integer number. However, for the convenience of introduction, these updates were called Atomium Galileo PPP, Atomium constrained PPP and Atomium integer PPP respectively and they were introduced in the section 2.3 to 2.5 accordingly.

2.3 Atomium Galileo PPP

Though Galileo hasn't reached its full constellation size yet by far (see Fig 2-66 which is made in April 2019), the benefit of combining GPS and Galileo signals for the positioning and timing services has been reported, such as in [73] and [74] respectively. The original Atomium uses GPS and GLONASS signals for the PPP computation, now it has been updated to include also Galileo signals. The process is introduced in the following sub-section.

2.3.1 Updating process

The satellite pseudorange measurements from any GNSS stations can be recorded in The Receiver Independent Exchange Format (namely RINEX observation file) for post-processing purpose. The RINEX V2 observation files that are provided on the IGS FTP site (ftp://cddis.gsfc.nasa.gov/) don't include Galileo measurements. In order to include the Galileo measurement, the RINEX V3 file is set as input instead in the new Atomium Galileo PPP. For the same reason, instead of IGS satellite products, IGS Multi-GNSS Experiment (MGEX) products [75] from one analysis center are used, including satellite orbit file (*.ORB), satellite/receiver clock file (*.CLK) and earth rotation parameters file (*.ERP). All the mentioned files are available on the IGS FTP.

As for GPS, the P (or P(Y)) code and carrier phase measurements on frequency L1 and L2 are used to build the ionosphere-free combination, the new PPP combines the Galileo measurements on E1 and E5a band.

The mathematic models of GPS code and carrier phase measurements that are used in the PPP computation keep the same as in the original Atomium PPP [51], which are expressed as

$$P_{IF} = R + c \cdot (T^R - T_S) + \mathrm{mf} \cdot \mathrm{zpd} + Tropo_{dry} + M_P + \varepsilon_P \quad (2)$$

$$L_{IF} = R + c \cdot (T^R - T_S) + \mathrm{mf} \cdot \mathrm{zpd} + Tropo_{dry} + \lambda_{IF} \cdot \mathrm{N} + \mathrm{W} + M_L + \varepsilon_L \quad (3)$$

where P_{IF} and L_{IF} are the ionosphere-free combination of the code and carrier phase measurements separately, R is the satellite-receiver geometric distance, c is the speed of light, T^R and T_S are the receiver and satellite clock offsets with respect to the reference time respectively, mf is the mapping function of the wet tropospheric delay and zpd is the corresponding wet tropospheric zenith path delay, $Tropo_{dry}$ is the dry tropospheric delay, λ_{IF} is the wavelength of the ionosphere-free combination, N is the phase ambiguity, W is the wind-up effect on carrier phase, M_P and M_L are the multipath effect on code and carrier phase measurements respectively, ε_P and ε_L are the noises on the corresponding measurements.

In order to add Galileo measurements in the PPP computation, only one more parameter needs to be estimated from the Galileo measurements, that is called Inter System Bias (ISB). ISB stands for the bias between the GPS and Galileo measurements, which is caused by the different hardware delays of the GPS and Galileo signals in the receiving system and the possible difference of the reference time for GPS and Galileo in the MGEX clock products. This ISB is set as an unknown constant in a daily batch in the current Galileo PPP, assuming it is stable enough. The ISB can be solved together with the station position, the receiver clock offsets, the wet tropospheric zpd and the float phase ambiguities. However, it was reported in [76] that not all the MGEX analysis centers treat the ISB as constant when generate their satellite products, therefore the products must be chosen with care.

It should be noted that the GNSS satellite position provided in the IGS/MGEX orbit product is at the center of mass, while the pseudorange measurements are based on the distance between the antenna phase centers of the satellite and the receiver. Hence it is necessary to convert the provided satellite position to the phase center position for further computation. The commonly used phase center corrections are provided in the file available on the IGS site [77], which includes the phase center offsets and variations for the GNSS satellite antennas and the common-used receiver antennas in the ground stations. The current version of this IGS file is igs14.atx, which is in ANTEX format [53].

Not like the phase center variation corrections to the GPS and GLONASS satellite antennas, which are nadir-dependent, these corrections for the Galileo satellite antennas are azimuth- and nadir-dependent. The azimuth angle is measured in the satellite-fixed right-handed coordinate system [53]. On the receiver side, the antenna phase center corrections for the Galileo signals are currently not available in the igs14.atx file at when the software were developed (February 2019), the temporary method that was used in the experiments is to apply the same receiver corrections on GPS L1 and L2 to Galileo E1 and E5a respectively. The magnitude of these antenna phase center corrections is generally around 100 mm (corresponding to 0.33 ns), and the mismatch of the corrections on L2 and E5a will mainly manifest as an offset in the related PPP time solution.

2.3.2 Processing and results

2.3.2.1 Test on the MGEX products from GFZ and CNES

It has been mentioned previously that the MGEX analysis centers may use different handling schemes to estimate the ISB(s) during the generation of their GPS/Galileo satellite products. In [76] the multi-GNSS PPP positioning was performed with three different ISB estimation strategies: as random walk noise, as white noise and as a random constant. It showed that the PPP positioning performances were very similar among these three ISB estimation strategies using the MGEX products from CODE, CNES/CLS (CNES for short) and WHU analysis centers, while for the PPP using the MGEX products from GFZ analysis center, estimating the ISBs as random constants caused worse positioning accuracy and longer convergence time compared to the results in which the ISBs were estimated as random walk or white noise.

In the current version of Atomium Galileo PPP, the ISB is estimated as a constant during the daily batch, therefore it must be tested first which MGEX product is more adequate for it. The products from the analysis centers GFZ and CNES were chosen here, which stand for the use of two different schemes as reported in [76].

The analysis centers GFZ and CNES have their own reference times in their satellite products. And in their satellite clock products, the GNSS satellite clock offsets with respect to their reference time are recorded every 5 min. Figure 2-4 presents the clock offsets of GPS satellite 32 and Galileo satellite 31 compared to the reference time of GFZ and CNES, obtained from the corresponding clock products. It can be observed that the reference times for the GPS clocks at the two centers were very stable and were very similar to each other, while the reference times for the Galileo satellite clocks showed some daily boundary jumps, especially the one at GFZ, which had tens of ns discontinuity at the daily borders.

It is known that the satellite products are estimated based on the daily measurements and a reference time is chosen for each separate day, which could induce discontinuity of the reference time at the daily border. To further investigate the coherence of the reference times used for the GPS and Galileo satellite clocks in the two analysis centers, the following experiment was carried out: since both clock products also provide the estimated clock difference between the reference time and the BRUX clock, combining these BRUX clock measurements and the satellite clock measurements at same epoch, the GPS and Galileo satellite clock offsets with respect to the BRUX clock were obtained. Then this “satellite clock – ref BRUX” was used instead of “satellite clock – reference time” as the input of the Galileo or GPS PPP. The PPP clock solution of the station BRUX which was “BRUX – reference time” was then converted into “BRUX – ref BRUX”. The new clock solutions of the Atomium Galileo-only PPP and GPS-only PPP using the GFZ and CNES products are displayed in Figure 2-5 and 2-6. In the upper parts of the figures, the clock solution “BRUX – ref BRUX” using the GPS and Galileo signals are plotted separately; meanwhile, the aligned

solutions, of which the daily jumps were removed, are plotted in the lower parts of the figures for better visualization. The daily solutions were aligned with the following strategy: in order to align the time solution of day 1 and day 2, the value at the first epoch of day 2 solution is predicted by applying the 2nd order extrapolation to the last hour's data of day 1, then the value at the same epoch is estimated again by applying the 2nd order interpolation (or extrapolation) to the first hour's data of day 2, then the solution of day 2 is shifted by the amount that is equal to the difference between these two estimated values to compensate the discontinuity.

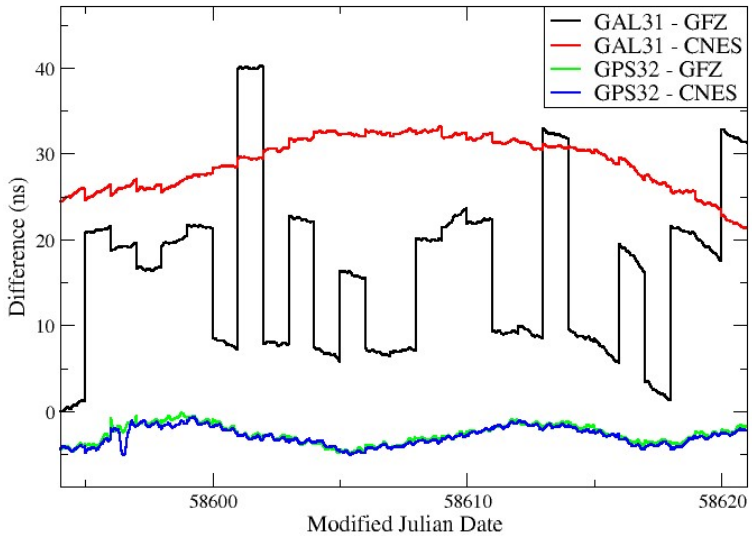

Figure 2- 4. Clock offsets of Galileo31 and GPS32 against GFZ and CNES reference time. Results are shifted for better comparison

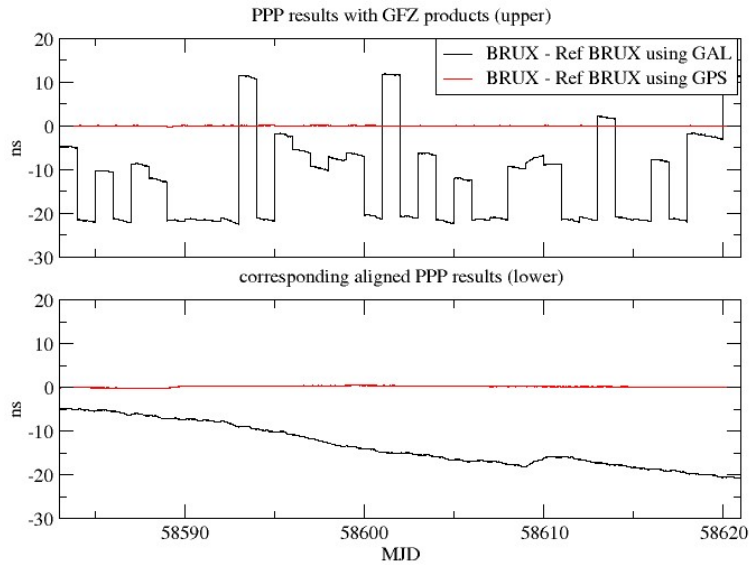

Figure 2- 5. "BRUX – ref BRUX" using Galileo or GPS measurements (shifted) at GFZ.

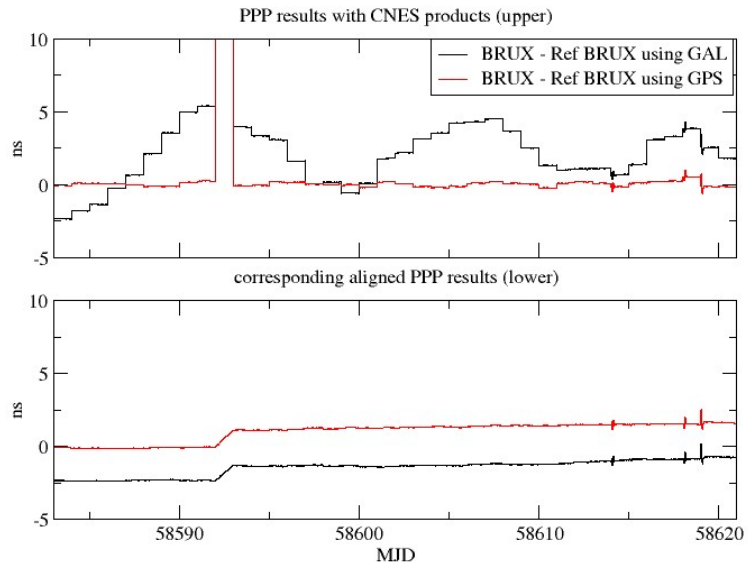

Figure 2- 6. "BRUX – ref BRUX" using Galileo or GPS measurements (shifted) at CNES.

From the aligned results in Figure 2-5 and 2-6 it is found that the GPS and Galileo time solutions using the CNES products are very stable and coherent with each other, while the ones using the GFZ products diverge from each other. It is probably because GFZ uses different reference times for GPS and Galileo. However, the reason could be also that GFZ's strategy of ISB estimation has a slightly different effects on the daily time measurements of GPS and Galileo in the clock products, which cause an accumulated error in the alignment over a long period. At last, the GPS + Galileo PPP and GPS-only PPP were carried out separately using the GFZ and CNES products for the estimation of "BRUX – ref BRUX" and the results are shown in Figure 2-7 and 2-8.

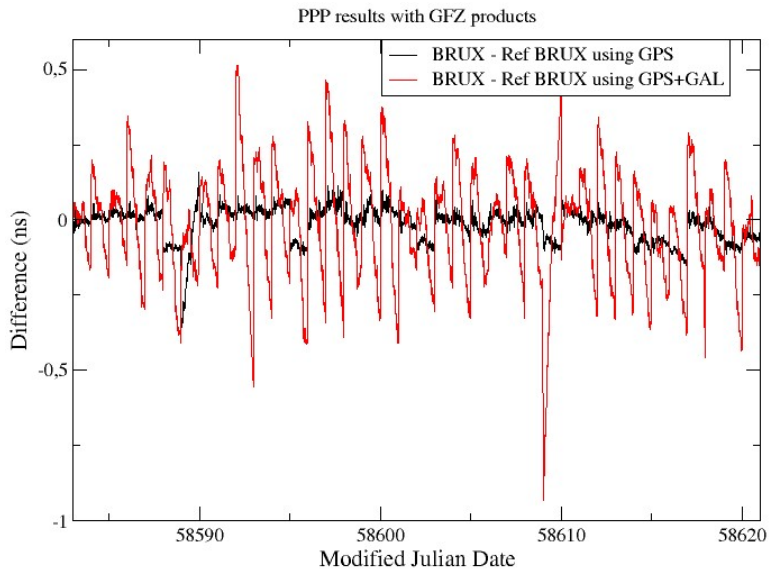

Figure 2- 7. "BRUX – ref BRUX" using the Galileo + GPS PPP with the GFZ products. Results are shifted for better comparison

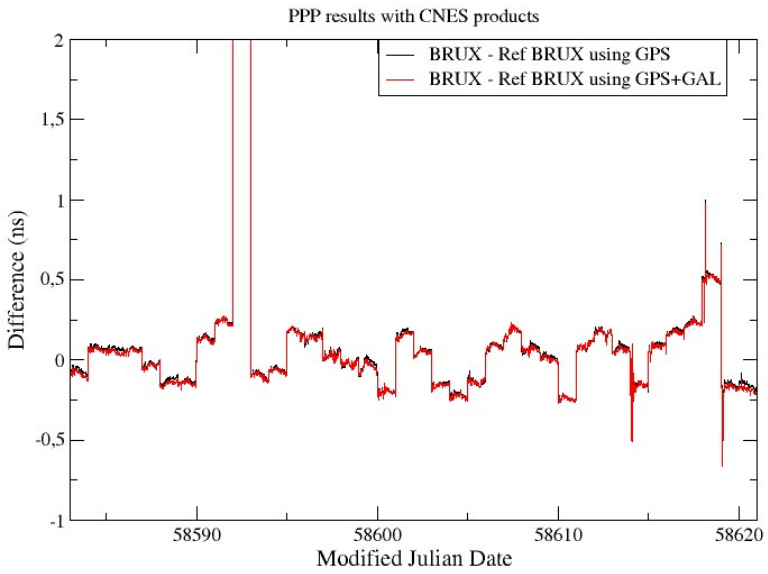

Figure 2- 8. "BRUX – ref BRUX using the Galileo + GPS PPP with the CNES products. Results are shifted for better comparison

It is observed from Figure 2-7 and 2-8 that, combing the GPS and Galileo measurements in the Atomium Galileo PPP using the GFZ products degrades the solution compared to the GPS-only results, while the GPS + Galileo and GPS-only results using CNES products are very similar. It indicates that GFZ possibly doesn't use the same ISB estimation strategy as in the Atomium Galileo PPP (in which the ISB is estimated as a constant value for one day) in the daily batch during the generation of its MGEX products. According to the results, the CNES MGEX products were therefore used for the test of the current updated versions of Atomium PPP in this dissertation.

2.3.2.2 CCD results with Galileo PPP

Since no Galileo measurement is provided by the stations in the "PPP - OPT" experiment, only the CCD links "BRUX – RTBS" at ORB and "GR01 – GR02" at INRIM were used here to study the performance of Atomium Galileo PPP. The two 1-month CCD PPP time transfer solutions using the GPS-only, Galileo-only and GPS + Galileo signals are shown in Figure 2-9 and Figure 2-10 separately. The results in both figures show good consistence by using the GPS and GPS + Galileo signals in the PPP, and the errors were generally within 0.5 ns over the whole period. The Galileo-only results show similar level of boundary jumps comparing to the GPS-only and GPS + Galileo ones at INRIM; while the Galileo-only results at ORB has significantly larger boundary discontinuity compared to the other two solutions. It is known that both stations at INRIM use the same type of GNSS receiver, which is Septentrio PolaRx4TR, while the station BRUX uses receiver Septentrio PolaRx4TR with multipath mitigation mode on and the station RTBS uses Septentrio PolaRx5TR with multipath mitigation mode off during the experimental periods. The larger discontinuity in the Galileo results at ORB may

have its origin in the GNSS receiver, and it needs to be investigated in future work. In this section, only the stability of these PPP solutions is studied.

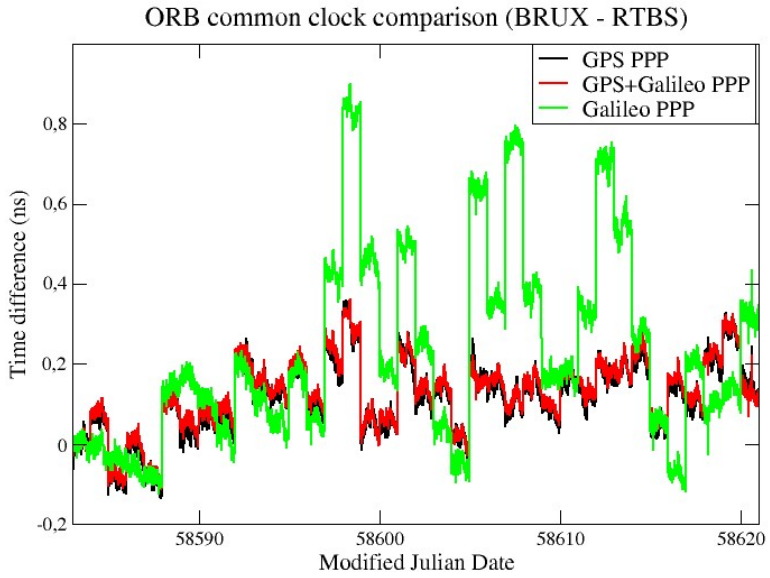

Figure 2- 9. CCD results at ORB with Atomium Galileo PPP

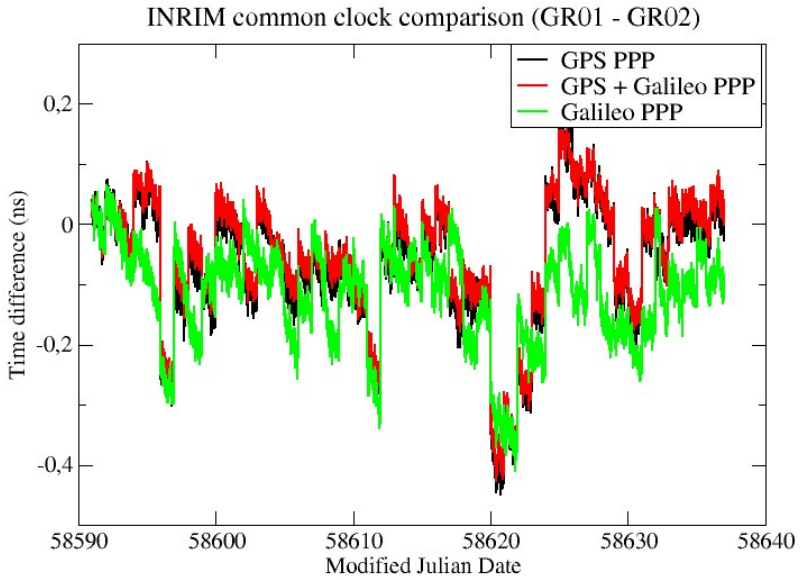

Figure 2- 10. CCD results at INRIM with Atomium Galileo PPP

Due to the existence of the daily boundary jumps, it's difficult to compare the stabilities of the results in Figure 2-9 and 2-10. A simple way to remove these daily boundary jumps is to align the daily time transfer solution using the 2nd order polynomial, which has been used for the alignment in Figure 2-5 and 2-6. However, the alignment will accumulate additional errors with the time, which can be found in Figure 2-11, where the aligned results of the solutions from Figure 2-9 are demonstrated. And Figure 2-12 gives another example of the additional errors caused by the alignment in the "PPP - OPT" experiment, in which the daily PPP solution generally follows the trend of the monthly NRCAN

PPP solution, while the alignment of the daily solution causes extra variations in the long term.

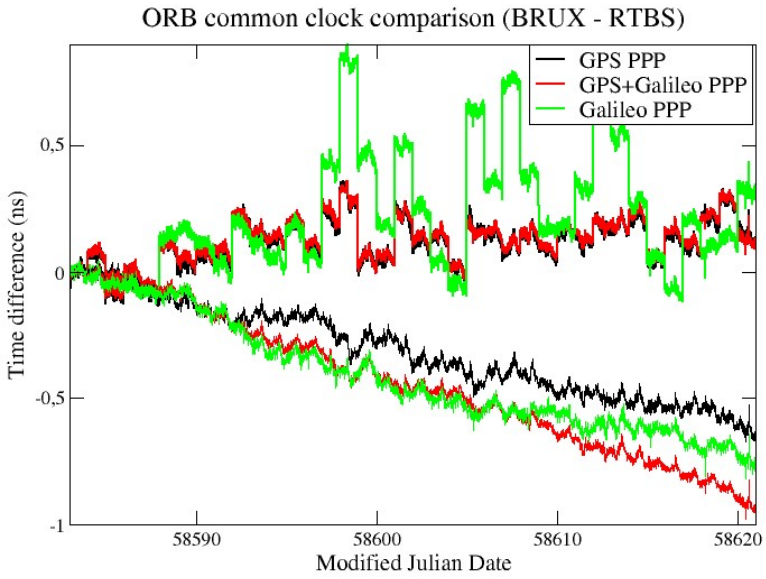

Figure 2- 11. PPP time transfer solution and the corresponding aligned results

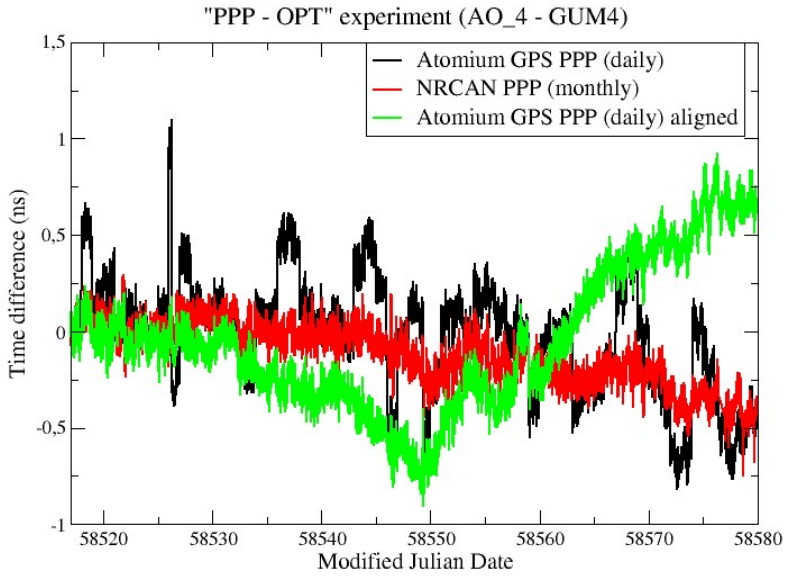

Figure 2- 12. Alignment errors over long terms in the “PPP - OPT” experiment

It should be noted that, the additional variations of the aligned results could be partly caused by the alignment itself, which is validated in the section 2.5 about integer PPP; meanwhile, the variations could also reflect the inaccuracy of the frequency determination in the float ambiguity PPP algorithms. The frequency determination of the PPP time transfer solution will be further studied in section 2.6. In this section, the frequency stability of the PPP time transfer solutions is studied based on 3-5 days aligned results to avoid the wrong estimation at the long

term, while the performance of PPP time transfer in longer term will be studied in section 2.6. 3 days measurements were taken from the solutions in Figure 2-9 and 2-10 for the alignment, and the corresponding results can be found in Figure 2-13 and Figure 2-14. The ADEVs of these aligned solutions are drawn in Figure 2-15 and 2-16 for the comparison of the frequency stability of the time comparison results. In addition, the ADEVs of other two 5-days aligned PPP time transfer solutions during the 6-months periods at ORB and INRIM are also plotted in Figure 2-17 and 2-18.

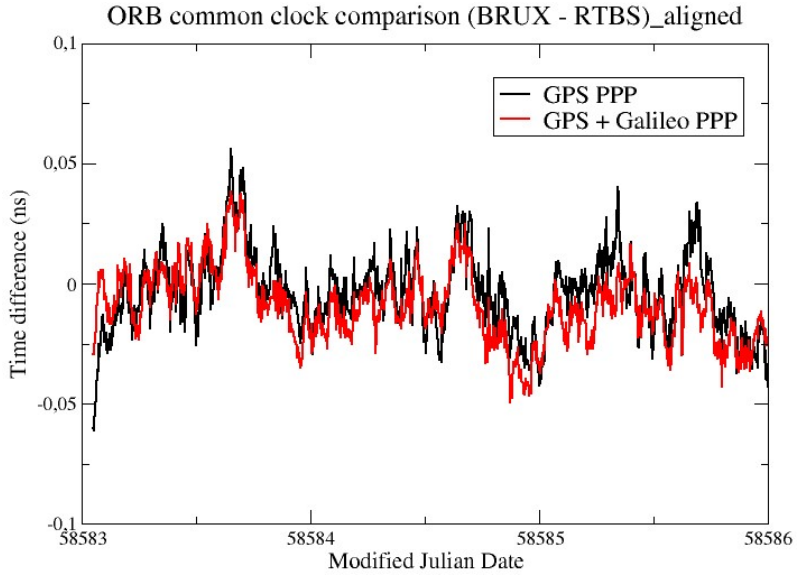

Figure 2- 13. 3-days aligned CCD results at ORB and INRIM

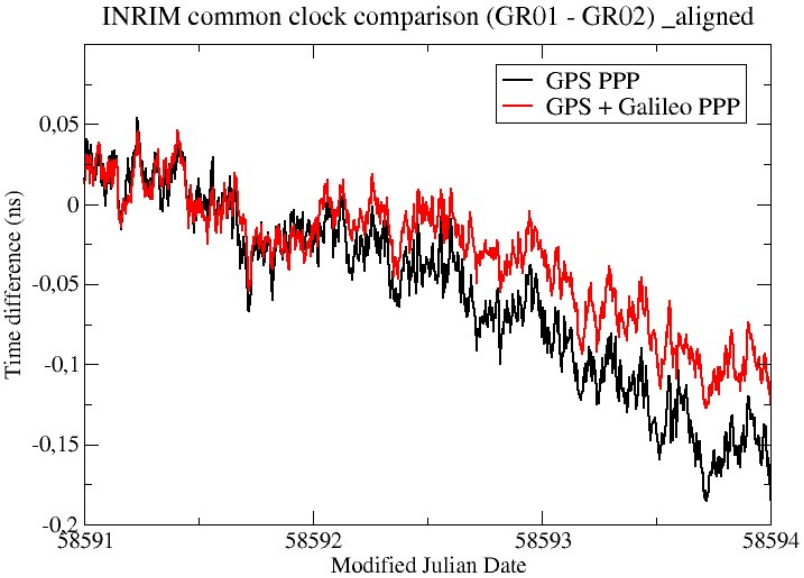

Figure 2- 14. 3-days aligned CCD results at ORB and INRIM

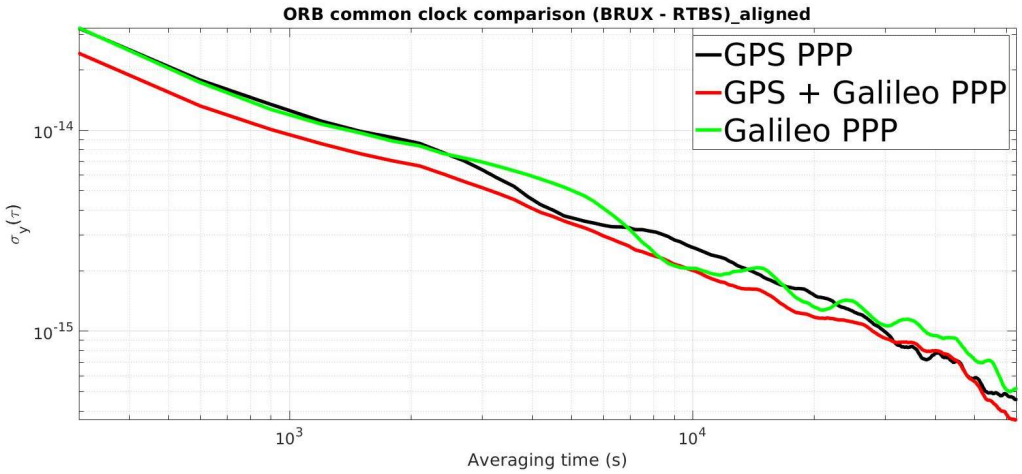

Figure 2- 15. ADEVs of the 3-days aligned CCD results at ORB (MJD 58288 - 58280)

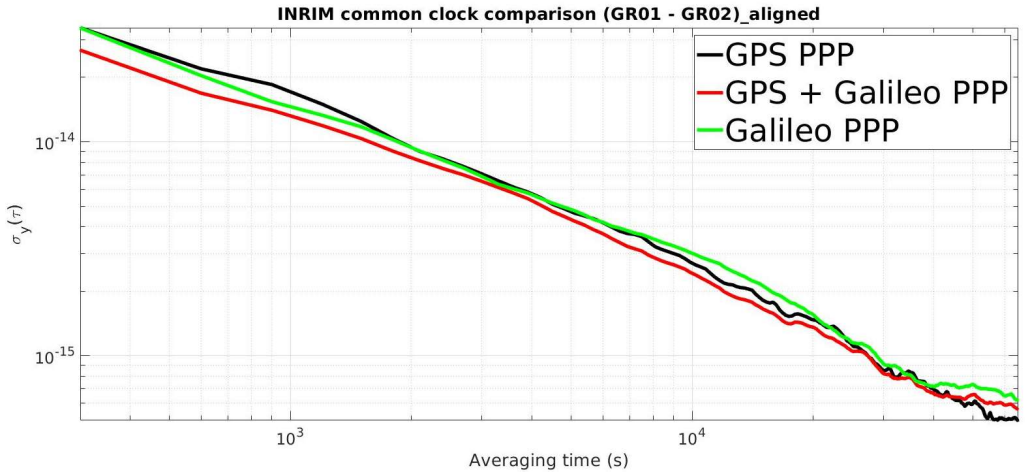

Figure 2- 16. ADEVs of the 3-days aligned CCD results at INRIM (MJD 58591 - 58593)

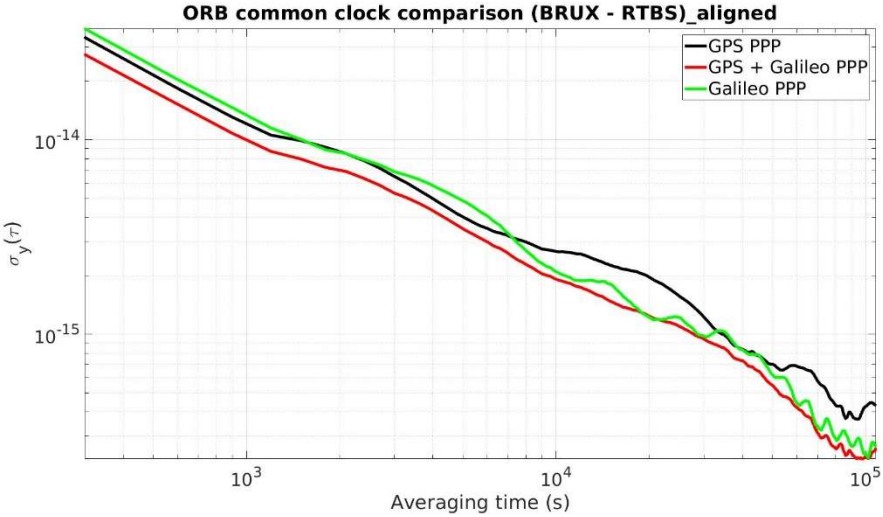

Figure 2- 17. ADEVs of the 5-days aligned CCD results at ORB (MJD 58376 - 58381)

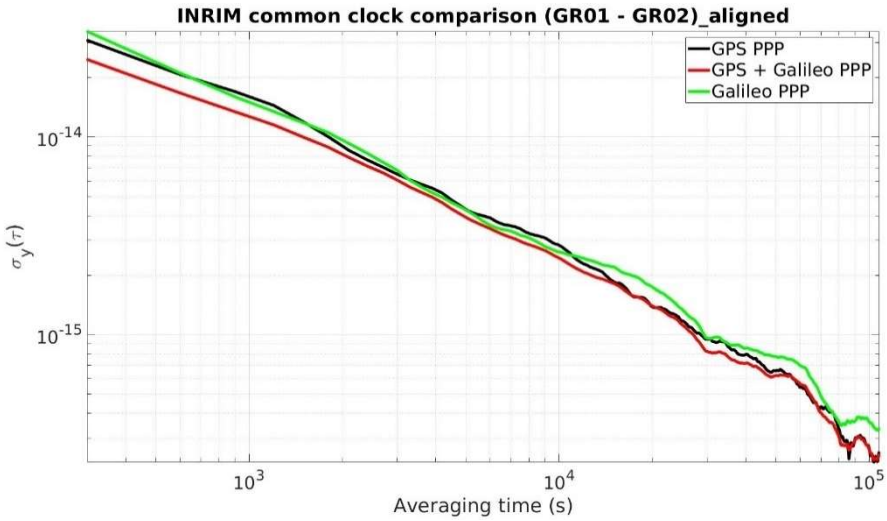

Figure 2- 18. ADEVs of the 5-days aligned CCD results at INRIM (MJD 58530 - 58535)

Due to the uncertainty at the long term, only the short-term frequency stabilities of the time transfer using Galileo, GPS and GPS + Galileo PPP are compared. In general, the GPS PPP and Galileo PPP time transfer show very similar performance at short term, while the GPS + Galileo PPP improved the short-term frequency stability of the time transfer compared to the GPS-only and Galileo-only PPP, as can be found in the ADEV figures. The improvement was generally in the range of 20% to 10% for the averaging time from 5 min to 2.5 hours. The long-term stabilities can only be compared precisely when multi-day continuous PPP time transfer solution can be provided.

2.3.3 Discussions

The current version of Atomium Galileo PPP only treats the ISB as a constant value in the daily batch, this limits its usage of satellite products to the ones which generate the ISB with the same (or similar) strategy (such as the products from CODE, CNES and WHU [76]). The future work will include the update of the ISB estimation strategy in the Atomium PPP to make sure it can use the MGEX products from all the analysis centers (for example, estimate the ISBs as random walk noise in the daily batch).

By adding Galileo signals to PPP computation, the short-term stability of the PPP time transfer is slightly improved. In order to study and improve the mid- and long-term stability, the mitigation of the daily boundary jump must be studied. This topic is further investigated in the next sections about the constrained PPP and the integer PPP.

In addition, the reason of the larger daily boundary jump in the Galileo-only PPP time transfer solution at ORB is still not confirmed, the effects of the GNSS receiver type and the receiver multipath mitigation function will be studied first.

2.4 Atomium Constrained PPP

The general idea of the constrained PPP is to restrict the white frequency noise in the receiver clock solution with a linear frequency model, in order to improve the short-term stability of PPP time transfer.

It was reported in [78] that a stochastic model could be applied on the receiver clock of high stability to improve the kinematic PPP positioning. [79] suggested a between-epoch constraint model for the receiver clock to improve the frequency stability of the real-time PPP time transfer. Also, some tests have been done with NRCAN PPP to study the effects of the constraint model on the PPP time and frequency transfer [80]. The algorithms of the constraint model used for the Atomium PPP are based on the ones described in [80] and have been modified so that it can adapt to the Atomium PPP. The algorithms of the constrained PPP and the scenarios where constrained PPP are applicable are introduced in the following subsections.

2.4.1 Developed algorithms

In order to measure a clock, usually the clock time or frequency deviations with respect to one reference are estimated, just as introduced in section 1.1.3. In this section, more conventional notations for these two quantities are used, and their relationship are expressed as follows [81]:

$$\mathrm{y(t)} = \frac{dx(t)}{dt} \tag{4}$$

where y(t) is the frequency deviation, and x(t) is the time deviation. The real GNSS signals are measured in discrete time, and equation (4) can be re-expressed as [82]

$$\mathrm{y[n]} = \frac{x[n] - x[n-1]}{\Delta t} \tag{5}$$

where Δt is the time interval between epoch n-1 and n.

The PPP clock solution of one station provides the time (deviations) measurements of the station clock with respect to the IGS/MGEX reference time at 5 min interval. Using equation (5), the related frequency deviations of the station clock can be computed. Assuming the station clock is mainly affected by the white frequency noise during the daily batch (which is generally true for the H-maser and Cs clocks by referring to Figure 1-3 and 2-2) and the IGS/MGEX reference time is stable enough during one day, the frequency deviations of the station clock measured by the PPP can be approximated by a frequency linear model (with an initial frequency and a frequency drift) plus the measurement noise from the PPP and the IGS products. Based on this principle, the algorithms of the constrained PPP were implemented in five steps as described below. The receiver clock refers to the atomic clock which is connected to the GNSS receiver in the station. These steps were previously introduced in the paper [65].

Step 1: Run the original Atomium PPP to obtain the clock solution "receiver clock – IGS/MGEX reference time" at 5 min interval. And the averaged frequency (deviation) of the receiver clock at each epoch is calculated as:

$$\mathrm{frq_i} = \frac{\mathrm{clock_{i+1}} - \mathrm{clock_i}}{\mathrm{t_{i+1}} - \mathrm{t_i}} \tag{6}$$

where $clock_i$ is the clock solution from the original PPP at epoch t_i.

Step 2: A linear model is built to fit the frequency data, and the frequency offset y0 and frequency drift d are obtained from the linear model:

$$\mathrm{frq_i} = \mathrm{y0} + \mathrm{d} * \mathrm{t_i} \tag{7}$$

An example of the process is shown in Figure 2-19.

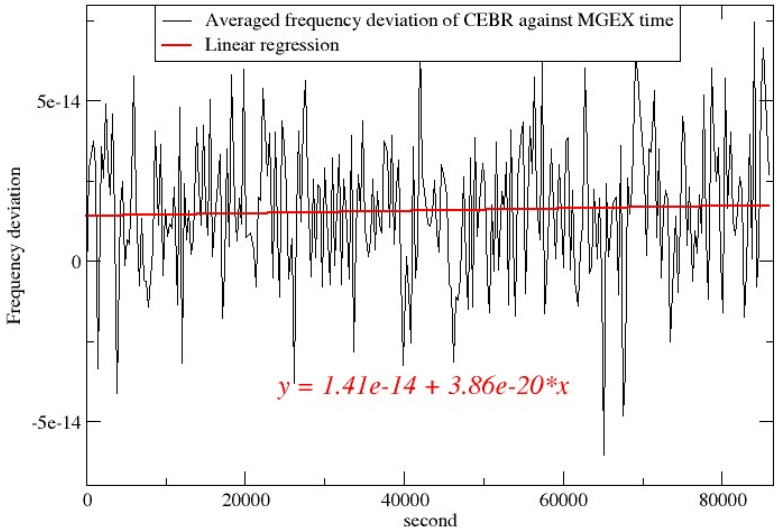

Figure 2- 19. An example of the frequency parameter estimations on the receiver clock of station CEBR

Step 3: From the estimated frequency parameters $(\mathrm{y0}, \mathrm{d})$, the relative changes of the clock in the time domain can be recomputed as:

$$\begin{aligned}\mathrm{delt_i} &= \mathrm{clock_{i+1}} - \mathrm{clock_i} \\ &= (\mathrm{y0} + \mathrm{d} * \mathrm{t_i}) * (\mathrm{t_{i+1}} - \mathrm{t_i})\end{aligned} \tag{8}$$

These recomputed clock changes can be used to restrict the evolution of the clock in the PPP clock solution (namely receiver clock constraints).

Step 4: The variances of the corresponding constraints are estimated as:

$$\sigma_i{}^2 = \left(ADEV(1s)\right)^2 * (t_{i+1} - t_i) \tag{9}$$

where $ADEV(1s)$ is the Allan Deviation of the receiver clock at 1 s. $ADEV(1s)$ of the receiver clock can be obtained from the clock specification document that is provided by the clock manufacturer or can be measured from the ADEV plot of the receiver clock (see Fig 2-2). The first method is adopted in the Atomium constrained PPP, the $ADEV(1s)$ of the commonly used atomic clocks CH1-75 H-maser and 5071A Caesium clock are 2e-13 [83] and 5e-12 [84] respectively. In case the receiver clock specification is not known, the classical value 2e-13 (for H-maser) or 5e-12 (for Caesium clock) will be used. Then the corresponding weight of the constraint $\mathrm{delt_i}$ can be estimated as:

$$W_i = \frac{\sigma^2}{{\sigma_i}^2} \tag{10}$$

where σ^2 is the a posteriori variance of the clock solution at epoch t_i which has been estimated in the original PPP.

Step 5: Re-run the PPP, adding the constraints to the receiver clocks. And the constrained receiver clock solution is obtained.

Furthermore, the constrained PPP has included two more functions: outlier recovery and multi-day constraint. Both functions can be switched on or off according to the demand.

The outlier recovery mode is on by default, and in this mode the outliers in the frequency data will be filtered out first before the estimation of the frequency parameters. Then the constraints are computed from the refined parameters, and the outliers in the constrained clock solution will be restricted and "pulled back" to stay within the normal noise level. However, the station may undergo some manual operations sometimes (for example, substituting the cable with new one which has different hardware delay), and this will cause a jump in the PPP clock solution. In this case, the outlier recovery mode will be switched off, and the constraint will not be applied around this phase jump (which will be detected by the algorithms), to make sure the constrained clock solution follows the true behaviour of the clock (actually the jump is not in the clock, but in the PPP clock solution before the new hardware delay calibration is applied).

The function of multi-day constraint is mainly used to remove the daily boundary jump and obtain a continuous multi-day PPP clock solution. The method is described as follows:

for each daily batch, besides the relative constraints, the receiver clock at the first epoch is further absolutely constrained based on the estimated clock at the last epoch of the previous batch and the increment predicted from the frequency model of the previous batch [65].

The multi-day constraint mode is off by default, as it may causes additional errors. It is recommended to switch it on to treat with some special problems which are introduced in the results section.

2.4.2 Processing and results

2.4.2.1 CCD results

The performance of constrained PPP time transfer was first estimated in the CCD experiments at ORB and INRIM. The clocks at the two stations are the H-masers, so the values of $ADEV(1s)$ were set to 2e-13 for both the PPP computations. The constraints were applied to both GPS-only and GPS + Galileo PPP, and the CCD results at ORB and INRIM are given in Figure 2-20 and 2-21 separately.

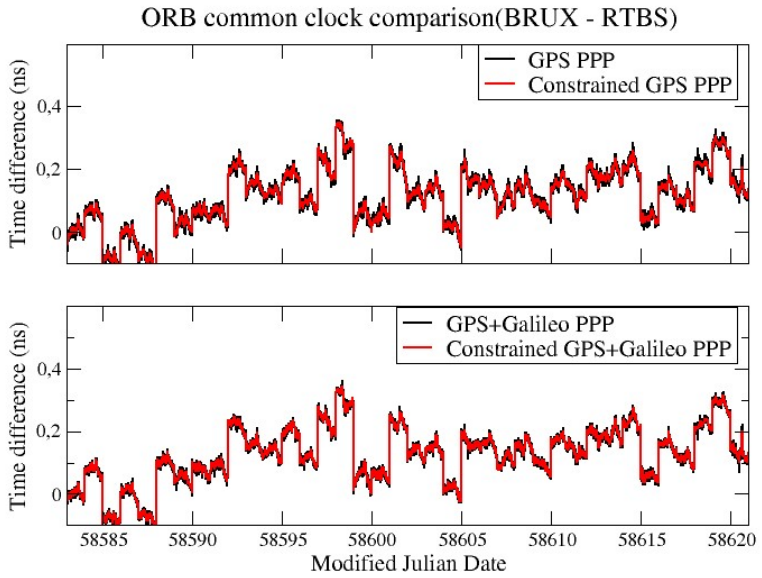

Figure 2- 20. CCD results at ORB with the constrained PPP

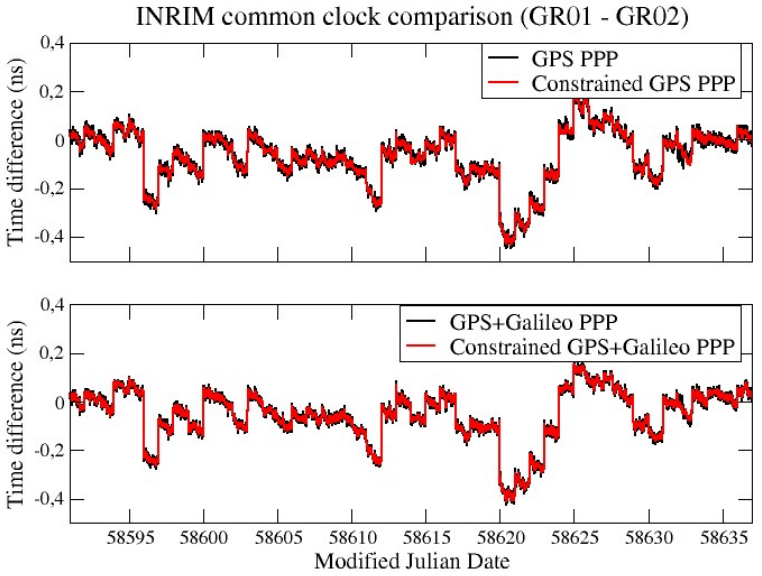

Figure 2- 21. CCD results at INRIM with the constrained PPP

It is found from Figure 2-20 and 2-21 that the constrained PPP results with both GPS and GPS + Galileo signals are aligned to the non-constrained ones. The noise of the time transfer solution was reduced by the constrained PPP inside the daily batch. Since the constrained PPP is also based on the daily PPP computation, the constrained results followed the same daily boundary jumps as appeared in the non-constrained ones.

Before further study on the constrained PPP performance, the correctness of the constrained PPP time transfer results referring to the original PPP needs to be investigated. Besides the linear frequency model that is used in constrained GPS PPP, the constraints were also estimated from an 2nd order frequency model and a wrong linear model in which the frequency parameters are increased by 50% intentionally, and these constraints were also applied to the constrained GPS PPP

to generate the CCD results at ORB during the period in Figure 2-20. The differences of the CCD results from GPS PPP and the constrained GPS PPP using these three models are plotted in Figure 2-22, in which the constrained GPS PPP with the suffix "_1st" uses linear frequency model, the one with "_2nd" uses 2nd order frequency model, and the one with "_1st*150%" uses wrongly estimated linear model. The data in Figure 2-22 are smoothed with a 5-hour sliding window just for a clearer comparison. Comparing the results in Figure 2-22 shows that linear frequency model is a proper model that could be applied to constrain the PPP clock solution with the purpose of improving the short-term stability of PPP time transfer, while making sure the constrained solution is consistent with the original PPP solution.

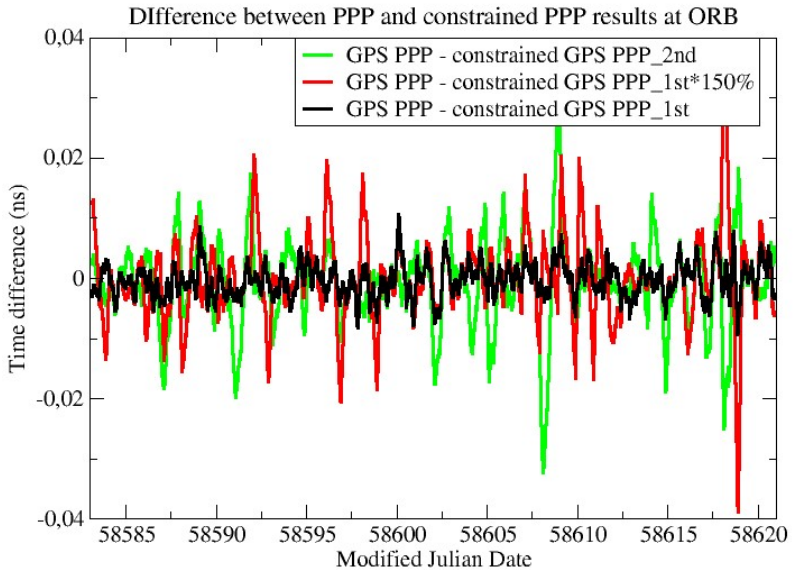

Figure 2- 22. PPP – constrained PPP with different constrained models at ORB (5-hours smoothing results)

For better comparison between the PPP and constrained PPP time transfer results, the alignment using 2nd order extrapolation was also carrier out on the data in Figure 2-20 and 2-21, and the corresponding 3-days aligned results are compared in Figure 2-23 and 2-24. The noise reduction using the constrained PPP at the short term is very clear as can be observed from the figures. A little divergence between the GPS constrained and non-constrained results at INRIM are discovered in Figure 2-24, it could be partly due to the alignment error at the border; in addition, it indicates that adding the constraints may slightly change the frequency deviations of the PPP time transfer solution, which will be studied in section 2.6 about the frequency accuracy of the PPP time transfer.

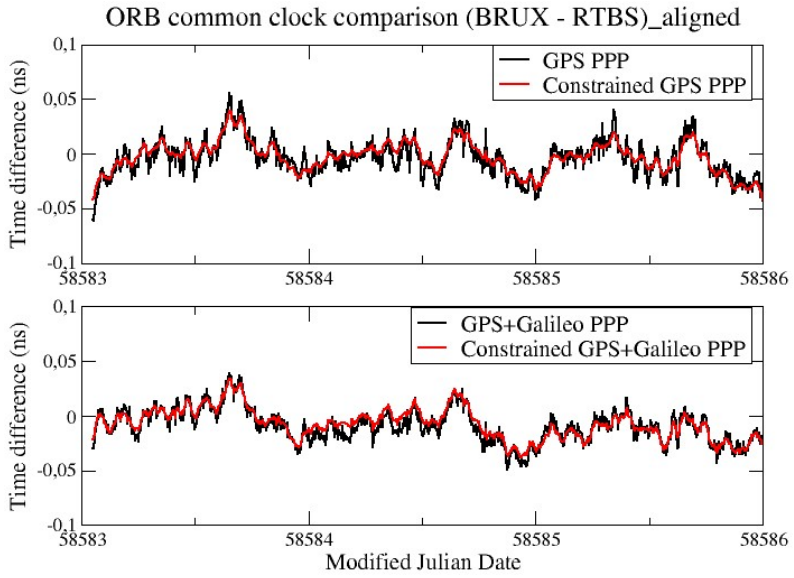

Figure 2- 23. 3-days aligned CCD results at ORB with the constrained PPP (MJD 58288 - 58280)

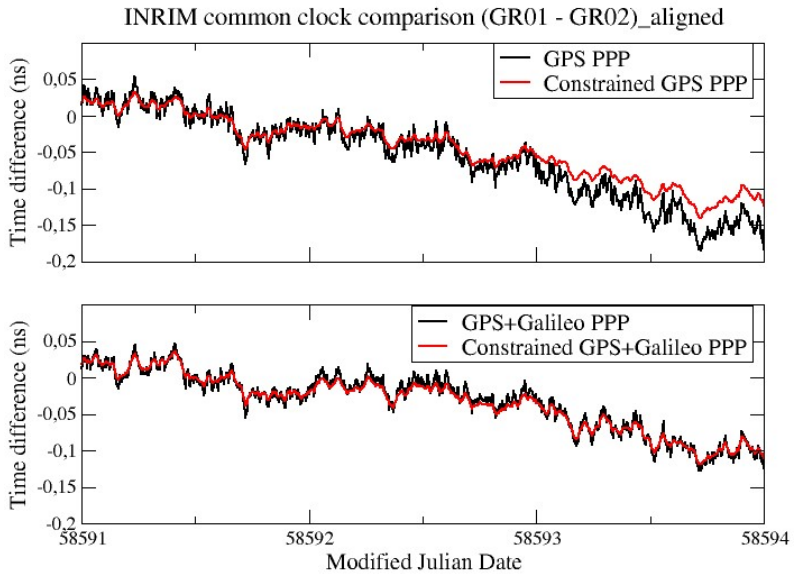

Figure 2- 24. 3-days aligned CCD results at INRIM with the constrained PPP (MJD 58591 - 58593)

In this section, only the frequency stability of the PPP time transfer solution is studied. To better conclude the improvement of the constrained PPP, the ADEVs of these PPP time transfer results (in Figure 2-23 and 2-24) are further plotted in Figure 2-25 and 2-26 respectively.

It can be discovered from the figures that the frequency stability of the time transfer solution using the constrained PPP were largely improved at short averaging times, and the amount of improvement reduced as the averaging times increased. The mean improvements at different averaging times in the two CCD experiments using the constrained PPP are reported in Table 2-1.

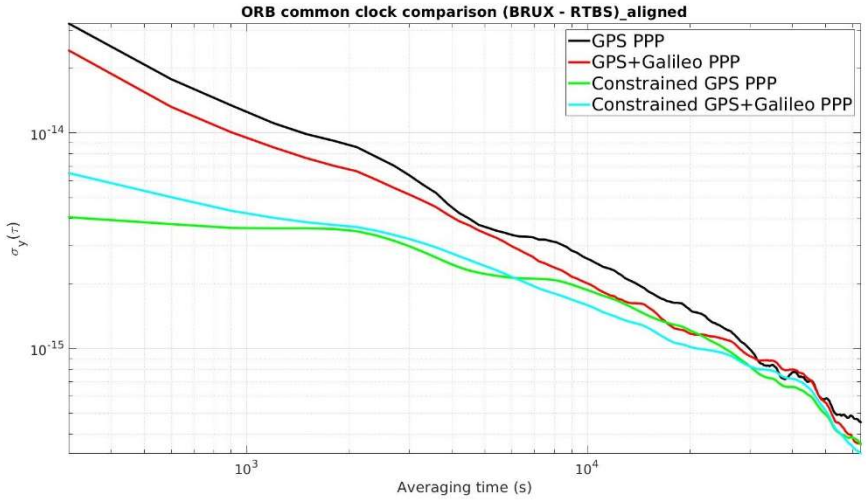

Figure 2- 25. ADEVs of the 3-days aligned CCD results at ORB

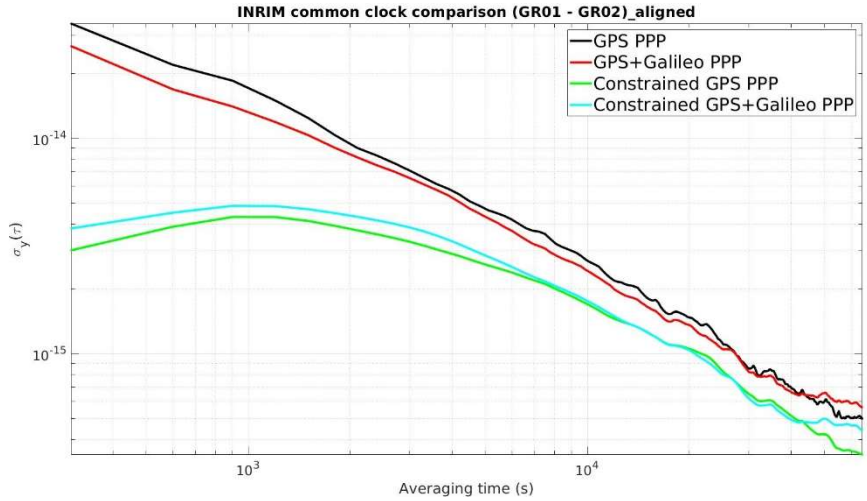

Figure 2- 26. ADEVs of the 3-days aligned CCD results at INRIM

Table 2- 1. The improvements of the frequency stability when apply constraints to the GPS PPP and GPS + Galileo PPP respectively

Averaging time	Improvement of the stability	
	GPS	GPS + Galileo
5 min	89.3%	79.4%
1 hour	50.0%	36.7%
3 hours	32.3%	23.1%
12 hours	21.1%	17.7%

From table 2-1, it is observed that improvement to the GPS-only PPP is larger at every averaging time when the constraint model is applied, compared to the GPS + Galileo results. Meanwhile, it can be found in Figure 2-25 and 2-26 that the lowest stability of the time transfer is generally provided by the constrained GPS-only PPP. The possible reason for these two phenomena is that there are

more satellite measurements in the GPS + Galileo PPP than in the GPS-only PPP at each epoch, and a single constraint with a fixed weight at that epoch will contribute more on the GPS PPP time solution than on the GPS + Galileo PPP time solution.

2.4.2.2 "PPP - OPT" results

Since the GNSS stations AO_4 and GUM4 only provides GPS observation data, only the GPS constrained PPP results were shown in the "PPP - OPT" experiments, and the IGS rapid products were used instead of the MGEX products as the input of PPP. The clocks in the two stations are also H-masers, hence the values of $ADEV(1s)$ remained as 2e-13 for both the PPP computations. Two monthly "PPP - OPT" results are selected to be plotted in Figure 2-27 for the comparison between constrained and non-constrained PPP solutions. The periods in the figure are MJD 58417-58447 (see the left plot of Figure 2-27) and the MJD 58506-58541 (see the right plot of Figure 2-27).

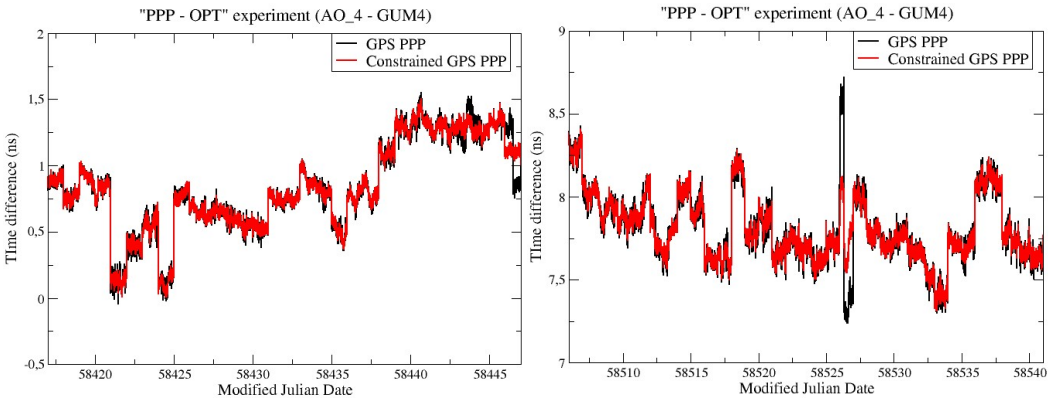

Figure 2- 27. "OPT - PPP" results using the PPP and constrained PPP during MJD 58417-58447 and 58506-58541

The first observation in Figure 2-27 is the distinct differences between the PPP and constrained PPP results during some periods, the results from one of these periods are replotted in Figure 2-28. The jump in the non-constrained PPP results was because all the satellites started with new tracks and all the carrier phase ambiguities were re-estimated at that exact moment. Most of this type of jumps happen at the daily border (daily boundary jumps), however they could also happen inside the daily batch due to the receiver problem or the PPP algorithms. As shown in Figure 2-28, the constrained PPP can overcome this discontinuity problem since the clock measurements inside the batch are all constrained relatively. And this trait of constrained PPP could also be useful to constrain the time measurements at the daily border and to obtain continuous time solution, which is the principle of multi-day constraint model that was introduced in section 2.4.1. The usage of multi-day constraint is introduced in the next subsection 2.4.2.3.

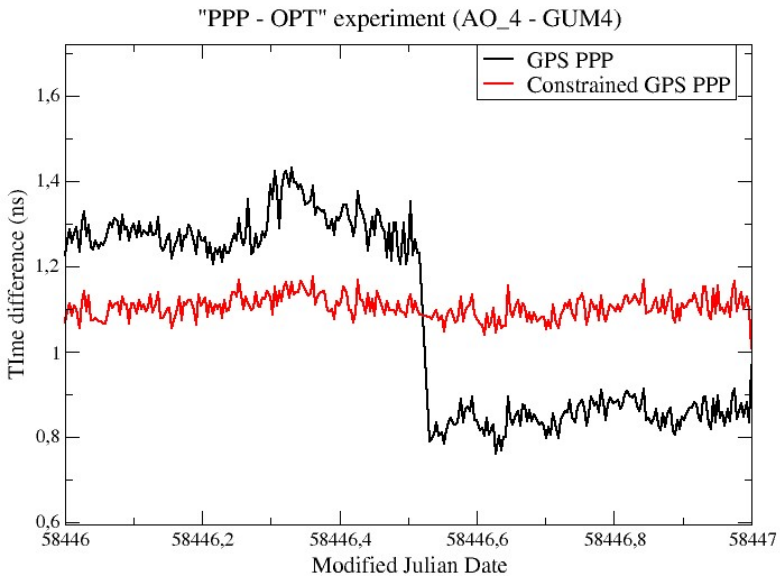

Figure 2- 28. Difference between PPP and constrained PPP results during MJD 58446

Then the ADEVs of the 5-day aligned PPP and constrained PPP results from the data in Figure 2-27 are drawn in Figure 2-29 and 2-30, corresponding to the period of MJD 58417-58421 and MJD 58506-58510 respectively.

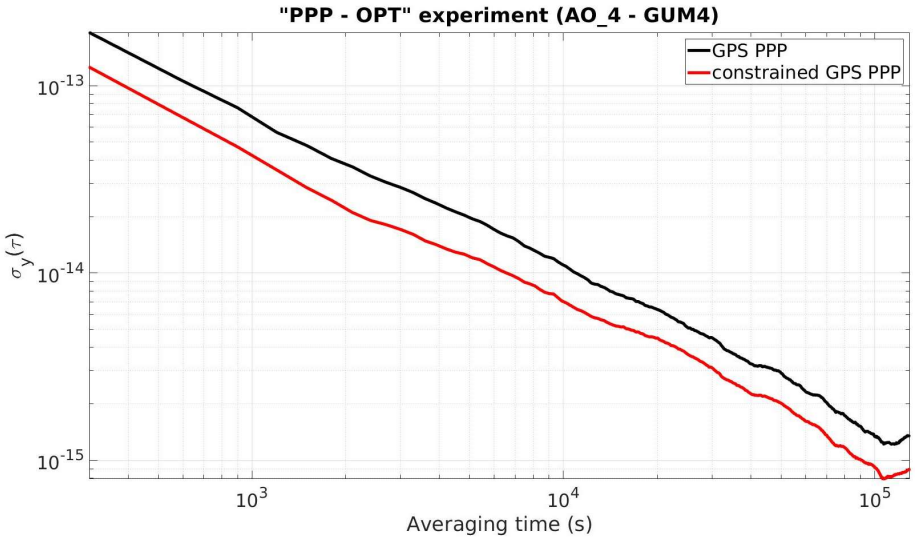

Figure 2- 29. ADEVs of the 5-days aligned PPP and constrained PPP time transfer solution during MJD 58417-58421

It can be discovered that the constrained PPP generally improves the frequency stability of the time transfer within one-day averaging; however, the improvement at the short term as can be observed in this experiment is not as much as in the former CCD experiments. The reason for this is illustrated in Figure 2-31 and 2-32.

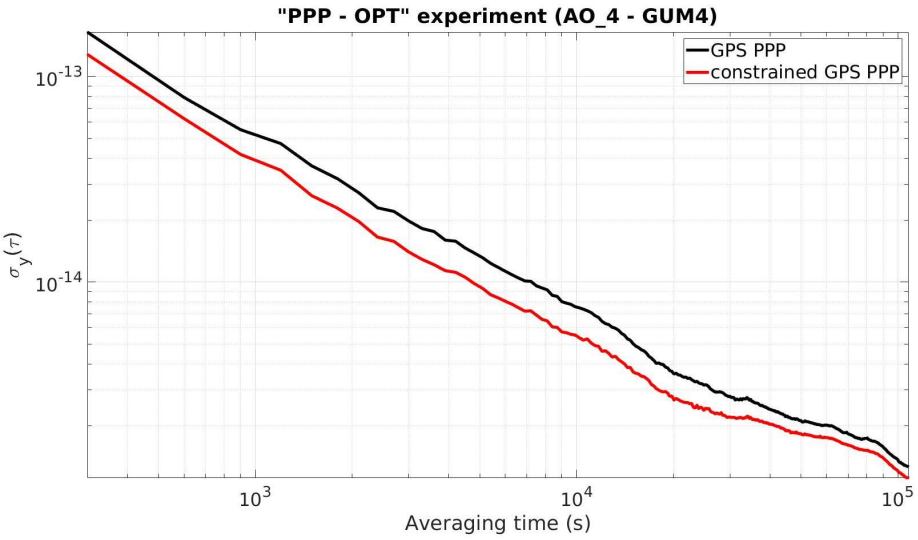

Figure 2- 30. ADEVs of the 5-days aligned PPP and constrained PPP time transfer solution during MJD 58506-58510

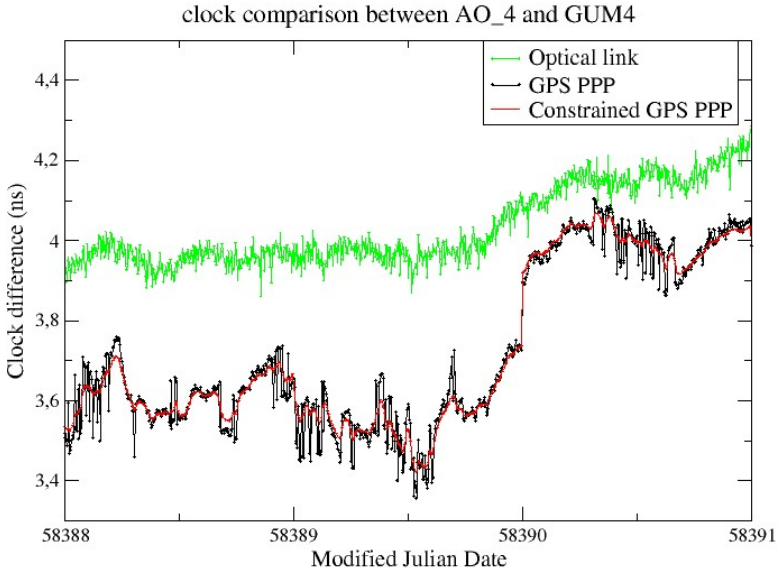

Figure 2- 31. Clock comparison between AO_4 and GUM4 using optical link and PPP

It can be discovered from Figure 2-31 that the PPP time transfer solution of "AO_4 – GUM4" has some short-term perturbations, the size of which is around 140 ps. These perturbations are present during the whole "PPP – OPT" experiment period, and the origin is probably in the GNSS receiving system of station GUM4 (personal communication from Dr. Gérard Petit at BIPM). Constrained PPP mitigates these short-term effects in the PPP time transfer solution, which can be seen in both Figure 2-31 and 2-32.

Figure 2-32 displays the frequency deviations at 5 min interval of the clock comparison results between AO_4 and GUM4 using optical link, GPS PPP and constrained GPS PPP during the whole experiment period, and the data gap in the figure represents the period when the GNSS measurements underwent some problems (reported in section 2.4.2.3).

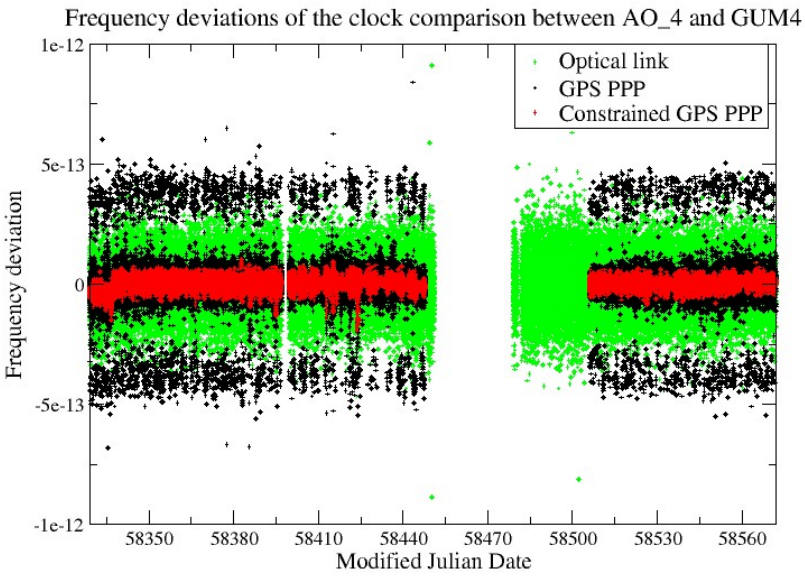

Figure 2- 32. Frequency deviations of the clock comparison results between AO_4 and GUM4

The short-term perturbations in the GPS PPP solution (black dots in Figure 2-32) are clearly visible in the frequency domain, which are represented as the black dots at around ±4.5e-13 (the corresponding size in phase domain is 4.5e-13 * 300 s = 135 ps) in the figure. Figure 2-32 demonstrates that the constrained PPP removed the effects from these short-term perturbations and also reduced the instantaneous frequency deviations in the PPP time transfer solution; Meanwhile, the improved instantaneous frequency deviations in the constrained PPP solution are also smaller than the ones in the optical link solutions (green dots), which indicates that the real improvement of constrained PPP time transfer at the short term in the "PPP - OPT" experiment as shown in Figure 2-29 and 2-30 is limited by the short-term stability of the optical link time transfer. For the sake of comparison, the ADEV of the optical link time transfer solution between AO_4 and GUM4 during a stable period is plotted in Figure 2-33.

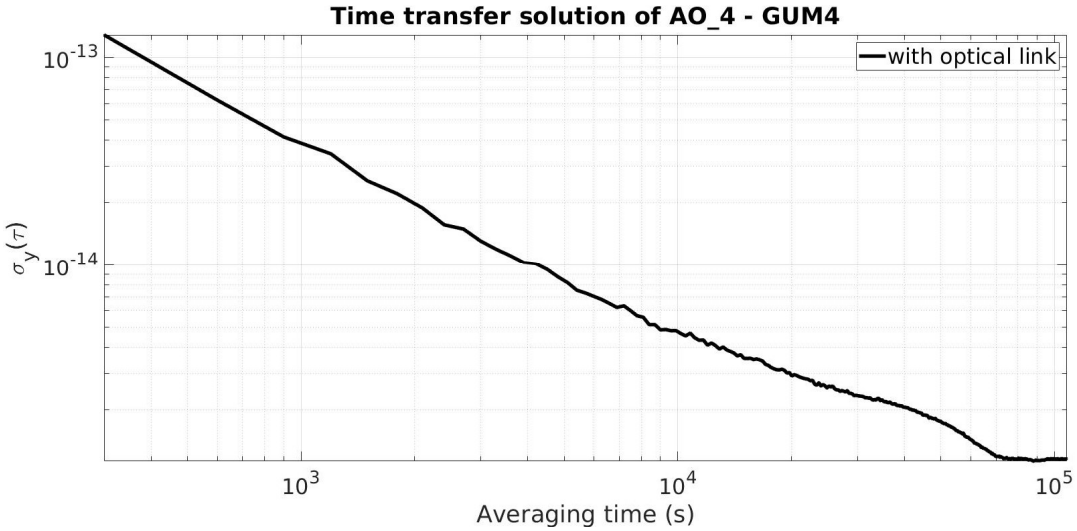

Figure 2- 33. ADEV of optical link time transfer solution of AO_4 – GUM4

Note that the actual performance of optical link solution could be better (personal communication from Dr. Gérard Petit at BIPM), here only report what is measured from the data at 5 min interval that are available on the BIPM FTP.

All the above PPP time transfer were carried out to study the performance of constrained PPP for the H-maser clock comparison. While its performance during clock comparison between a H-maser and a Caesium clock was also tested in the following experiment. As seen in Figure 2-34, the clock of station BRUX (H-maser) and the clock of station KIRU (Caesium clock) are compared during MJD 58583-58585 using PPP and constrained PPP. There is no significant difference between these two results, neither between their ADEVs, which are not plotted here. The reason is that the clock in the station KIRU is a Caesium clock, due to its own clock noise, the $ADEV(1s)$ was set to 5e-12 in the constrained PPP to reduce the weights of the constraints (see equation 10), so the clock solution won't be over constrained. As a result, the constrained PPP has minor effect on the Caesium clock solution, and the stability of the final clock comparison results between the two clocks were dominated by the Caesium clock noise.

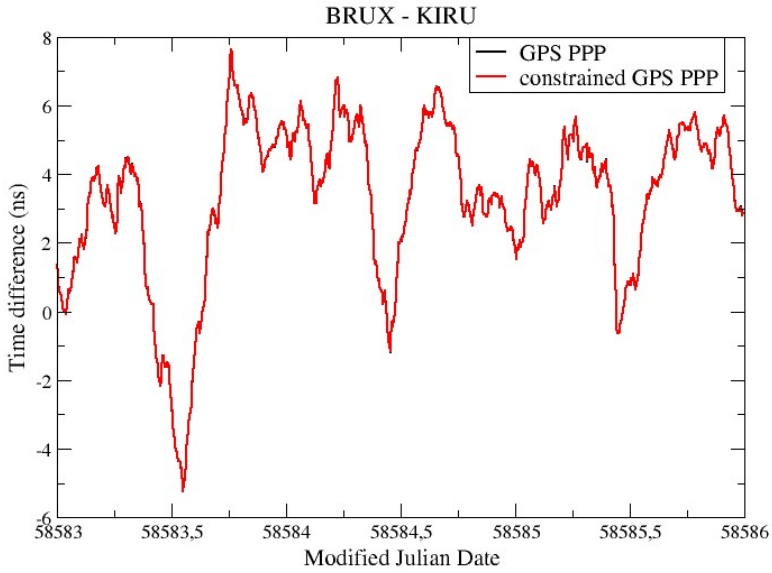

Figure 2- 34. Clock comparison between BRUX and KIRU using PPP and constrained PPP

2.4.2.3 More results about Constrained PPP

As already discussed in subsection 2.4.2.2, constrained PPP can be used to restrict the discontinuity in the PPP time solution. The multi-day constraint is a function to constrain the clock measurement change at the daily border in order to obtain a multi-day continuous time solution. As shown in Figure 2-35, the multi-day constrained PPP well removed the boundary jumps and aligned the daily solutions in the CCD experiment at ORB compared to the original PPP results.

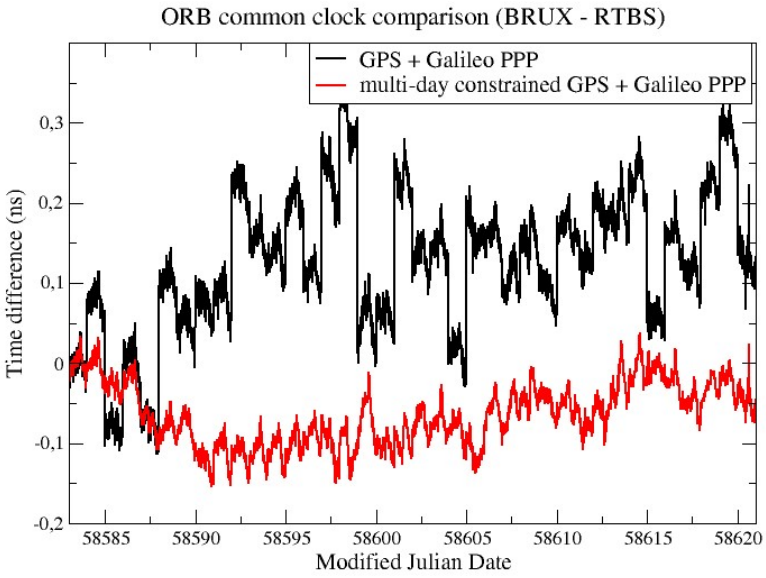

Figure 2- 35. The PPP and multi-day constrained PPP time transfer

Though better stability of time transfer solution can be obtained at longer term by using multi-day constraint, additional noises were also introduced to the time transfer measurements within the daily batch. The main reason is that the current version of multi-day constrained PPP only constrain the clock measurements at the daily border according to the real clock change, ignoring the discontinuity of the IGS clock products. In fact, the IGS products are also generated based on daily measurements, hence its clock products may also have daily boundary jumps. A more correct way to align the daily PPP time measurements is to consider the discontinuity of the clock products, besides the receiver clock change. The new version of multi-day constrained PPP will be developed and studied in future work. In the dissertation the multi-day constrained PPP time transfer solution is only used as a tool to further check the correctness of constraint model that is applied to the clock measurements, and the details can be found in the following part of this subsection, which introduces the application of constrained PPP to the noisy PPP clock measurements.

It was found that at the station GUM4 the receiver clock measurements from PPP were very noisy for about two months during the “PPP - OPT” experiment. The problem was fixed after some modifications in its receiver have been observed. Since these extreme noises were only present in the PPP solution (see Figure 2-36), the origin of this problem was probably in the GNSS receiver at GUM4.

In order to reduce the noise of the PPP clock solution at GUM4, constrained PPP was used, with its outlier recovery mode on. Figure 2-37 displays the receiver clock offsets with respect to the IGS reference time in GUM4, which are estimated by the constrained PPP and the original non-constrained PPP during the period.

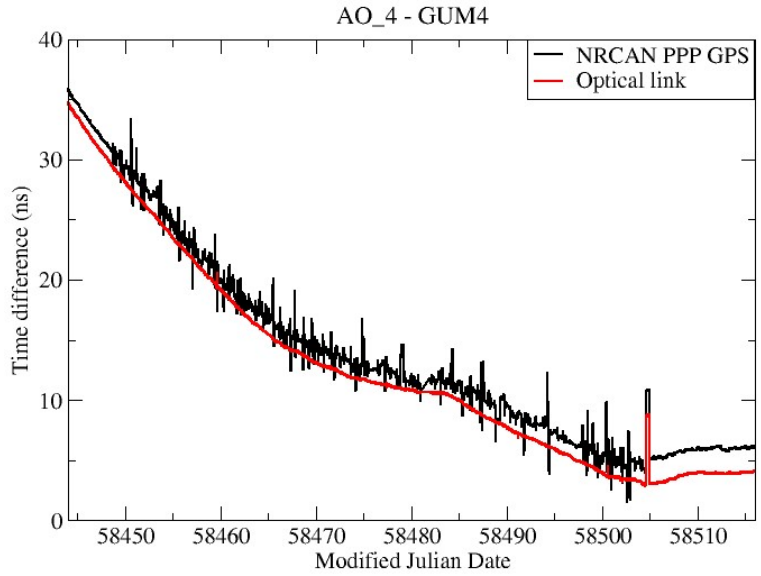

Figure 2- 36. Clock comparison between AO_4 and GUM4 via PPP and optical fibre

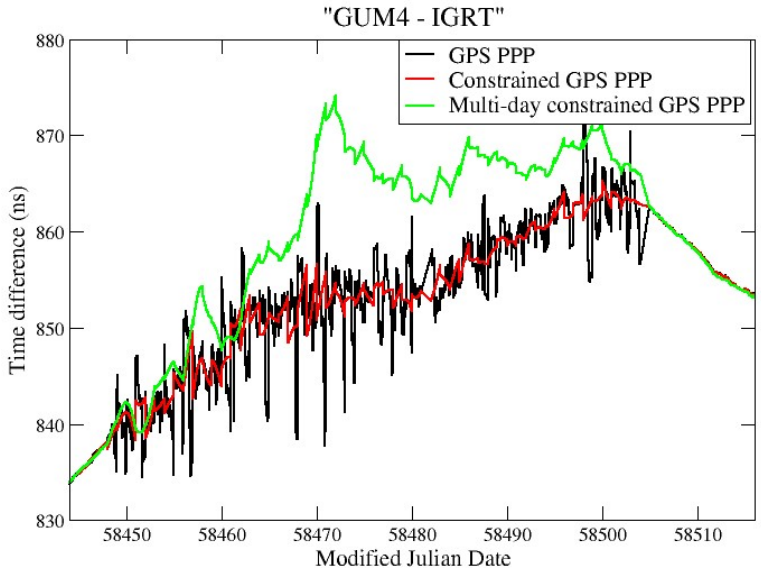

Figure 2- 37. Noise reduction in the clock measurements using the constrained PPP

Figure 2-37 shows that the constrained PPP reduces the noise in the receiver clock measurements compared to the non-constrained PPP results during the problematic period. However, the constraint model in the constrained PPP were estimated with high uncertainties from the extremely noisy clock measurements, as a result, the multi-day constrained PPP results showed great divergence compared to both the original PPP and constrained PPP results. It is expected that if more correct constraint models could be estimated, the constrained PPP and multi-day constrained PPP would further reduce the noise in the PPP clock solution and their results would not diverge from each other. In order to validate the consumption, more accurate frequency deviation measurements of "GUM4 –

IGRT" ($Frq_{GUM4-IGRT}$) are needed for the estimation of the constrained model, and the following strategy was applied for this purpose:
the idea was to re-estimate the frequency deviations of "GUM4 – IGRT" ($Frq_{GUM4-IGRT}$) using external frequency measurements. For example, by combing the Frq_{AO_4-IGRT} that were estimated from PPP solution and the Frq_{AO_4-GUM4} that were estimated from the clock comparison using another reliable technique. There are many other techniques that are used for accurate time transfer, such as the optical fibre link, TWSTFT and T2L2 [85]. In this case, the available clock comparison results between AO_4 and GUM4 using optical fibre link were taken to estimate the Frq_{AO_4-GUM4}. Then $Frq_{GUM4-IGRT}$ was estimated as the difference of Frq_{AO_4-IGRT} and Frq_{AO_4-GUM4} at every 5 min interval.

Finally, the frequency parameters were computed from these refined frequency measurements and were used to build the constraint to constrain the receiver clock at GUM4. In Figure 2-38, the constrained PPP clock solution at GUM4 using the re-estimated constraints (in red line) is compared with the original non-constrained solution (in black line) and the related multi-day constrained PPP clock solution.

The noise in the clock solution was highly reduced by using the constrained PPP with the re-estimated constraints (in red) as can be seen in Figure 2-38. However, the daily boundary jumps in the constrained clock solution were very large (up to 5 ns) due to the noisy measurements. By using the multi-day constrained PPP, a more stable PPP time solution at GUM4 during the problematic period was obtained.

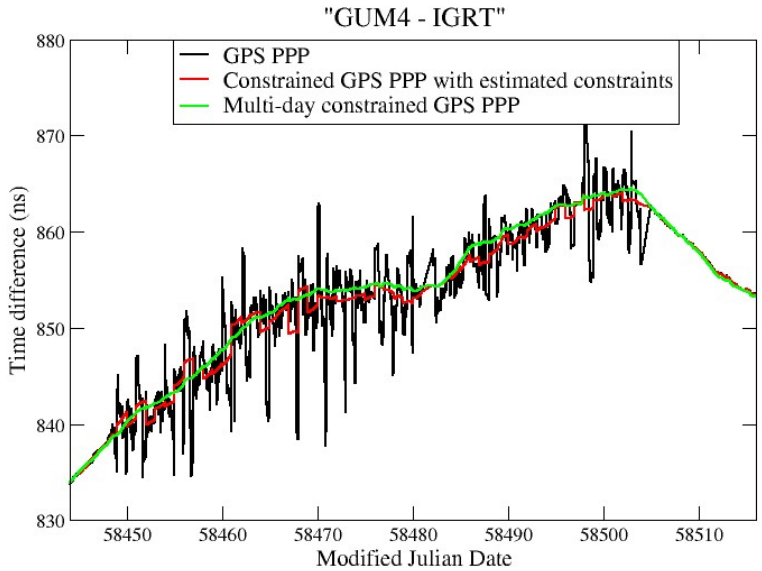

Figure 2- 38. Constrained PPP solutions with the re-estimated constraints

The previous experiment indicated that, if the constraint models could be estimated correctly, the constrained PPP would reduce the noise of the clock solution efficiently in the noisy environment; meanwhile, the multi-day constrained PPP could be used to produce a more stable clock solution in case the size of the daily boundary jump has high impact on the continuity of the daily

solution; in addition, if the constraint models are correct, both the constrained and multi-day constrained PPP clock solution will stay aligned to each other at long term.

However, it is not significative in practice to retrieve "good" PPP clock solution using other already existing solutions of that clock. Therefore, it is necessary to estimate the PPP constraint models using its own GNSS data. The reason for the noisy PPP clock solution of GUM4 is that the receiver of the station lost the track of satellites more frequently during the problematic period, which caused a lot of cycle slips in the carrier phase measurements during the satellite tracks, therefore, much more carrier phase ambiguities had to be fixed in the least square computation of PPP, and as a result, the more noisy PPP clock solution was generated.

One way to remove the effect of the cycle slip problem to the carrier phase measurement is to calculate the relative change of the carrier phase measurements, since the abnormal change at the epoch when the cycle slips happened can be easily removed by a filter. The relative change can be expressed as

$$dL_{IF} = L_{IF}^{i+1} - L_{IF}^{i} \tag{11}$$

where L_{IF}^{i+1} and L_{IF}^{i} are the carrier phase measurement from one satellite at the epoch i+1 and i respectively, and dL_{IF} is the relative change of the carrier phase measurements between these two adjacent epochs. According to equation (3), equation (11) can be re-expressed as

$$\begin{aligned} dL_{IF} = {} & dR + c \cdot dT_S + dTropo_{dry} \\ & + \left(mf^{i+1} \cdot zpd^{i+1} - mf^{i} \cdot zpd^{i}\right) + c \cdot dT^R \end{aligned} \tag{12}$$

where the relative change of geometric distance (dR), satellite clock offset (dT_S) and the dry tropospheric delay ($dTropo_{dry}$) can be computed by using the IGS products and code measurements, the unknowns are the zpd at each epoch and dT^R, which is the relative change of the receiver clock offset (the time deviation). The quantity dT^R is exactly what we need to compute the frequency deviation of the receiver clock, referring to equation (5). It should be note that, to compute the geometric distance in equation (12), the antenna position of the station is needed as an input, this position can be obtained from the PPP running on the same day, or on another day in case the measurements of the current day are too noisy.

The zpds and the relative changes of the receiver clock time deviation can be solved in least square computation, which was explained in [52]. However, by the time when this dissertation was finished, the related least square algorithms haven not been well developed, and the zpds were not correctly estimated. Therefore, an alternative method was chosen in order to solve the equation (12): first, the zpds during the days when there was no GNSS measurement problems are computed directly by PPP, and the zpds during the problematic period are estimated out of the computed zpds in the previous days by linear extrapolation; then the relative changes of the time deviation are obtained from equation (12) and used to compute the related frequency deviations, which are used to estimate the constraint model in the constrained PPP. Figure 2-39 displays the frequency deviations of the receiver clock offsets that were estimated in the GPS PPP and

the frequency deviations estimated by the carrier phase measurements using equation (12), and it can be observed that the noise in the frequency data has been largely reduced by using the carrier phase measurements during the problematic period. The clock solutions of GUM4 by using the PPP and the constrained PPP with the refined constraints that were estimated from the carrier phase measurements are plotted in Figure 2-40.

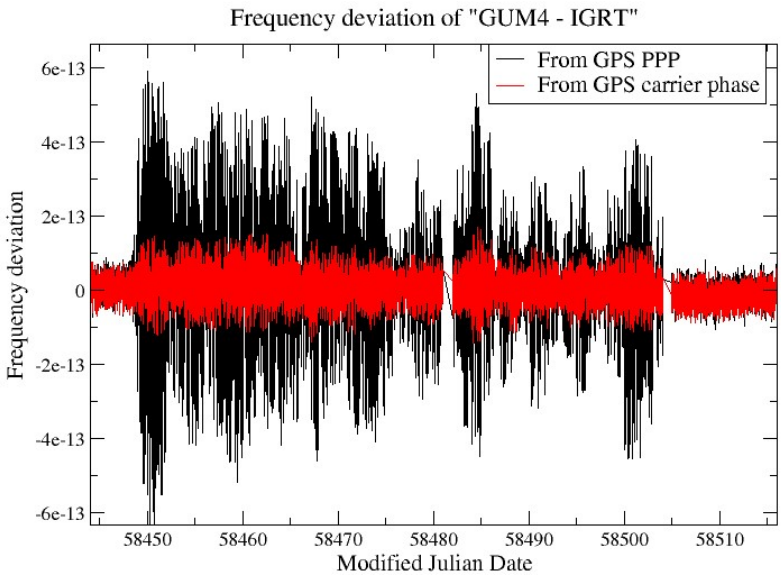

Figure 2- 39. Frequency deviations of GUM4 clock estimated by PPP and carrier phase measurements

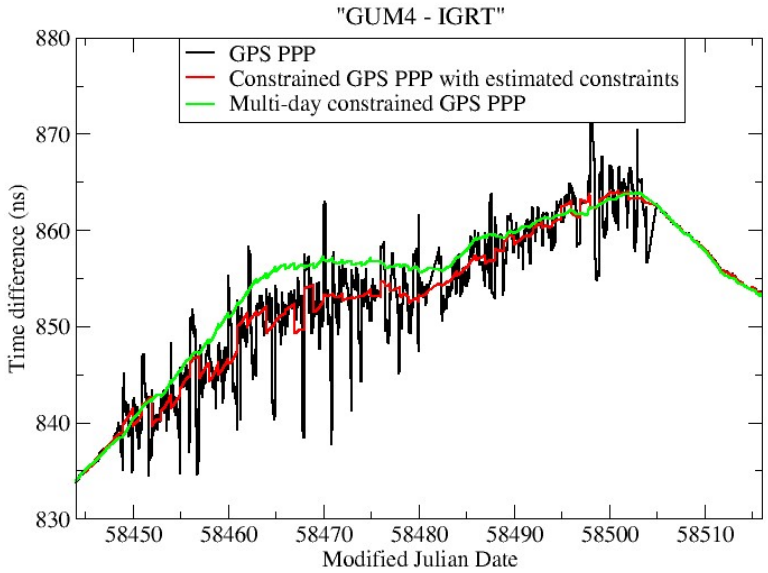

Figure 2- 40. Constrained PPP solutions with the re-estimated constraints using carrier phase measurements

As shown in Figure 2-40, with the constraints estimated from the carrier phase measurements, the constrained PPP clock solution of GUM4 (the red lines) shows very similar trend to the one in Figure 2-38 and both have the similar size of daily boundary jump. However, since the zpd s in equation (12) were not well

computed but estimated by extrapolation, the estimated constraints were still not accurate enough, and this inaccuracy caused slightly increased noise in the daily clock solution and the divergence of the multi-day constrained results (the green lines in Figure 2-40). The more correct method (least square) to solve the equation (12) will be developed in future work, and the application of constrained PPP in the noisy environment and the advantage of using carrier phase measurements for the constraint model estimation will be concluded.

2.4.3 Discussions

The results of the constrained PPP experiments suggest that: 1. constrained PPP could be used to further improve short-term stability of PPP time transfer between H-masers, but it has little effect on the clock solution of Caesium clock or other clocks which are with worse quality; 2. constrained PPP can be used to overcome the discontinuity problem inside daily batch due to the loss of track in the receiver; 3. with the well-estimated constraint model, constrained PPP can reduce the noise of the clock solution efficiently when the measurements are very noisy; 4. carrier phase measurement has its advantage for the constraint model estimation in constrained PPP, however, the related algorithms still need to be developed to have a better performance; 5. constrained PPP, with the multi-day constraint function switched on, can be used to obtain continuous time solution by removing the daily boundary jump, this function needs to be upgraded to considering the daily discontinuity of the IGS clock products, and before the upgrade, this function is only used to check the correctness of the estimated constraint model.

2.5 Atomium Integer PPP

Integer PPP is the PPP that fixes the carrier phase ambiguities as integers during the computation. The integer nature of the carrier phase ambiguities in the classic PPP (such as the NRCAN PPP and the old version of Atomium PPP) is ignored, and the float values are estimated with the help of the code measurements. It was shown in [71] that the stability of the GNSS time transfer is improved by using the carrier phase measurements with integer ambiguity resolution, and the random walk noise with the origin in the float ambiguity estimation is also eliminated. In [86] a new method for the integer ambiguity resolution on the un-differenced carrier phase measurements was introduced, and the related PPP had a precision of centimetre level.

Currently, the GNSS integer satellite products (called GRG products) from the CNES/CLS (CNES for short) IGS analysis center are available on the IGS FTP for the single receiver users to perform the integer PPP time transfer [87]. Both the GPS and Galileo integer products are provided by CNES, but the Galileo product is not regularly available by the time when the software have been developed (March 2019). Therefore, the current version of Atomium integer PPP

is only based on the GPS measurements. The general term "integer PPP time transfer" is used to express the clock comparison in the phase domain by using integer PPP.

2.5.1 Developed algorithms

The GRG products from CNES include the estimations of the satellite clock, the satellite orbit, the earth rotation parameters (ERP) and the satellite wide-lane biases (WSB). There are mainly three steps to compute the integer PPP clock solution with the GRG products: 1. Resolve the wide-lane (WL) integer ambiguity; 2. Resolve the narrow-lane (NL) integer ambiguity; 3. Compute the final integer solution. These steps were previously described in the paper [65].

Step 1: WL integer ambiguity. The Melbourne-Wubbena (MW) combination is built at each epoch using the phase and code measurements for each GPS satellite, which is expressed as:

$$\mathrm{MW} = (\alpha_{\mathrm{WL}}\mathrm{L1} - \beta_{\mathrm{WL}}\mathrm{L2}) - (\alpha_{\mathrm{NL}}\mathrm{P1} + \beta_{\mathrm{NL}}\mathrm{P2}) \quad (13)$$

where (L1, L2) and (P1, P2) represent the carrier phase measurements and the P (or P(Y)) code measurements on L1 and L2 band separately, $(\alpha_{WL}, \beta_{WL})$ and $(\alpha_{NL}, \beta_{NL})$ are the coefficients in front of the related measurements for the MW combination. The equation (8) can be re-expressed as:

$$\frac{\mathrm{MW}}{\lambda_{\mathrm{WL}}} = \mathrm{N_{WL}} + \mathrm{WRB} - \mathrm{WSB} \quad (14)$$

where λ_{WL} is the WL wavelength (in meter), $\mathrm{N_{WL}}$ is the integer ambiguity in the WL combination (in cycle), WRB is the WL receiver bias, and WSB is the WL satellite bias that is provided by the GRG products.

After correcting the WSB using the GRG WSB products, the real-valued $\mathrm{N_{WL}}$ and WRB are estimated by each satellite track and each epoch separately using the linear least square method. To avoid the singularity, the WRBs are constrained to make sure their estimated values are continuous and stay within the 0 to 1 WL cycle during the first day estimation. The current strategy of constraining the WRBs in the software is: In the first iteration, the WRBs are absolutely constrained to the mean of the WRBs that have been estimated from the previous day, or to 0.5 WL cycle if it's first day estimation, and in the second iteration, the estimated WRBs from the first iteration are used to constrain the WRBs; in addition, to ensure the continuity of the estimated WRBs, a relative constraint is also applied to constrain the relative change between the adjacent WRBs. After the second iteration, both float N_{WL} and WRBs are computed. Passing though the bootstrapped estimator [88], the N_{WL} are all decorrelated from each other, and then most of their values are already close enough to some integer values, then these N_{WL} are fixed to their closest integers for each satellite track. WRBs are solved as the remaining fractional WL cycles in equation (14) at each epoch.

During the decorrelation between the ambiguities in the GNSS bootstrapping method, the predicted probability of the success of each ambiguity resolution is also estimated, which is called the success rate [88]. In this step of the software, there are two conditions that need to be fulfilled before fixing the $\mathrm{N_{WL}}$ to an

integer: the corresponding success rate is over 90% and the real value of that N_{WL} is not too far from an integer (smaller than 0.25 WL cycle). The tracks with not fixed N_{WL} will be excluded in the following computations. The key for this step is to have a continuous WRB estimation avoiding the 1 cycle estimation error inside the daily batch and at the daily border. To make sure the coherent estimation of WRB in the multi-day solution, the mean value of the estimated WRB in the previous day is chosen as the absolute constraint for the WRB estimation of the current day.

Step 2: the GPS ionosphere free (IF) code and carrier phase combinations are re-expressed as:

$$P_{IF} = \rho + T^R + \mathrm{zpd} + \mathrm{e} + \varepsilon_P \tag{15}$$

$$L_{IF} = \rho + T^R + \mathrm{mf} \cdot \mathrm{zpd} + \lambda_{NL}\left(N_1 + \left(\frac{\lambda_{WL}}{\lambda_2}\right)N_{WL}\right) + \mathrm{W} + \mathrm{e} + \varepsilon_L \tag{16}$$

where P_{IF} and L_{IF} are the code and carrier phase IF combinations, ρ is the distance between satellite and receiver phase center, T^R is the receiver clock offset, zpd is the wet tropospheric zenith path delay, mf is the mapping function, W is the wind-up effect to be corrected, e is the other common errors between code and phase measurements (e.g. troposphere dry component delay, relativistic effect, satellite clock error), ε_P and ε_L are the code and phase noises, λ_{NL} is the NL wavelength, N_1 is the integer ambiguity to be resolved, and N_{WL} is the WL integer ambiguity that has already been fixed in step 1. Since $\lambda_{NL} = 17\lambda_{IF}$ = 10.7 cm, it is much easier to resolve the integer ambiguity in equation (16). One real-valued N_1 is computed per satellite track combining the equation (15) and (16) in the least square computation, and the integer value of N_1 is determined using the same strategy as fixing the WL ambiguities in step 1, that is: fixing N_1 to the closest integer of the decorrelated ambiguity, as long as the related success rate is over 90% and the distance between the float N_1 and the closest integer is smaller than 0.25. The satellite track without fixed integer N_1 will be filtered out.

Step 3: At this step the two ambiguities in equation (16) have already been fixed to integers, and the equation (16) can be re-expressed as:

$$L_{IF} - \lambda_{NL}\left(N_1 + \left(\frac{\lambda_{WL}}{\lambda_2}\right)N_{WL}\right) - \mathrm{W} - \mathrm{e} = \rho + T^R + \mathrm{mf} \cdot \mathrm{zpd} + \varepsilon_L \tag{17}$$

with the already estimated variables on the left and the unknowns on the right, which include the receiver position (in ρ), the receiver clock offset and the wet tropospheric zpd. The wind-up corrections (W) have been computed in step 2 together with the ambiguities.

Since now the IF carrier phase measurements are not ambiguous anymore. They are used to estimate the final PPP solutions in the least square without the IF code measurements.

If the WRB estimations are coherent (without WL cycles jump) during the whole period and the ambiguities are resolved correctly at both stations, the sizes of the discontinuities at the daily borders (or inside the daily batch) for the integer PPP time transfer solution are the integer multiple of the λ_{NL}, therefore the continuous solution for multiple days can be easily obtained by alignment.

However, if the discontinuity is caused by any hardware change in the receiving chain of the station, the same alignment strategy may not work anymore. Since the real values of WRB have changed since that moment, constraining the WRB estimation will push the integer cycle estimation error in the N_{WL} in equation (14) and cause a bias of integer multiple of $\lambda_{NL}(\lambda_{WL}/\lambda_2)N_{WL}$ in the clock solution as can be seen in equation (17).

2.5.2 Processing and results

2.5.2.1 WRB estimation

As explained previously, before using the integer PPP clock solution, the continuity of the estimated WRBs need to be checked first. As illustrated in Figure 2-41, when hardware change (or problems) happens in the station AO_4, it will be manifested in the estimated WRBs as a jump. The jump will introduce a discontinuity in the integer PPP clock solution which could not be compensated by integer multiple of λ_{NL}. Additionally, since the estimation of WRBs are constrained in the integer PPP, when an unexpected WRB jump happens, some correct measurements might be filtered out as outliers, which might increase the noise of the final clock solution on that day. Note that the higher variation of the estimated WRBs in the station GUM4 was not caused by any hardware change, it was probably due to some diurnal effects to that station (multipath, temperature variation etc.).

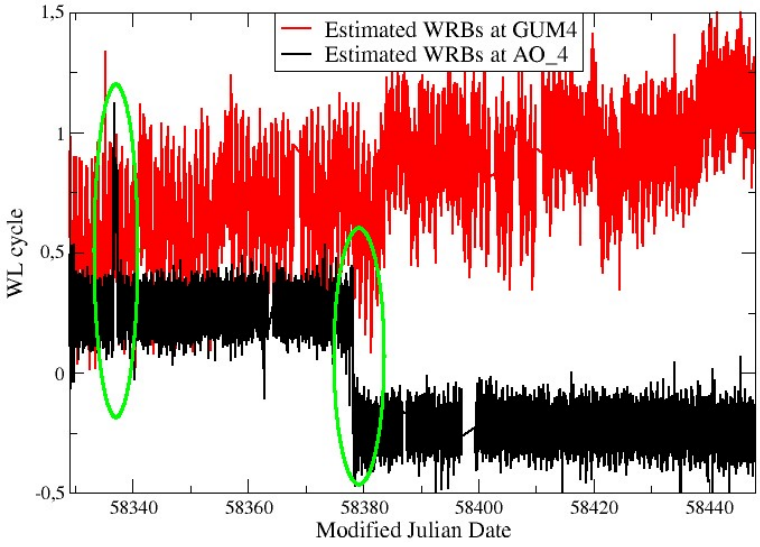

Figure 2- 41. Hardware change in the station AO_4

In addition, the continuous WRB estimation is not always guaranteed in the current version of integer PPP software. As shown in Figure 2-42, in the first two days computation, the software failed to constrain the WRBs which are around 0.5 WL cycle, and the estimated values jumped by 1 WL cycle in the middle of the days. This 1-cycle estimation error rarely happened (2 to 3 times in the whole 22 months experimental period). The software will be updated to conquer this problem in future work.

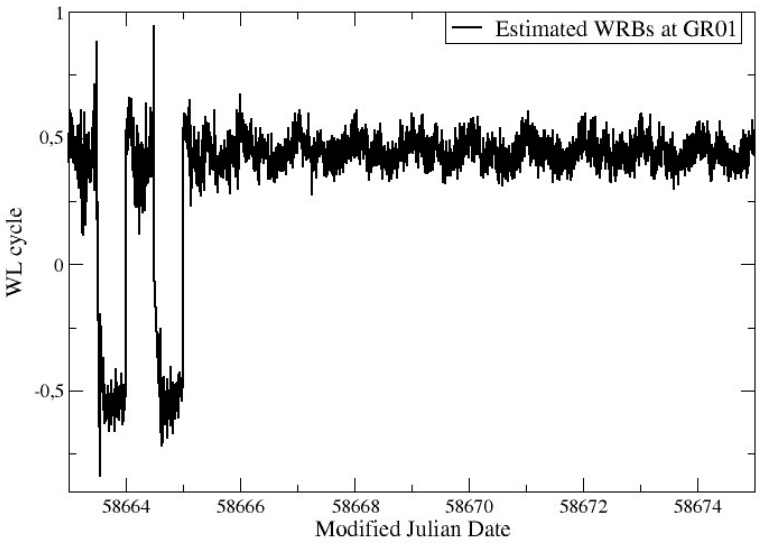

Figure 2- 42. The software failed to estimate the continuous WRBs

Since this discontinuity problem in integer PPP solution is not compensated easily as in the float PPP, in the phase domain only the clock comparison results using integer and float PPP during the period when the WRBs of the stations are continuous are compared in the following part of section 2.5.2.

2.5.2.2 CCD results

In the CCD experiments at ORB and INRIM, the fixing rates of the ambiguities in step 1 and 2 of the integer PPP are normally over 90% and 95% respectively during all the experimental periods.

Figure 2-43 demonstrates an ideal situation of the WRB estimations in the CCD experiment at ORB. Since the multipath mitigation option is off in the station RTBS, the estimated WRBs in RTBS has a larger daily variation, as can be seen in the figure.

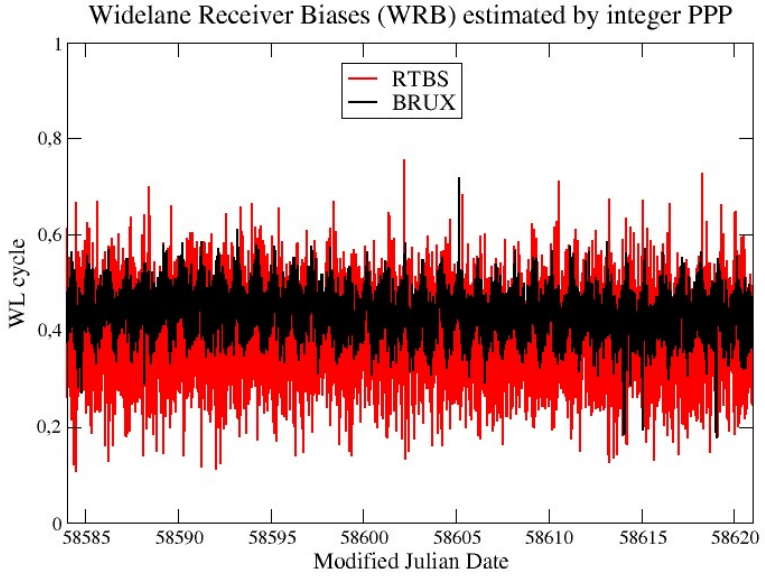

Figure 2- 43. WRB estimation in the ORB CCD experiment

The corresponding integer PPP time transfer solution in this CCD experiment is then displayed in Figure 2-44. The red lines in Figure 2-44 are the original integer PPP time transfer solution with the discontinuity at the daily border. The sizes of these discontinuities and the shifted sizes for the alignment are summarized in Table 2-2. The aligned integer PPP results are drawn in black lines in Figure 2-44.

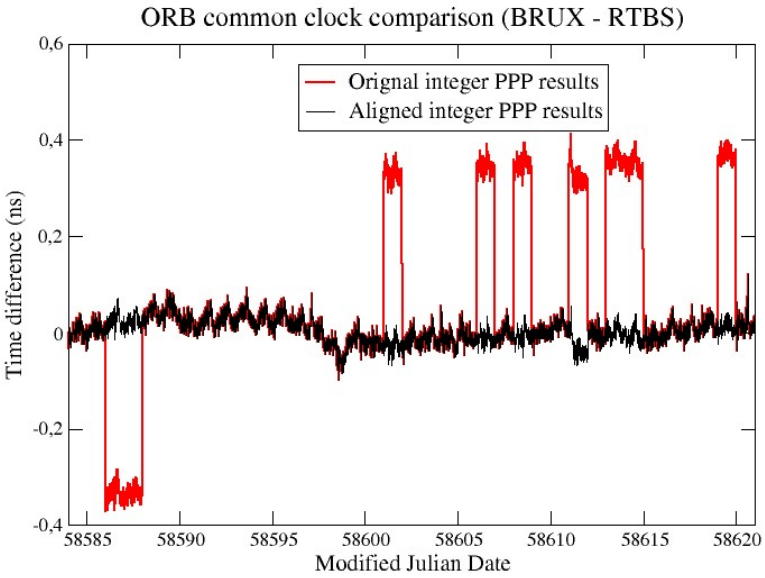

Figure 2- 44. CCD experiments at ORB with integer PPP

Table 2- 2. The discontinuities of the integer PPP time transfer solution

MJD	size in λ_{NL} cycle		MJD	size in λ_{NL} cycle	
	Discontinuities	Actual shift		Discontinuities	Actual shift
58585	-0.09	0	58603	-0.06	0
58586	-1.05	-1	58604	-0.03	0
58587	-0.02	0	58605	0.02	0
58588	1.01	1	58606	0.98	1
58589	0.02	0	58607	-1.02	-1
58590	-0.02	0	58608	1.05	1
58591	0.06	0	58609	-0.97	-1
58592	-0.01	0	58610	0.05	0
58593	-0.04	0	58611	0.91	1
58594	-0.00	0	58612	-0.87	-1
58595	0.04	0	58613	1.05	1
58596	-0.01	0	58614	-0.02	0
58597	-0.03	0	58615	-1.03	-1
58598	-0.07	0	58616	0.02	0
58599	0.03	0	58617	-0.06	0
58600	-0.08	0	58618	0.05	0
58601	0.94	1	58619	0.98	1
58602	-1.03	-1	58620	-0.99	-1

To evaluate the performance of the integer PPP time transfer, its continuous results (simply called integer PPP results hereafter) are compared with the results from the original Atomium PPP which estimates the float ambiguities (called float PPP for the simplicity) as shown in Figure 2-45. Meanwhile, two continuous float PPP results are also plotted in the same figure for the comparison, which are aligned PPP results (in green) and multi-day constrained PPP results (in blue).

The alignment of the float PPP daily results ignored the integer λ_{NL} cycle, only simply aligned the daily results at the border using the 2nd order extrapolation.

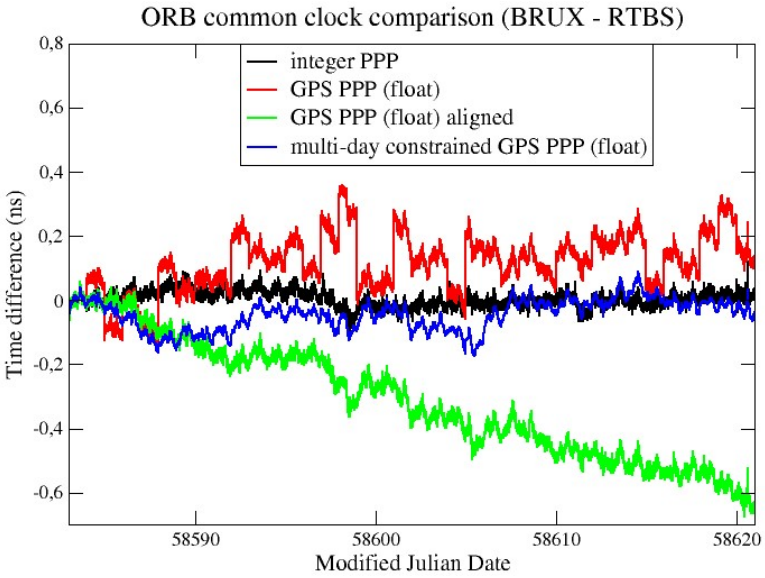

Figure 2- 45. CCD experiments at ORB with integer PPP and float PPP

The integer PPP time transfer solution showed great improvement of the stability compared to the float PPP solutions, as can be observed in Figure 2-45. The long-term stability of the float PPP time transfer was mainly contaminated by the daily boundary jump. Aligning the discontinuous float results improved the stability, but it caused an accumulation of error (0.6 ns in a month). Using the multi-day constraint function to obtain the continuous float PPP solution relatively reduced the accumulated errors compared the aligned float PPP results, however, additional noises are introduced inside the daily results since the algorithms still need to be upgraded to consider the discontinuity of the IGS clock products (see section 2.4.2).

The results in Figure 2-45 are further compared in the form of ADEVs as shown in Figure 2-46.

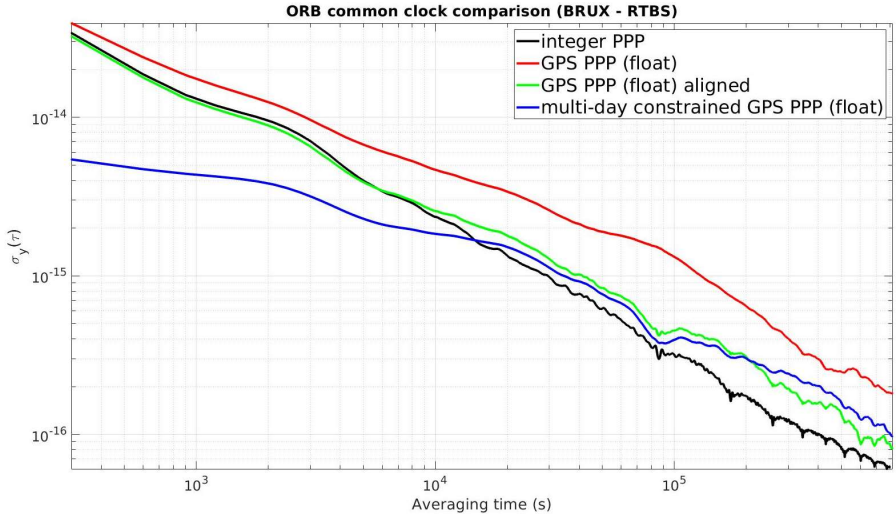

Figure 2- 46. ADEVs of the integer and float PPP time transfer solution in the ORB CCD experiment

It can be found in Figure 2-46 that the integer PPP improved the stability of the time transfer at all time span compared to the float PPP. The two continuous float PPP results (in green and blue) had comparable/better short-term stability, but the long-term stability was still worse than the one of the integer results. Comparing between the integer PPP and aligned float PPP results indicates that, the short-term stability of the time transfer doesn't improved by using integer PPP instead of float PPP, the worse estimated stability of the float PPP time transfer (in red lines) at the short term is mainly due to the effect of the daily boundary jump on the estimation. In this experiment, with 4 days averaging on the integer PPP time transfer solution, the 10^{-16} frequency stability could be achieved.

Since the algorithms of the multi-day constrained PPP is still not complete, its results are not present in the following comparison. In addition, the monthly (or longer period) results are used in this section for the study of long-term stability of PPP time transfer solution, the aligned results are not included in the following comparisons, since the alignment may introduce additional variations in the long term. An example of the additional alignment error can be observed in Figure 2-47, where the integer PPP results are aligned simply using the 2nd order extrapolation (in green lines) just as for the float PPP results. In the following parts of this section, integer PPP results are only compared with the original float PPP results in the term of ADEVs. The improvements of the time transfer stability at different averaging times by using the integer PPP instead of the float PPP (corresponding to the black and red lines in Figure 2-46) are reported in Table 2-3.

Table 2- 3. The improvements of the time transfer stability by using the integer PPP

Averaging time	**Improvement of the stability**
5 min	13,3%
1 hour	31.2%
3 hours	50.2%
12 hours	63.3%
1 day	80%
5 days	65.3%

The results from the 1-month CCD experiments at INRIM are also compared in the Figure 2-47 and 2-48, corresponding to the phase measurements and their ADEVs. Additionally, two longest continuous periods in the 6-month CCD experiments at ORB and INRIM were chosen to compare the integer PPP and float PPP time transfer, and their ADEVs are plotted in Figure 2-49 and 2-50 respectively. The results from these CCD experiments show that after 3-4 days averaging, the frequency transfer stability of 10^{-16} can be reached by using integer PPP.

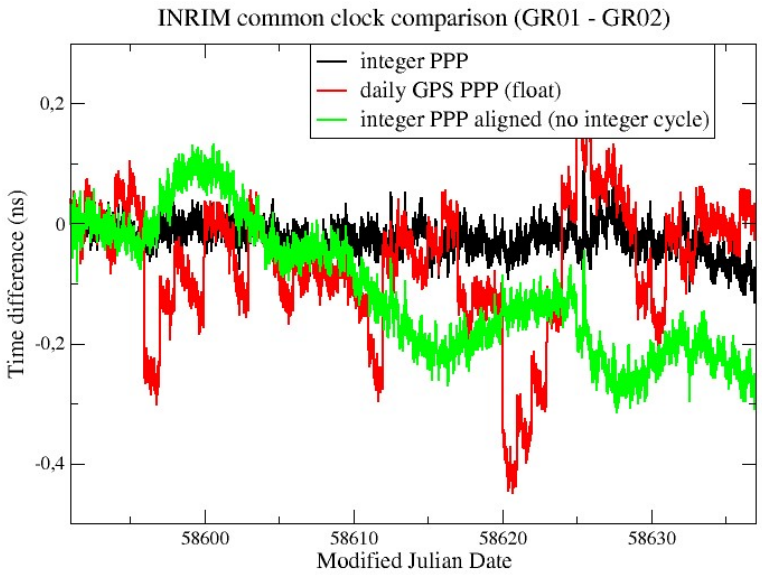

Figure 2- 47. CCD experiments at INRIM with integer PPP and float PPP, the alignment (in green) of integer PPP results ignores the integer λ_{NL} cycle discontinuity in order to show the alignment error.

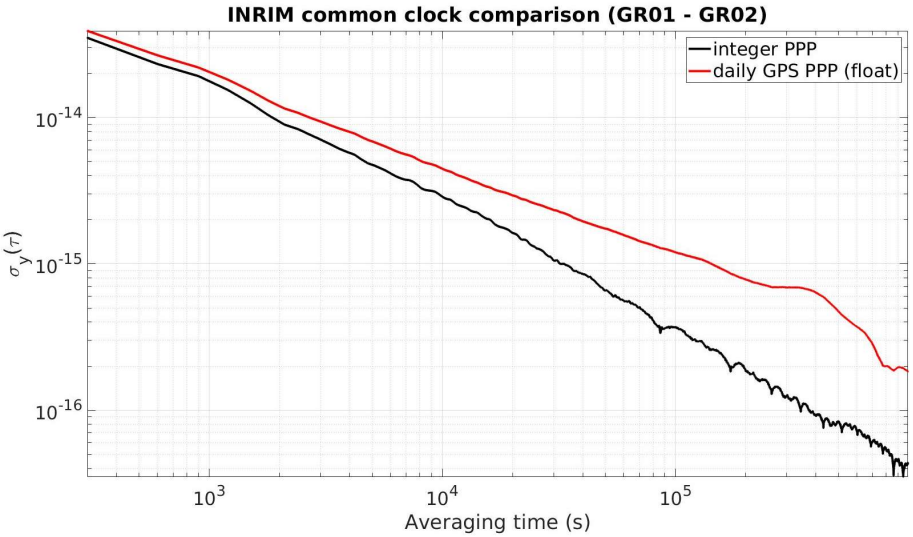

Figure 2- 48. ADEVs of the integer and float PPP time transfer solution in the INRIM CCD experiment

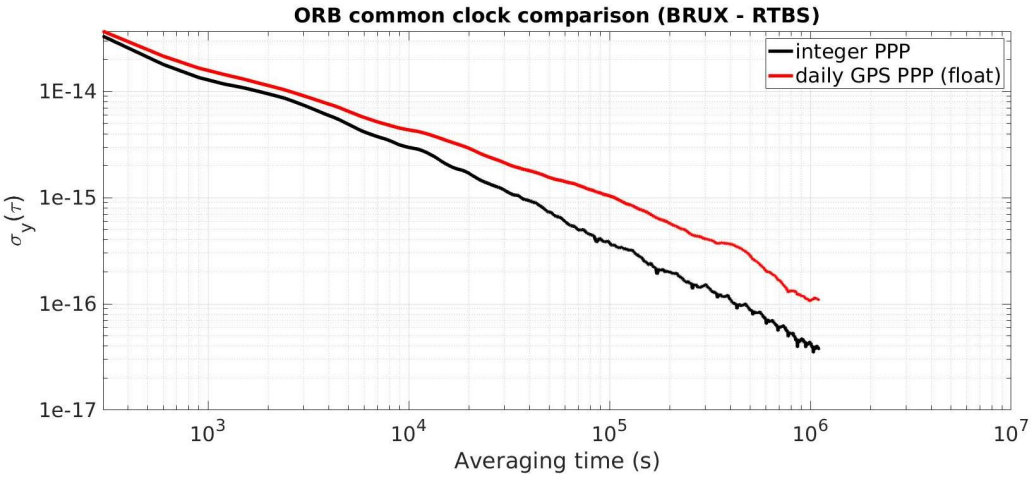

Figure 2- 49. ADEVs of the integer and float PPP time transfer solution during anther longer period at ORB

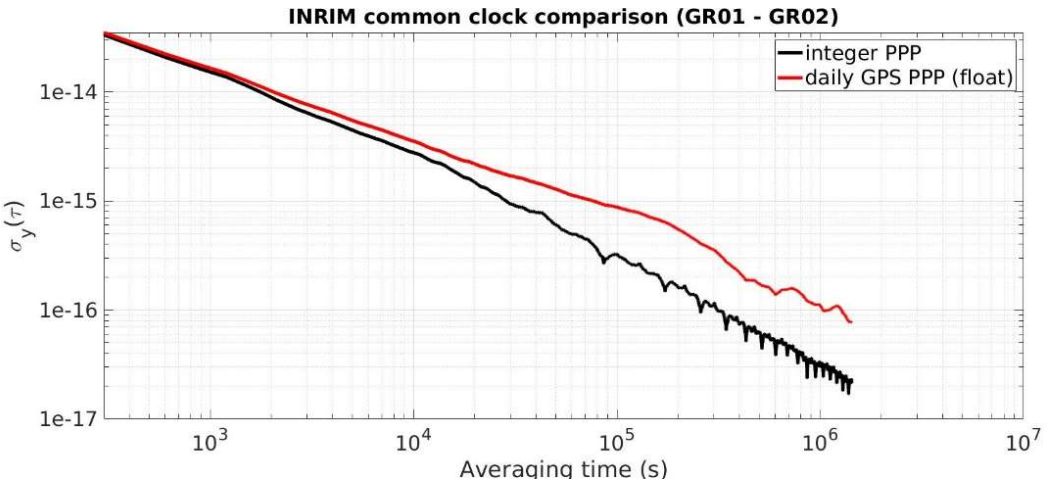

Figure 2- 50. ADEVs of the integer and float PPP time transfer solution during anther longer period at INRIM

2.5.2.3 "PPP - OPT" results

During the "PPP-OPT" experiments between station AO_4 and GUM4, the fixing rates of the ambiguities in step 1 and 2 of the integer PPP are normally over 85% and 90% respectively during the experimental periods, except the period with noisy measurements that was reported in section 2.4.2.3.

In the "PPP – OPT" experiments, the Atomium integer PPP time transfer was compared with the NRCAN PPP time transfer. The NRCAN PPP is a float ambiguity PPP with multi-day computational batch that is used by BIPM for the international clock comparison. Therefore, the comparisons were carried out during the periods when the NRCAN PPP time transfer results were within the same computational batch, which means no boundary jump was present.

The comparisons in the two test periods are selected to be demonstrated in the left and right plots of Figure 2-51. A drift of 0.8 ns and another of 0.4 ns in the NRCAN PPP results were observed in the two periods. These additional errors could be due to the random walk noise generated in the float ambiguity estimations [71].

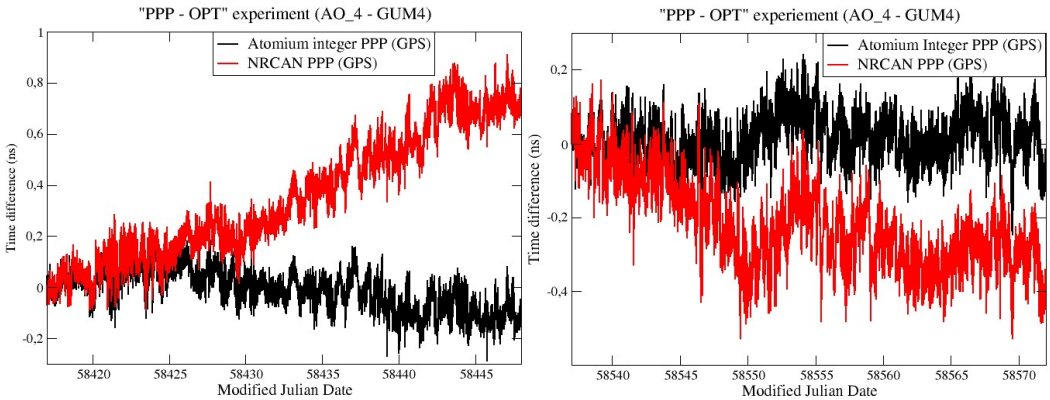

Figure 2- 51. Comparison of integer PPP and NRCAN PPP time transfer results

The ADEVs of the measurements in Figure 2-51 are then compared and displayed in Figure 2-52 and 2-53. The figures indicate that the integer PPP improves the frequency stability of the time transfer solution from 2.5 hours averaging to longer term, compared to the NRCAN PPP solution. The 10^{-16} frequency stability could be reached by the integer PPP time transfer with 9-10 day averaging in these "PPP - OPT" experiments.

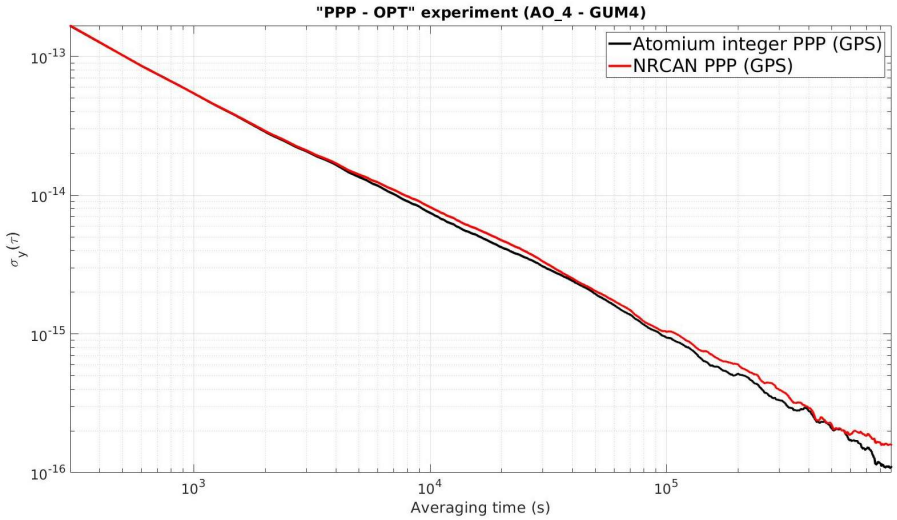

Figure 2- 52. ADEVs of the integer PPP and the NRCAN PPP results as given in the left plot of Figure 2-32

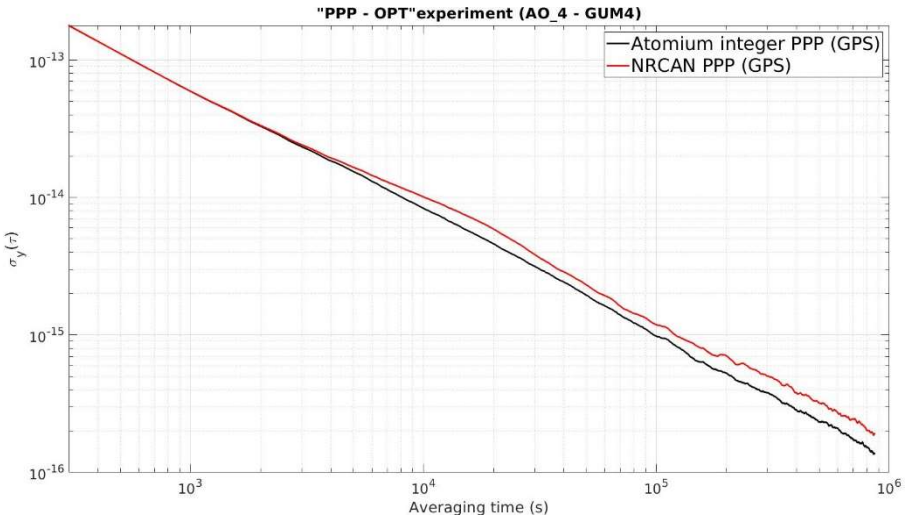

Figure 2- 53. ADEVs of the integer PPP and the NRCAN PPP results as given in the right plot of Figure 2-32

In [69] the integer PPP technique implemented by the CNES was tested in the same "PPP - OPT" experiment during different periods. It was reported in [69] that the frequency transfer stability of 10^{-16} can be achieved with 5 days averaging by integer PPP in the experiments, while the difference is that the performances were studied with the Modified Allan Deviation. Therefore, the data in Figure 2-53 are re-plotted in the form of Modified Allan Deviation in order to compare

them with the results reported in [69]. As shown in Figure 2-54, the current version of the Atomium integer PPP has very similar performance of the frequency transfer accuracy compared to the results in [69].

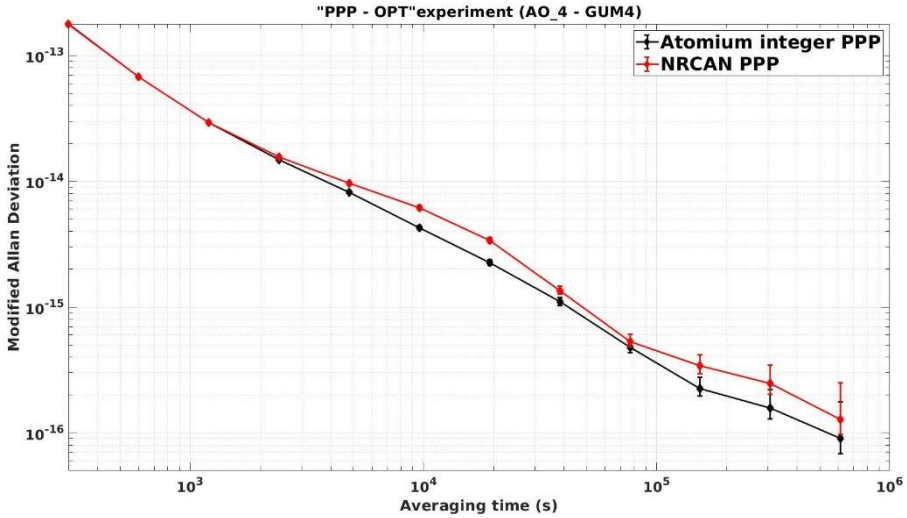

Figure 2- 54. Modified Allan Deviations of the integer PPP and the NRCAN PPP results as given in the right plot of Figure 2-51

2.5.3 Discussions

The integer PPP showed its advantage to the current float ambiguity PPP techniques on the frequency stabilities of the time transfer at mid-term and long-term averaging times, and with 3 to 10 days averaging the frequency stability of 10^{-16} could be reached. Meanwhile it removed the obvious random walk noise in the clock solutions caused by the float ambiguity estimation.

However, the current version of Atomium integer PPP still can't 100% guarantee the continuous WRB estimations during all the test periods, and it introduced occasionally a 1-cycle estimation error. This problem will be fixed in the future work.

This original integer PPP solution can be used for the frequency transfer only. However, since integer PPP can provide long-term continuous results without drift after the alignment as shown in the previous results, it also could be used for the time transfer if its solution is calibrated occasionally by another accurate time solution, as suggested in [85].

The current Atomium integer PPP will be updated to include the Galileo measurements when the daily Galileo integer products are regularly available, and its performance will be investigated. Furthermore, as the integer PPP improves the long-term stability of the time transfer and the constrained PPP improves the short-term and mid-term stability of the time transfer, the constrained integer PPP could be an interesting topic that will be studied in future research.

2.6 Frequency accuracy of PPP time transfer solution

Not like the clock comparison in the phase domain, in which a period of continuous PPP clock solution needs to be found for easier comparison, the comparison in the frequency domain can be carried out in the whole period, since the value at the epoch with phase discontinuity can be easily filtered out as outliers. Figure 2-55 shows the related frequency deviations of the Atomium integer and float PPP time transfer solutions between BRUX and RTBS at ORB during the period MJD 58678 - 58796 when the measurements and GRG products are continuously available (only GPS results are plotted in the figure for a clearer visualization), these frequency deviations were computed using the equation (5).

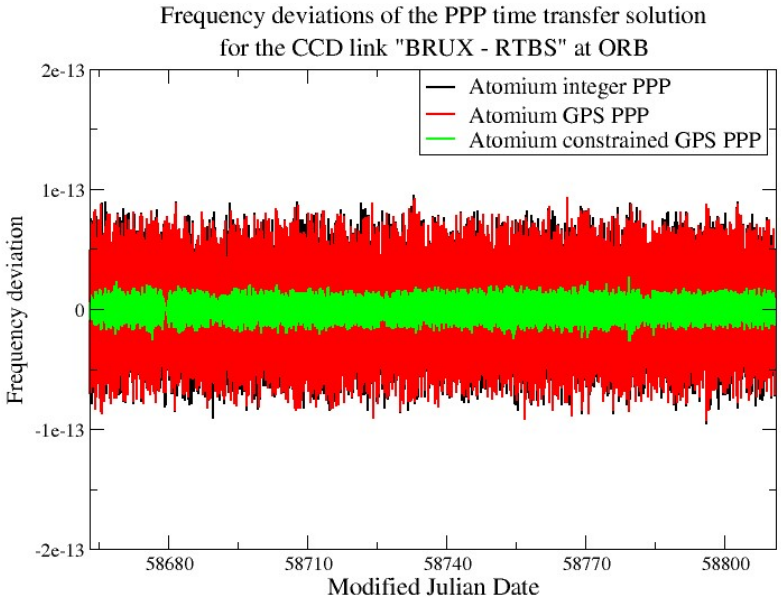

Figure 2- 55. Frequency deviations of the PPP time transfer solutions between BRUX and RTBS

To better compare the frequency accuracy of the related PPP time transfer solutions, the monthly frequency deviations were estimated from the data in Figure 2-55 by averaging the data with a 30-days sliding window. The corresponding monthly frequency offsets of the Atomium integer and float PPP time transfer solutions for the CCD link “BRUX - RTBS” at ORB are compared and plotted in Figure 2-56, and the monthly frequency offsets of the constrained PPP solutions are also demonstrated in Figure 2-57.

From Figure 2-56 it can be seen that all the float PPP solutions (including GPS-only, Galileo-only and GPS + Galileo ones) have very similar frequency accuracy, and their monthly frequency offset varies between 0 and -7e-16 during the 4 months testing period, which is corresponding to an accumulated phase error between 0 and -1.8 ns in a month (see equation 5); Meanwhile, the integer PPP provides much more accurate frequency solution: the frequency offsets are generally centered around zero, and within the range of ±2e-16 (corresponding to the phase error of ±0.52 ns in a month)

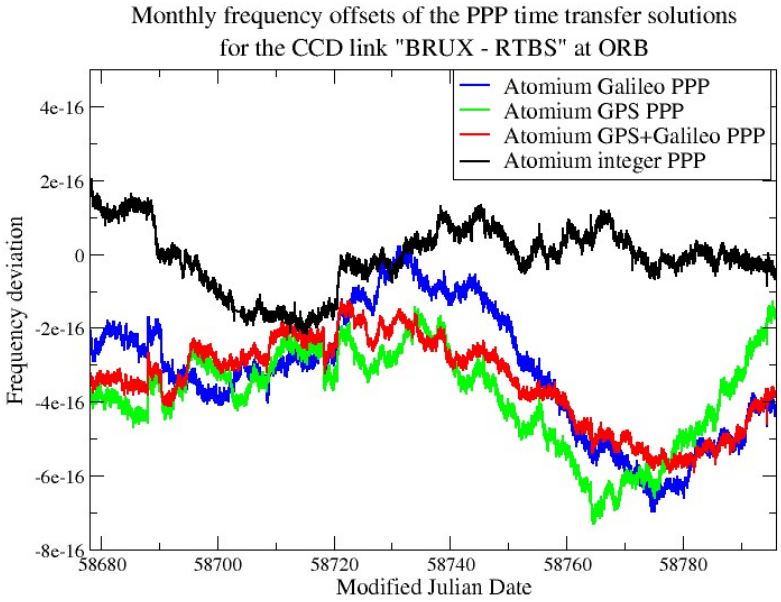

Figure 2- 56. Monthly frequency offsets of the PPP time transfer solutions between BRUX and RBTS (integer and float PPP results)

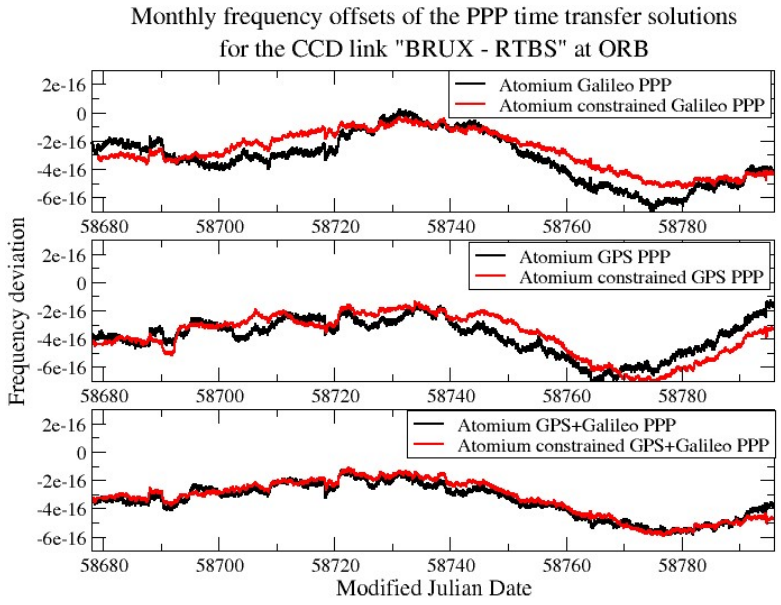

Figure 2- 57. Monthly frequency offsets of the PPP time transfer solutions between BRUX and RBTS (constrained and non-constrained results)

Figure 2-57 indicates that Atomium float PPP and its corresponding constrained PPP have similar frequency transfer accuracy; in addition, the closer similarity between the GPS+Galileo PPP and its related constrained PPP results indicates that the constraint models could be estimated more accurately based on more GNSS satellite measurements.

Then, the comparisons of the frequency accuracy of the PPP time transfer solutions for the link “GR01 – GR02” at INRIM during MJD 58680 – 58796 are given in Figure 2-58 and 2-59. Similar performance of the integer PPP solution can be found in Figure 2-58; However, the float PPP solutions show the frequency offsets very different from each other. The Galileo PPP solution has the largest

frequency offset (around -6e-16); while the GPS PPP solution shows a clear frequency drift from 2e-16 to -5e-16 during the 4-month period; combing GPS and Galileo in the PPP reduces the frequency offset compared to the Galileo-only solution and mitigate the frequency drift (from -2e-16 to -4e-16) compared to the GPS-only solution. The reason for the clear distinction between the GPS and Galileo PPP frequency transfer is still not very clear, the daily effects on the GPS and Galileo signals at these two stations probably need to be further investigated. The magnitudes of the frequency offsets of the float PPP and corresponding constrained PPP solutions are generally the same, while the constrained PPP provides slightly more stable frequency comparison results in the long term, as can be seen in Figure 2-59.

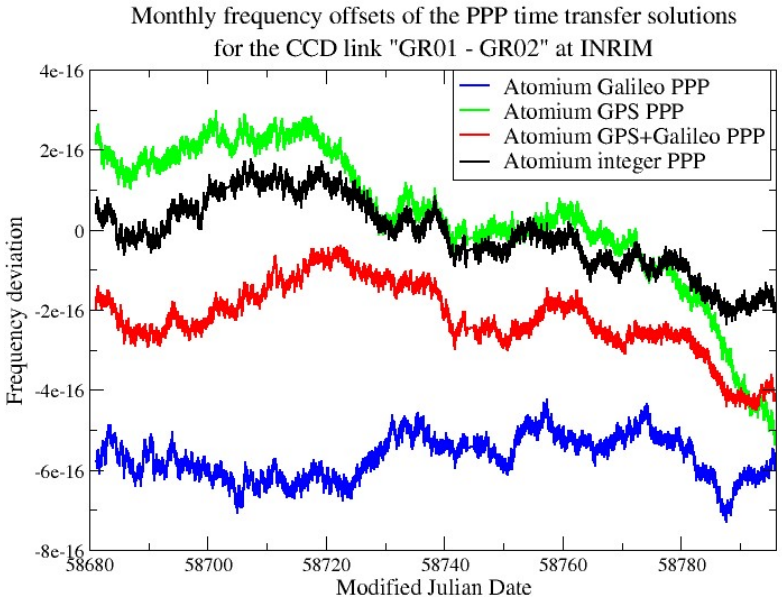

Figure 2- 58. Monthly frequency offsets of the PPP time transfer solutions between GR01 and GR02 (integer and float PPP results)

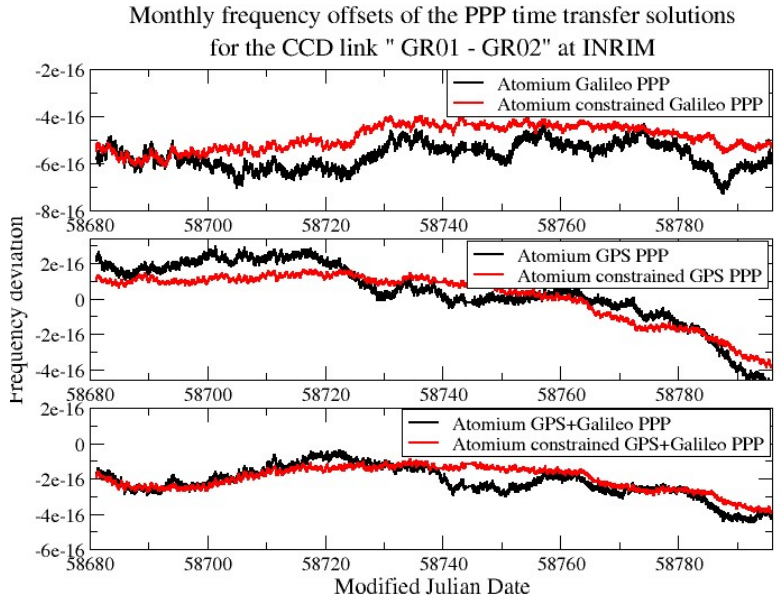

Figure 2- 59. Monthly frequency offsets of the PPP time transfer solutions between GR01 and GR02 (constrained and non-constrained results)

Moreover, it should be mentioned that, the large frequency offset in the float PPP solution doesn't manifest directly in the long-term phase comparison results using the daily Atomium PPP. For example, it is found in Figure 2-58 that Atomium Galileo PPP time transfer solution has a very stable frequency offset around -6e-16, which means an accumulated phase error around -6.1 ns in the whole 4 months period; however, this phase error is not present in the original Galileo PPP time transfer solution (black lines) as can be seen in Figure 2-60, while this accumulation of phase error is clearly visible in the aligned results (red lines) in the same figure. It indicates that the trend of the daily PPP solution (caused by the daily frequency offset) could be different from the trend of the actual PPP solution in the longer term. This mismatch is probably due to the errors in the daily float ambiguity estimation, by checking the improvement of using GPS integer PPP instead of GPS float PPP in both CCD experiments; in addition, the stable frequency offset in the Galileo solution in Figure 2-58 shows that there could be a constant frequency offset that is not compensated in the Galileo PPP computation in the INRIM CCD experiment. It was reported in [89] that any inconsistence of the measurement time in the two receivers or any code-phase clock measurement bias in one of the receivers will cause additional frequency offset in the daily solution, therefore, the synchronism of the Galileo measurements in the two receivers at INRIM needs to be further studied in future work.

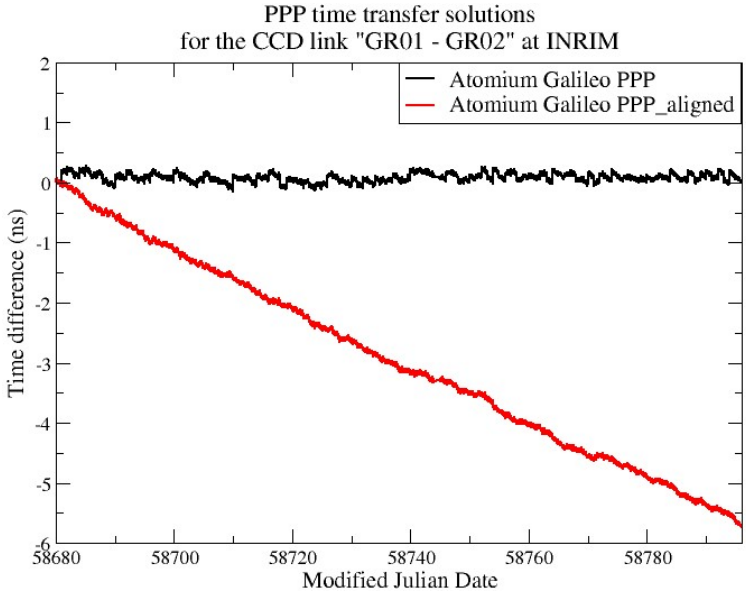

Figure 2- 60. Clock comparison of GR01 and GR02 in the phase domain using Atomium Galileo PPP

In the "PPP - OPT" experiment, since NRCAN PPP time transfer solution is based on the monthly computational batch, the average value of the frequency offsets in each monthly computational batch is computed. For a better comparison between the NRCAN and Atomium PPP, the absolute values of the computed monthly frequency offsets are plotted in Figure 2-61. During the 7 months period, the Atomium integer PPP frequency comparison results show the best accuracy,

with the size of monthly frequency offsets always below 2e-16; while the Atomium GPS float PPP and NRCAN GPS float PPP have similar monthly frequency transfer accuracy (from 0 to 6e-16).

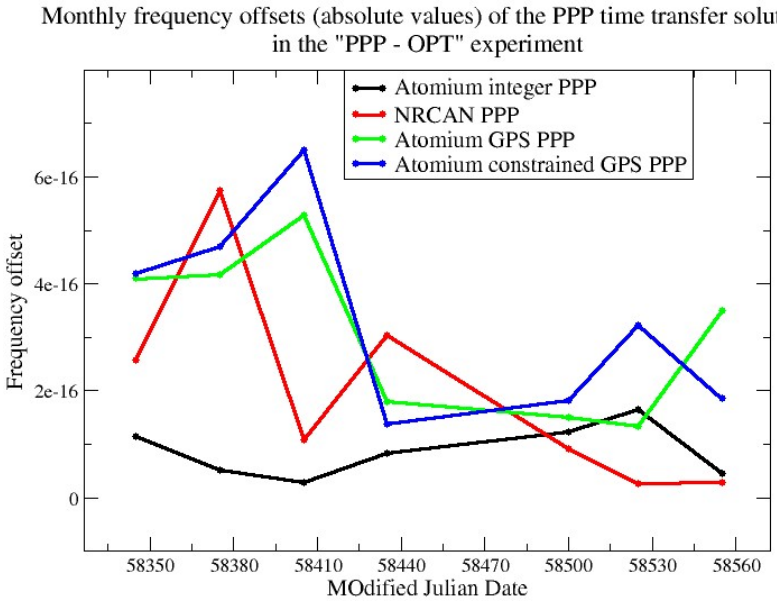

Figure 2- 61. Sizes of monthly averaged frequency offsets (within each NRCAN computational batch) of the PPP time transfer solutions in the “PPP - OPT” experiment

The previous results in this section indicate that, integer PPP frequency transfer is very stable, and the size of the monthly frequency offset is normally within 2e-16, which is corresponding to 0.52 ns accumulated phase error in one month; float PPP, either Atomium or NRCAN, provides less accurate frequency transfer solution, and the largest monthly frequency offset is around 7e-16, which means 1.8 ns error in the monthly batch; adding constraint to the receiver clock improves only the PPP frequency transfer stability in the short term but not the accuracy.

2.7 Improved PPP algorithm applications: upgrade of DEMETRA timing monitoring services

The current version of Atomium PPP is the core software that is used for the DEMETRA timing monitoring and steering service. As a result of the improved time transfer performances of these new Atomium PPP algorithms which have been presented in the previous sections, it was decided to integrate these new versions of Atomium PPP into the DEMETRA server to upgrade the current service.

2.7.1 Time Monitoring and Steering service

The "Time Monitoring and Steering" service provides the user the time difference between the user clock and the reference time scale of DEMETRA from the near real-time and daily post-processing PPP solution. The computation is based on the GNSS signal observation data collected at the user and INRIM side, the process is described in Figure 2-62.

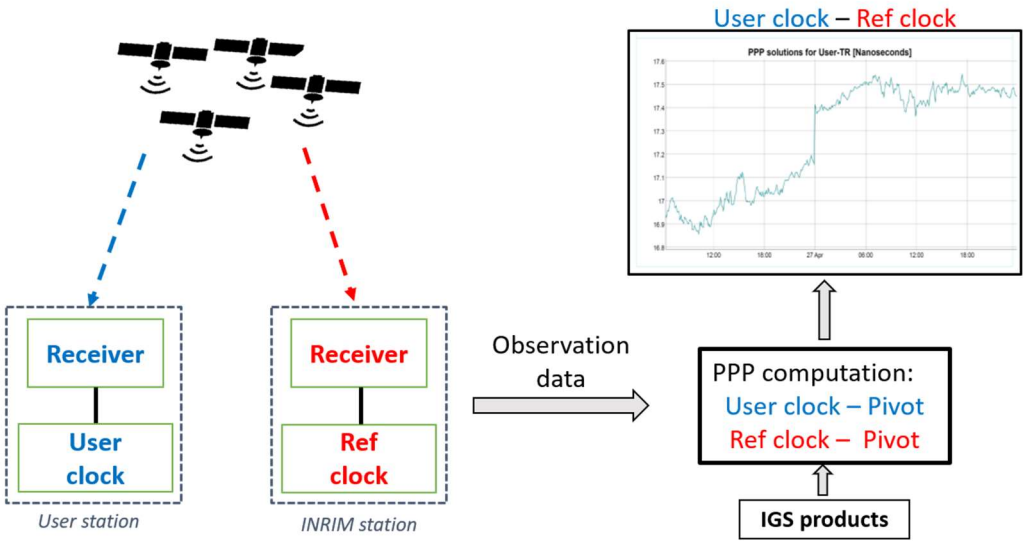

Figure 2- 62. The process to compute the time difference between user clock and the reference clock. Pivot is the IGS reference time when the IGS satellite products are used (namely, IGST, IGRT and IGUT, corresponding to the reference time of the IGS final products, rapid products and ultra-rapid products)

The user, which is equipped with a GNSS receiver, transmits its GNSS observation data hourly to the DEMETRA platform, then the PPP software that is integrated in the server will compute both the clock differences "User clock – IGS reference time" and "DEMETRA ref clock – IGS reference time" at 5 min interval, and the synchronization error "User clock – DEMETRA ref clock" is estimated by computing the difference of these two PPP clock solution. With the IGS ultra-rapid products, the user synchronization error is estimated in near real-time based on the hourly computed PPP solution, and the daily PPP solution, which has a better accuracy but a latency of 2 days, is also provided using the IGS rapid products.

Note that, the "user clock" in this dissertation always refers to the clock that need to be measured at the user side, it can be either the internal clock of the GNSS receiver or an external clock (such as H-maser, caesium, rubidium atomic clock) used to drive the GNSS receiver. On the other side, the "DEMETRA ref clock" is chosen to be the UTC(IT), which is based on a H-maser steered to the UTC.

By monitoring the user clock, the user will be alerted for any anomaly that happens on its clock, such as the phase or frequency jump, at the mean time some steering parameters that are estimated based on the monitoring data will be sent to

the users for the alignment to UTC if it's needed. Moreover, the quality monitoring data (such as satellite sky-plot, multipath) at the user station are also recorded and available on the user's personal area of the DEMETRA web page. As an example, a part of one user interface is exhibited in Figure 2-63.

Variable Name	Value
Satellite azimuth and elevation (plane)	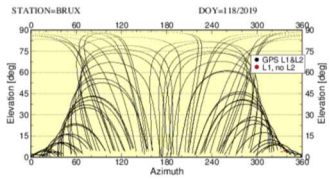 (https://www.demetratime.eu/getfile/11/2971)
Satellite elevations	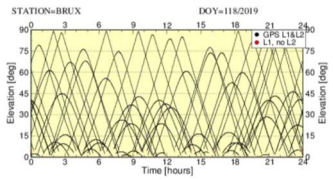 (https://www.demetratime.eu/getfile/11/2972)
Number of observed satellites	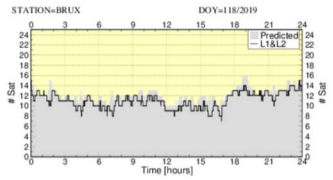 (https://www.demetratime.eu/getfile/11/2970)
Satellite azimuth and elevation (polar)	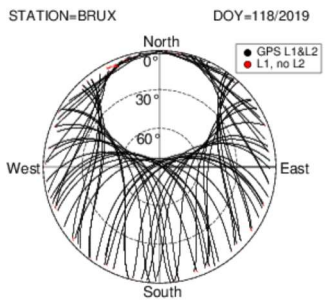 (https://www.demetratime.eu/getfile/11/2973)
PPP solutions for User-TR	17.45 Nanoseconds
Prediction for N days of UTC-User	-0 Nanoseconds
Steering parameters for user	-0 Relative unit
Max clock jump in the last 24 hours	0 Nanoseconds
Daily number of cycle slips	964
Max frequency jump in the last 24 hours	0 Relative unit

Figure 2- 63. Quality control data (truncated) of one user station on the DEMETRA website

2.7.2 Updated DEMETRA timing monitoring service

Since the steering parameters provided in the "timing and steering" service for the alignment of the user's clock to UTC are based on the performance of the time monitoring, the improvements of the steering service are not mentioned specifically in this section.

The two improved versions of the Atomium PPP that were introduced in section 2.3-2.5 have been integrated in DEMETRA server to upgrade the timing monitoring part of the DEMTETRA "time monitoring and steering" services. Three new types of daily results including the GPS + Galileo PPP solution, the constrained GPS (+Galileo) PPP solution and the integer GPS PPP solutions are provided in parallel besides the original GPS PPP one. These daily solutions are produced for the users who need post-processed services. The upgraded time monitoring services will have higher robustness and availability, provide time solutions with increased frequency transfer stability and accuracy; in addition, new services such as noise reduction with constrained PPP will also be studied in practice. Meanwhile, the new near real-time solution (hourly solution) using the GPS + Galileo PPP will be available very soon and benefits the users who need their clock synchronized more frequently and quick reaction to the anomalies in their clocks.

In addition, the new quality control data including Galileo measurements have also been available in the DEMETRA database, the examples are given in Figure 2-64 to Figure 2-67.

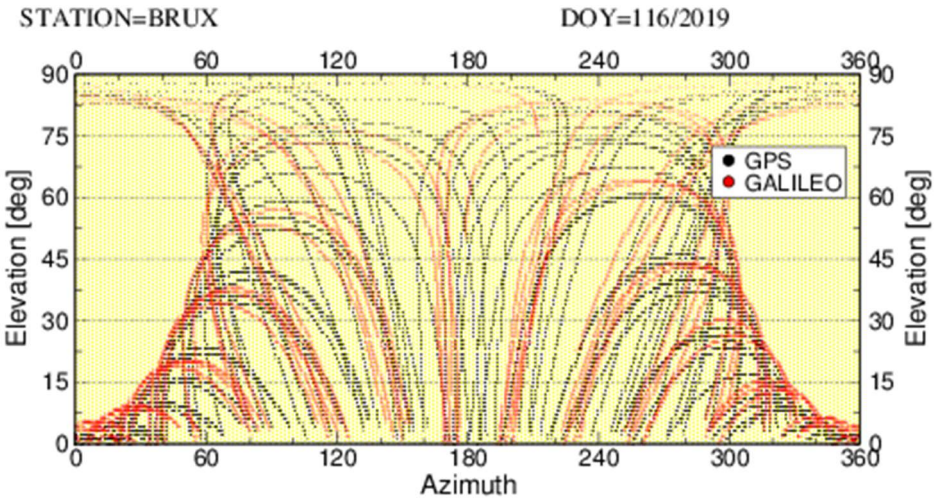

Figure 2- 64. Satellite azimuth - elevation (plane) plot

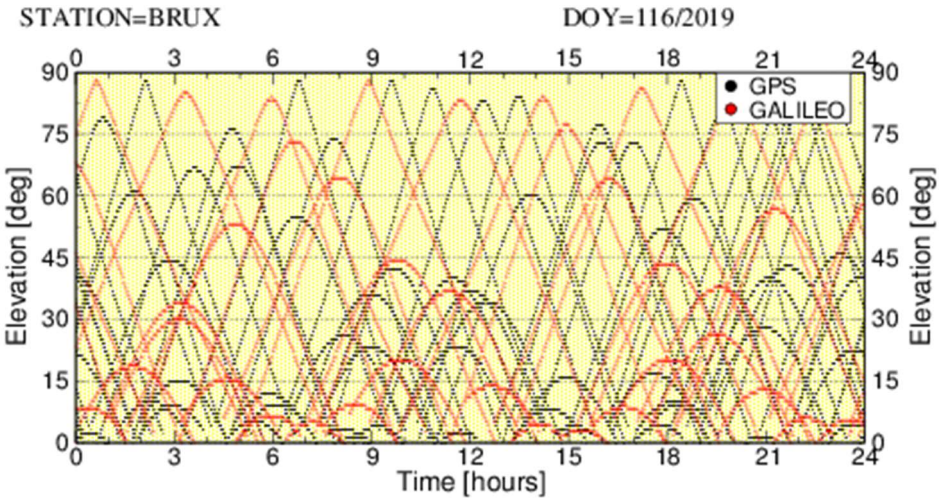

Figure 2- 65. Satellite elevation plot

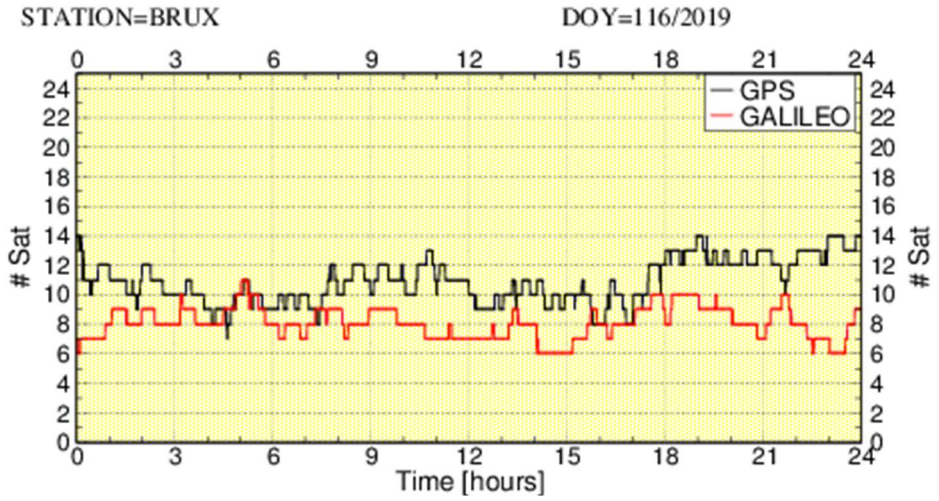

Figure 2- 66. Number of observed satellite plot

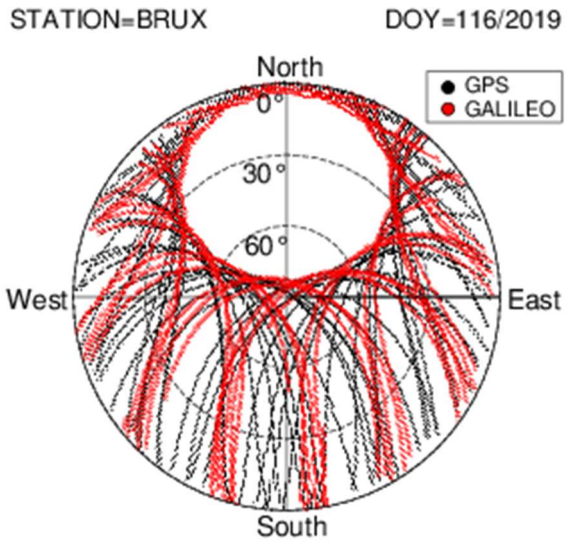

Figure 2- 67. Satellite azimuth - elevation (polar) plot

Chapter 3

Real-time detection of GNSS satellite clock frequency anomalies

This chapter is mainly about real-time detection of the frequency anomalies in the GNSS satellite clocks. As already explained in section 1.5, the real-time GNSS positioning and timing applications rely on the quality of the broadcasted navigation message. Since the satellite-user range measurements are based on the reading of the satellite and user clocks, if there is an unexpected clock anomaly happens in the satellite clock, the final GNSS solution could be affected.

In section 3.1 the typical GNSS satellite clock frequency anomalies are introduced, and their effects on the final GNSS timing or positioning are illustrated with some examples. Section 3.2 generally describes the principle of the frequency jump detector. In section 3.3, the primary method that generates the real-time frequency measurements of the GNSS satellite clocks is proposed and its performance in the frequency anomaly detection are reported. Section 3.4 further introduces two alternative methods for the real-time frequency measurement that can be used as an independent way for the jump detection. The conclusions are made in section 3.5. At last, the possible application of the proposed methods in the DEMETRA project is discussed in section 3.6.

3.1 Satellite clock anomaly

Each GNSS satellite operates its own satellite clock, meanwhile it broadcasts in its navigation message three coefficients (satellite clock offset, drift and drift rate) to the users. The users build the second order polynomial (first order polynomial for GLONASS) with the received three coefficients to predict the synchronization error of that satellite clock referring to its system time [17].

The typical anomalies that happen on GNSS satellite clocks are time and frequency jumps, these jumps are normally not compensated in the broadcasted navigation messages in time, for example, the prediction of the GPS satellite clock

error is usually updated once per day. As it is already known, the GNSS solution is based on the clock measurements, an unknown jump that happens in the satellite clock will cause a wrong estimation of the satellite-receiver range and therefore increases the positioning and timing error.

Compared to the jump happening in the time domain, the frequency jump is more difficult to be detected and it may cause more serious problems in the clock measurements, since the time deviation is the integral of the frequency deviation (referring to equation 4 and 5 in chapter 2). For this reason, this part of the work mainly focuses on the frequency jump detection in the GNSS satellite clock.

In order to detect any frequency jump in the satellite clock, a reference time scale is needed to measure the frequency deviations of the clock. The IGS and MGEX final satellite clock products provide the most accurate GPS and Galileo satellite clock phase offsets referring to their reference time respectively. These phase measurements of the satellite clocks can be transferred to the corresponding frequency measurements using the equation (5).

Figure 3-1 shows a clear frequency jump in the clock of the GPS satellite02 (GPS02), which is measured by IGST (note that the measurement in the IGS clock product is satellite clock – IGST, while the quantities in the figure is IGST – satellite clock). The original frequency measurements at 5 min interval are plotted in black line, and the smoothed ones with 25 min sliding window are in blue line for a clearer observation.

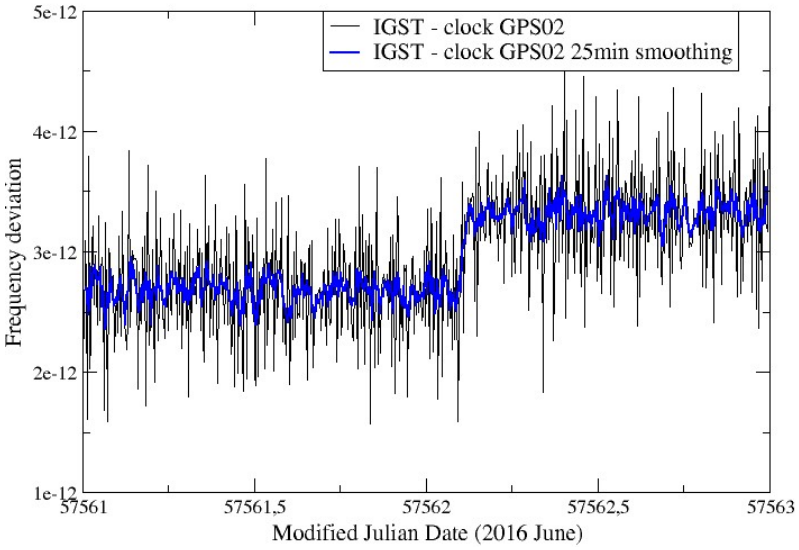

Figure 3- 1. A GPS satellite frequency jump happened on 23 June 2016

The size of the detected jump in Figure 3-1 is around 7.5×10^{-13}. According to the equation (5), this frequency jump will cause a clock error of 2.7 ns in one hour, which is corresponding to 81 cm error on the pseudorange measurement (distance=velocity of light × time). If the clock data of the GPS02 is updated after 1 day, the clock error will reach 64.8 ns, which means 19.4 m error on the pseudorange measurement until the update. In practice, this satellite will be discarded without any doubt for the GNSS positioning or timing when its

measurement error is noticeably large compared to the other satellites. However, this issue of frequency jump needs to be alerted when it happens, and the corresponding satellite must be discarded before it causes any positioning or timing error that can't be ignored anymore.

In order to study the effect of the frequency jump of the GPS02 clock to the user's positioning service, the IGS station HRAO was chosen to estimate its antenna positions using the GPS satellite signals during the day when this frequency jump happened. The precise coordinate of the station antenna is first estimated by Atomium PPP for that day and it is chosen as the reference position. Since Atomium PPP uses IGS post-processed clock products to obtain the satellite clock data, its computed coordinate is not affected by the problematic satellite GPS02. Then the GPS standard positioning at HRAO was carried out, which uses the satellite navigation messages for the estimation of the satellite positions and clock offsets, and its 3D positioning residual error referring to the reference position at each epoch was recorded.

In Figure 3-2, the effect of the problematic GPS02 to the GPS standard positioning solution of IGS station HRAO is shown. The change of 3D positioning residual errors with time are plotted, the results in the figure are smoothed with 25 min sliding window to make a distinction between different lines.

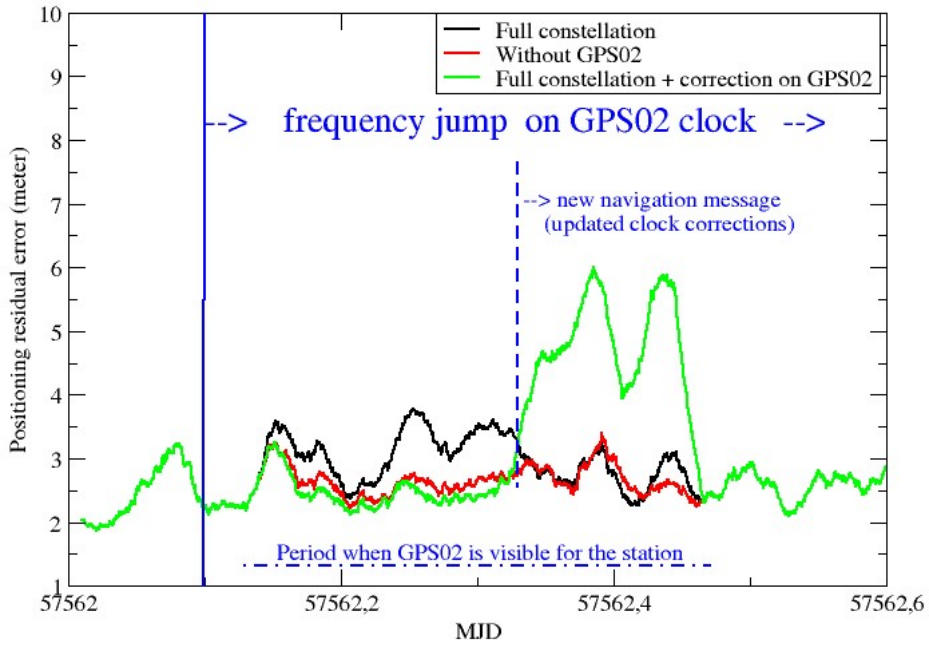

Figure 3- 2. The 3D positioning residual error at HRAO with or without GPS02

In Figure 3-2, the blue solid horizontal line indicates the start of frequency jump on the GPS02 and the blue dash line indicates the time when clock data of the GPS02 is updated in the navigation message (the end of the frequency jump). Black line represents the positioning errors using all the GPS satellites including the GPS02. Red line stands for the positioning errors using the constellation

without the GPS02. Moreover, since the size of the jump is well measured, the accumulated error with time on the pseudorange measurement could be calculated, so another solution is to keep using the full constellation for the positioning, correcting the errors caused by the frequency jump on the GPS02, of which the results are shown in green line.

It is observed in the figure that, the residual errors of the three solutions are very similar at the beginning since the clock error on the GPS02 is small. The positioning error using the uncorrected GPS02 signals starts to increase over time until this frequency jump is compensated in the new navigation message of the GPS02. This additional positioning error which is caused by the GPS02 reaches 1 m in about 4 hours. Meanwhile, using the corrected GPS02 signals shows the lowest positioning error before the update of navigation message in the GPS02 since more correct measurements are used. Usually the corrections on the GPS02 signals should be stopped after the frequency jump has been corrected in the updated navigation message. However, for illustrative purpose only, these corrections to the GPS02 are adopted during the whole period when the GPS02 is visible for the station HARO, and the results shows higher error after the update of the GPS02 navigation message just as expected.

Besides the effect on the GPS positioning, the frequency jump on the GPS02 clock also causes error in the GPS time solution. The R2CGGTTS software [44] was used to estimate the receiver clock offset with respect to GPS system time (GPST) at HRAO on the same day. As shown in Figure 3-3, due to the direct effect of the frequency error on the time measurement, when the GPS02 is included to compute the receiver clock offsets with respect to GPST at HRAO, a clear drift is observed, comparing to the solution without using the GPS02. However, due to the lack of reference, Figure 3-3 only summarises that this frequency jump in the satellite GPS02 causes a divergence, the size of which reaches 4 ns within 4 hours, in the time solution.

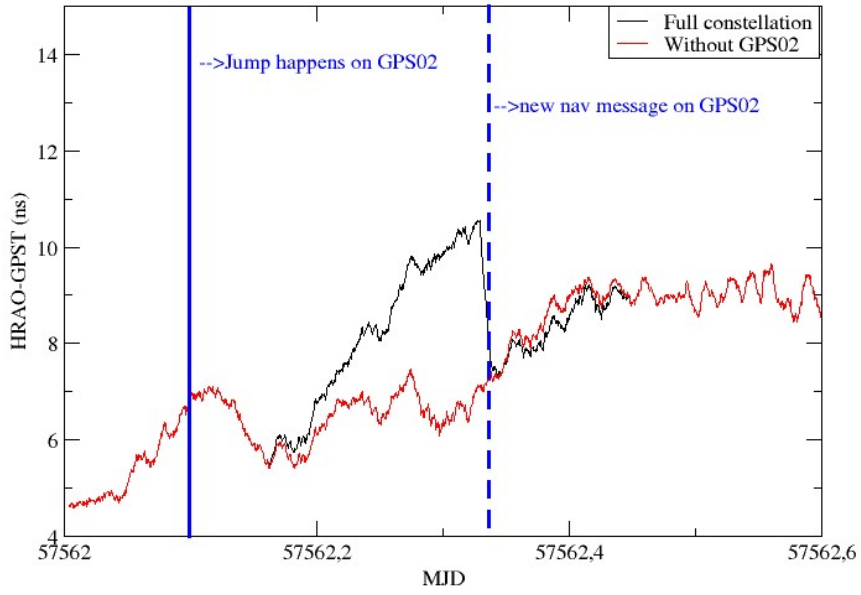

Figure 3- 3. Receiver clock at HARO against GPST with or without GPS02

It is worth mentioning that, discarding the problematic satellite is not always an optimal choice, since the accuracy of the positioning does not only depend on the satellite measurements, but also depends on the geometric distribution of the satellites, namely GDOP [90]. So, in the case that the frequency jump on the satellite is too small to dominate the positioning error (for example, with the size 1×10^{-13}), and keeping using that satellite will retain a good GDOP at the same time, then the user can choose to continue using that problematic satellite.

Adding corrections on the problematic satellite signals is not strongly recommended unless there are not enough visible satellites or the GDOP can be improved by using that problematic satellite. The reasons why the satellite frequency corrections should be used with caution are: 1. The corrections are based on precisely measured size of the frequency jump, which is not guaranteed due to the measurement noise and the stability of the reference time scale; 2. The frequency jump is not always in the form of an frequency offset, which makes the corrections hard to be computed; 3. The improvement to the positioning is usually very small if the frequency jump is not very large, it's easier to discard the satellite if there are still enough visible satellites to keep the good geometric distribution.

Figure 3-4 gives another example of the positioning and timing results at station BRUX during the period when there is a frequency jump of 3×10^{-1} in the GPS13 satellite (G13).

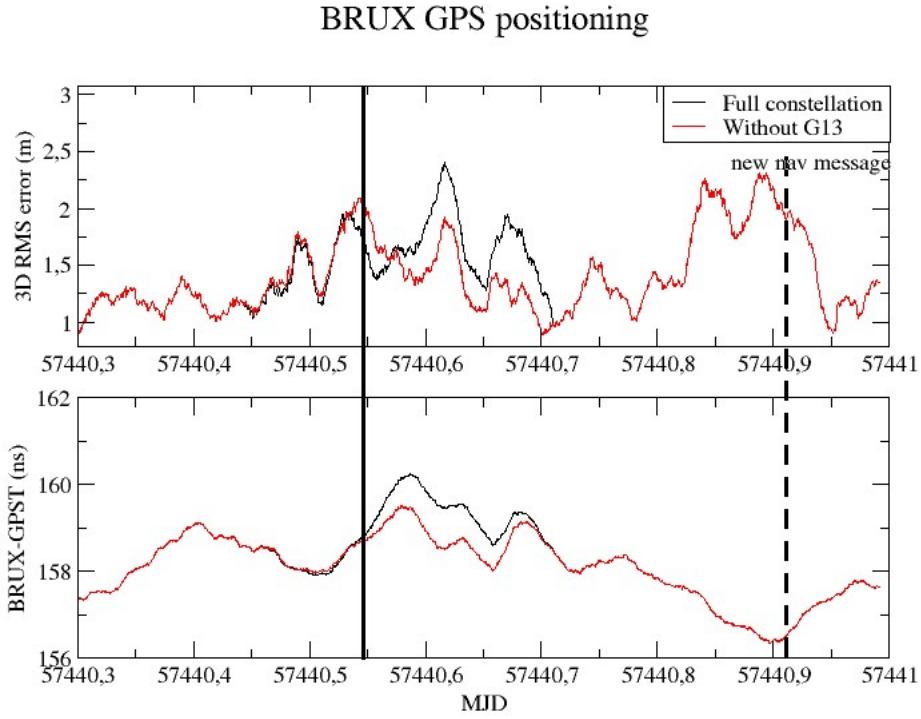

Figure 3- 4. Positioning and timing errors at BRUX during the usage of problematic satellite GPS13

The G13 becomes invisible for station BRUX before the update of the navigation message, so the differences between the solutions can only be found around the period of the MJD 57440.43 – 57440.73 when the G13 is visible. The

size of the jump happening on the G13 is very small, it can be seen from the figure that by using the problematic G13 for the positioning at the beginning of the jump causes even less position errors, since it's better to keep the G13 for a better GDOP. However, as the phase errors on the G13 accumulate over time, the advantage to exclude the G13 starts to emerge.

Compared to the complex situation in GPS positioning, the problematic satellite affects the GPS timing solution in a clearer way even if it is a tiny frequency jump, as indicated in the lower plot of Figure 3-4. It is also found that the divergence in the clock solution by using the G13 doesn't increase linearly as in Figure 3-3. It is because the phase error from the G13 doesn't accumulate very fast due to the small frequency jump, while its contribution in the final time solution reduces quickly as the satellite elevation keeps decreasing before it becomes invisible for BRUX (the weight of the measurement from one satellite in the time solution is proportional to its satellite elevation).

3.2 Frequency jump detector

The software to detect the frequency jump on the GNSS satellite has already been developed at INRIM based on the method that was described in [82], and its principle is displayed in Figure 3-5. Based on the provided satellite clock frequency measurements against a reference time scale (such as the IGST), the frequency jump detector can detect and report the position of the jump with minutes of delay. The detection process consists of four steps: 1) the trend of the first N_1 frequency values is estimated; 2) the predicted trend of the next N_2 values (μ_p) based on the previous N_1 values is computed; 3) the N_2 values are smoothed with a sliding window of length N_3 to reduce the noise and 4) the differences of the smoothed values and the predictions μ_p are measured, if the difference is larger than the threshold, a frequency jump is declared at that epoch.

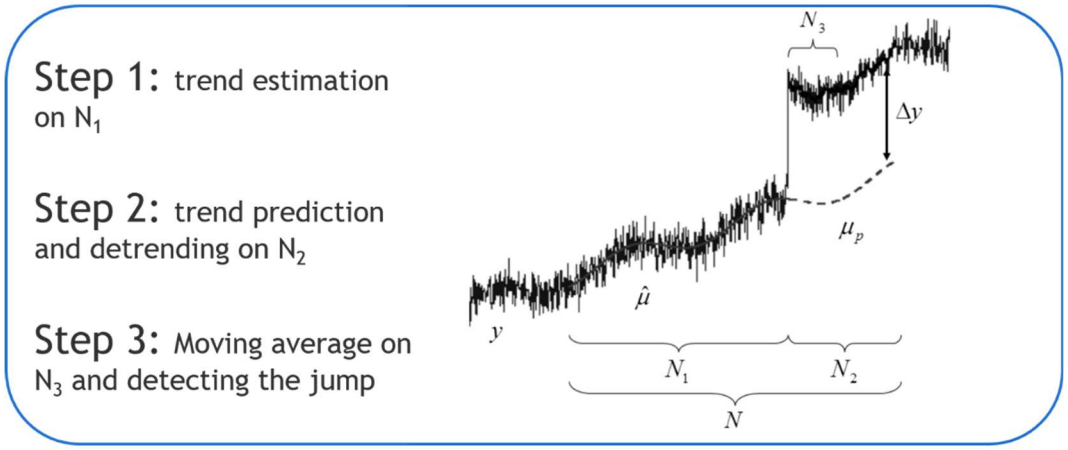

Figure 3- 5. Principle of the frequency jump detection method [82]

This frequency jump detector has been tested by using the frequency measurements from the IGS/MGEX final products. As suggested in [82], the

frequency data are smoothed with a 50 min sliding window (N_3=10 for the 5-min interval IGS products), which means 25 mins delay of the detection. In practice, a frequency jump as small as 2×10^{-13} can be precisely detected by the detector using the IGS products.

Compared to the quick detection of the jump in the frequency jump detector, the IGS/MGEX products are generated in a post-processing way. The most precise products are available with a delay of over 10 days, even the rapid products are provided after 1 day. The IGS also has real-time products, such as the ultra-rapid products and the real-time service (RTS) products [91]. However, the real-time part of the ultra-rapid product is based on the prediction and the reference time of the RTS clock product changes over time, which makes them not suitable for the detection purpose if used directly.

In the next two sections, three methods are proposed to provide the real-time frequency measurements of the GNSS satellite clocks, that can be used by the detector for the quasi-real-time frequency jump detection. Two of the methods are based on a ground reference time in the laboratory, while the other method uses a satellite clock as the reference.

3.3 Method with ground reference

3.3.1.1 Background

In addition to the IGS reference time, some time laboratories also provide very accurate reference time scales, such as UTC(ORB) [92] and UTC(IT) [93]. These two UTC(k) are based on the H-masers, which provide very stable reference frequency which can be utilized to measure the frequency deviations of the GNSS satellite clocks through the GNSS station they are connected to. An example is given in Figure 3-6, in which the frequency jump on the GPS02 (reported in Figure 3-1) was measured again by UTC(IT) thought the connected station GR01. As already explained in the section 1.3, by receiving the broadcasted navigation message from the GPS02 at GR01, the phase offsets of the GPS02 clock with respect to UTC(IT) can be computed, and then the frequency deviations are further estimated using equation (5).

The short availability of the UTC(IT) measurement is because the satellite GPS02 can only be measured when it is visible to the station GR01. The two results using code and carrier phase measurements are plotted in grey and green respectively in Figure 3-6. The corresponding smoothed data are in blue lines. Note that the code, carrier phase and IGS measurements in Figure 3-6 are all with 30 second interval, while the IGS measurements in Figure 3-1 are with 5 minutes interval.

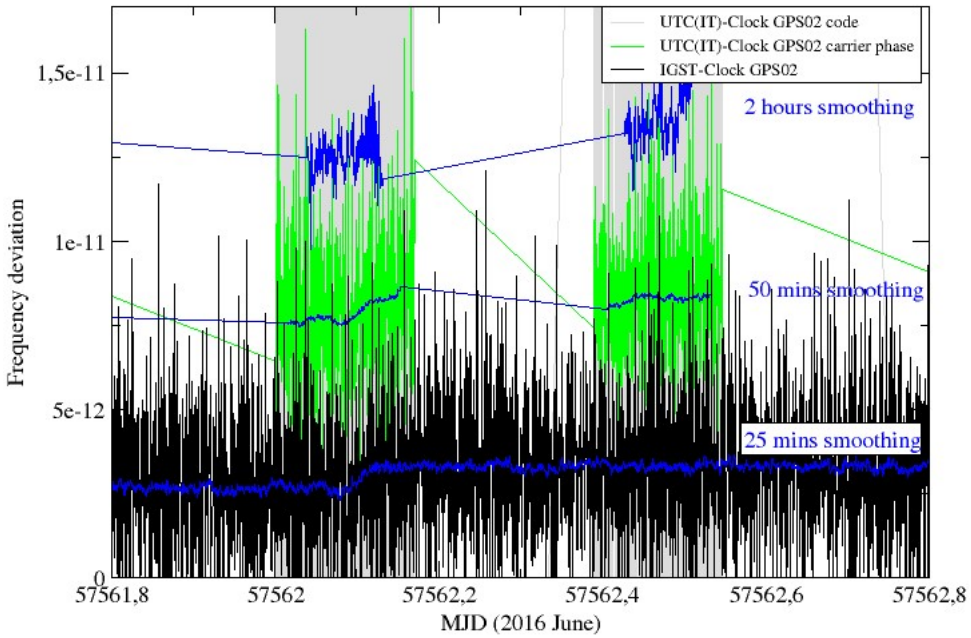

Figure 3- 6. Frequency measurements (30 s interval) of GPS02 clock referring to UTC(IT) and IGST

Figure 3-6 shows that the frequency jump on the GPS02 can be seen from both the IGS measurements and the carrier phase measurements. While the code measurements are too noisy to display this jump. The stability of the three measurements are further compared in the form of ADEVs in Figure 3-7. It is observed that it is possible to monitor the satellite frequency change against a good ground reference by using the real-time carrier phase measurements instead of using the IGS post-processing measurements.

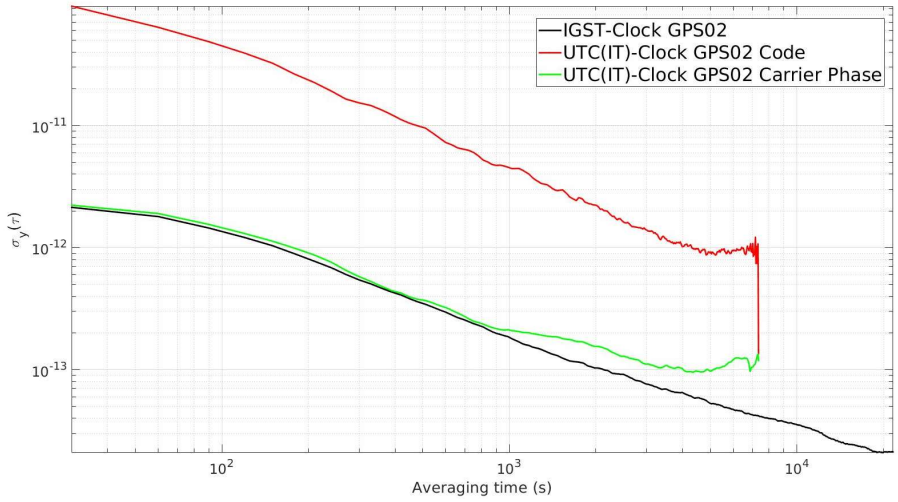

Figure 3- 7. ADEVs of the carrier phase measurements, code measurements and IGS measurement

However, due to the measurement gaps as shown in Figure 3-6, it's impossible for a single station to monitor continuously the satellite clock by receiving the broadcasted signals. Meanwhile, the quality of the measurements

from a single station are highly affected by the elevation of the satellite (atmospheric and multipath errors are higher for the low elevation satellites).

A method that can continuously monitor the satellite clock frequency anomalies using the ground reference was proposed in this work, and the details are described in the next subsection.

3.3.1.2 Developed algorithms

This method is based on the real-time distributed GNSS observation data from a global station network (for example, the stations that participate the IGS real-time service [42]). The related software has been developed and is now being tested. For the computational efficiency in the test phase, the minimal number of stations that are evenly distributed around the world were selected (40 stations for the GPS monitoring and 31 stations for the Galileo monitoring). These stations were selected from the IGS/MGEX tracking network [94]. In the current test phase, UTC(ORB) is used as the ground reference, therefore the station BRUX which is connected to UTC(ORB) must be included. The whole process of the method consists of the following steps:

Step 1: The coordinates of the selected stations are computed based on the observation data of the previous day using the Atomium PPP.

Step 2: Every 30 s the GPS/Galileo observation data are collected from all the stations including BRUX. Correcting the signal propagation errors in the carrier phase measurements of each station (the same as have described in the PPP algorithms before), the differences between each satellite clock and each station clock (if the satellite is visible for the station) are estimated separately. Since the carrier phase ambiguities are not fixed, these clock differences estimated from the carrier phase measurements don't provide accurate time information. However, by using equation (5), the satellite clock frequency (deviation) measurements respect to each station clock can be accurately computed. The discontinuities in the frequency measurements due to the change of ambiguities are filtered out easily in the frequency domain as the outliers. The prediction parts of the IGS ultra rapid satellite orbit products are used in this step to estimate the satellite positions in real-time.

Step 3: From step 2, the frequency deviations of each satellite clock against the station clocks at 30s interval have been obtained. The frequency deviation of the satellite i against the clock of station j (which is not BRUX) at one epoch is expressed as $Frq_{(\text{station j – sat i})}$, and it can be further expressed as $Frq_{(\text{BRUX – sat i})} - Frq_{(\text{BRUX-station j})}$. Passing all these frequency measurements at one epoch into the least square algorithms, the frequency deviation of each satellite clock against the BRUX clock (which is UTC(ORB)) and the frequency deviation of each non-BRUX station clock against the BRUX clock at that epoch are computed. The least square solution of the matrix computation $b = Ax$ is $\hat{x} = (A^T A)^{-1} A^T b$. At each epoch, the matrix b is filled by the estimated frequency measurements $Frq_{(\text{station j – sat i})}$, x is the matrix of the unknowns $Frq_{(\text{BRUX – sat i})}$ and $Frq_{(\text{BRUX-station j})}$,

A is the coefficient matrix in front of x. Examples of these matrices at one epoch are given as follows.

$$b = \begin{bmatrix} Frq(BRUX - sat1) \\ Frq(station2 - sat1) \\ Frq(station3 - sat1) \\ \cdots \\ Frq(BRUX - sat2) \\ Frq(station3 - sat2) \\ Frq(station5 - sat2) \\ \cdots \\ \cdots \end{bmatrix}$$

$$A = \begin{pmatrix} 1 & 0 & \cdots & 0 & 0 & 0 & 0 & 0 & \cdots \\ 1 & 0 & \cdots & 0 & -1 & 0 & 0 & 0 & \cdots \\ 1 & 0 & \cdots & 0 & 0 & -1 & 0 & 0 & \cdots \\ \cdots & \cdots & \cdots & \cdots & \cdots & \cdots & \cdots & \cdots & \cdots \\ 0 & 1 & \cdots & 0 & 0 & 0 & 0 & 0 & \cdots \\ 0 & 1 & \cdots & 0 & 0 & -1 & 0 & 0 & \cdots \\ 0 & 1 & \cdots & 0 & 0 & 0 & 0 & -1 & \cdots \\ \cdots & \cdots & \cdots & \cdots & \cdots & \cdots & \cdots & \cdots & \cdots \\ \cdots & \cdots & \cdots & \cdots & \cdots & \cdots & \cdots & \cdots & \cdots \end{pmatrix}$$

$$x = \begin{bmatrix} Frq(BRUX - sat1) \\ Frq(BRUX - sat2) \\ \cdots \\ Frq(BRUX - station2) \\ Frq(BRUX - station3) \\ Frq(BRUX - station4) \\ Frq(BRUX - station5) \\ \cdots \end{bmatrix}$$

Step 4: Keep running the step 3 at every 30 s, the frequency deviations of the satellite clocks are continuously measured by UTC(ORB). These frequency measurements are filtered first to remove the outliers and then pass though the frequency jump detector for the possible frequency jump detection in the satellite clock. The previously described steps are further illustrated in Figure 3-8 as a flow chart.

Two versions of software have been developed accordingly: one version provides GPS satellite clock frequency measurements using the RINEX 2 observation files and IGS ultra rapid orbit products, the other version is fed by the RINEX 3 observation files and GFZ ultra rapid orbit products and is used to monitor the Galileo satellite clock frequency anomaly.

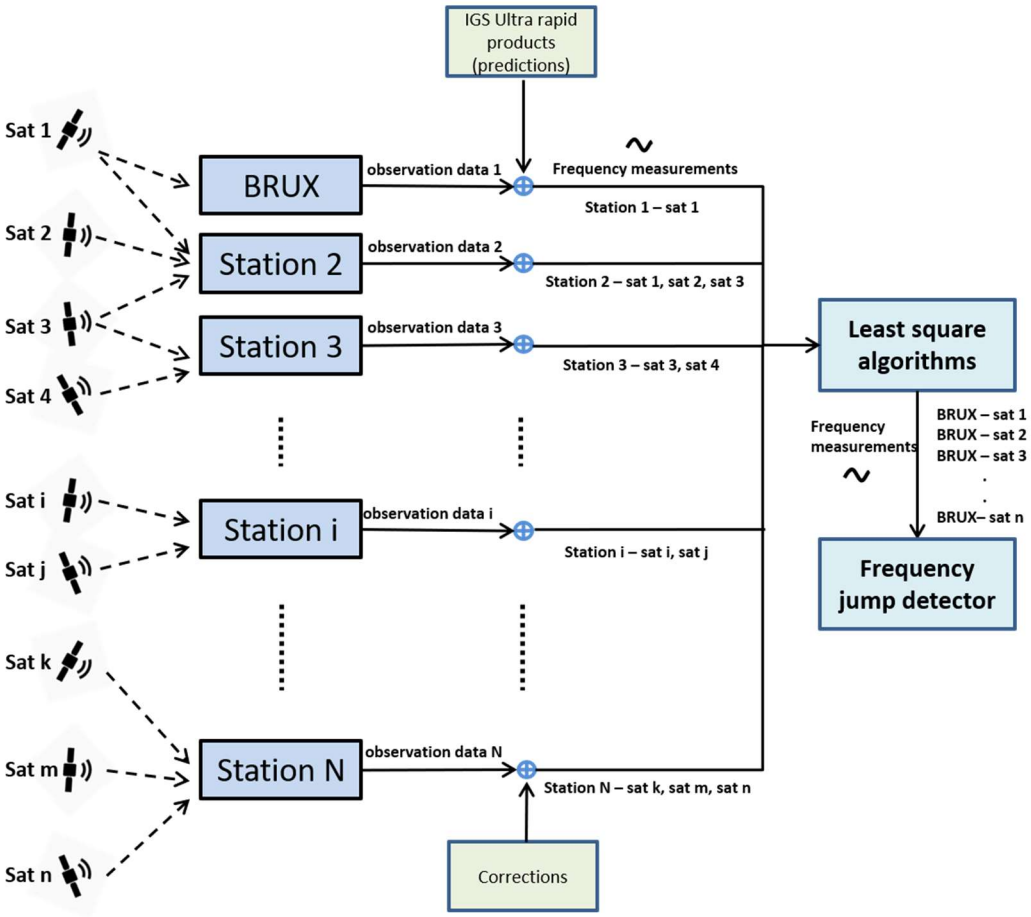

Figure 3- 8. Principle of real-time satellite clock frequency monitoring with the ground reference UTC(ORB) at BRUX

3.3.1.3 Performances

Currently there are different types of atomic clock on the GPS satellites of several generations, and the details can be found on the GPS navigation center website [20]. In Figure 3-9 the real-time frequency measurements of three typical types of GPS satellite clocks using the proposed method are compared with the post-processed ones using the old method, where IGST is used as the reference. In the Figure, the satellite clocks from the GPS satellite 10, 02 and 24 are chosen to represent the rubidium clock on GPS IIF satellite (IIF Rb), rubidium clock on GPS IIR satellite (IIF Rb) and caesium clock on GPS IIF satellite (IIF Cs) respectively. The distinctions between the lines of different colours in the figure generally reflect the measurement stabilities of the clocks on the three generations of the GPS satellites, however this figure doesn't provide any evidence of the true GPS satellite clock qualities, since the stabilities of these clock measurement are also affected by the measurement noise and the quality of the reference used.

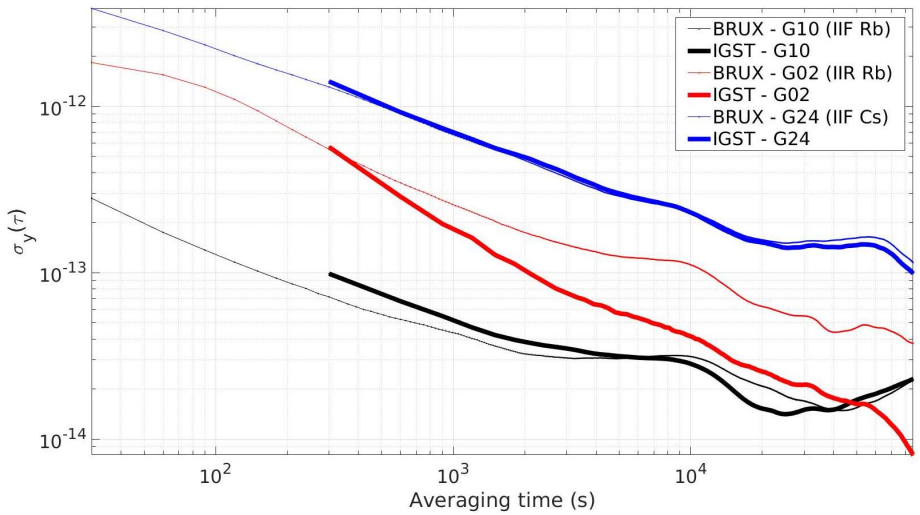

Figure 3- 9. Comparison of the real-time measurements (reference BRUX, thin lines) and the post-processed measurements (reference IGST, thick lines) in the form of ADEVs

The frequency measurements from both methods show very similar precisions, as can be observed from Figure 3-9, except for the IIR Rb on the GPS satellite 02. The reason for the worse performance on the IIR Rb using the real-time method is still not clear, it could be due to the errors that were still not well estimated in the software. Also, it should be noted that IGS measurements in the figure are phase data; while the real-time measurements are frequency data and were transformed to phase data for the computation of ADEVs. Nevertheless, the proposed method, which uses limited number of tracking stations, has shown its potential to measure satellite clocks in real-time as needed for the real-time satellite clock frequency jump detection purpose.

Another important information that can be obtained from the ADEVs in Figure 3-9 is how long we need to average the frequency measurements to see a frequency jump of a certain size. Empirically speaking, to detect a frequency jump of size N, the frequency jump detector needs to average the frequency measurements over T min around that epoch (corresponding to T/2 min delay of the detection) to reduce the measurement noise to have a precision of N/5, then the jump is easy to be detected since the measurement noise is 5 times smaller than the size of the jump. For example, in order to detect a frequency jump of 1×10^{-12} on an IIF Rb clock or IIR Rb clock, an averaging over about 50 s or 25 min is needed to limit the precision of the real-time measurements to 2×10^{-13} (see Figure 3-9), if the jump is then detected successfully, the detection delay is 25 s or 12.5 min. In practice, the detection delay is much less: within 30 min delay, a jump with the size as small as 5×10^{-13} can be detected in all the IIF Rb and IIR Rb clocks. However, due to the poorer stability of the IIF Cs clock measurements, the small/medium size jump in it can't be easily detected within short delay. In general, for a frequency jump over 1×10^{-12} in an IIF Cs clock, it needs about 1 hour to detect it. A clearer observation of the effects of the averaging on the frequency measurements of the three clocks is demonstrated in Figure 3-10.

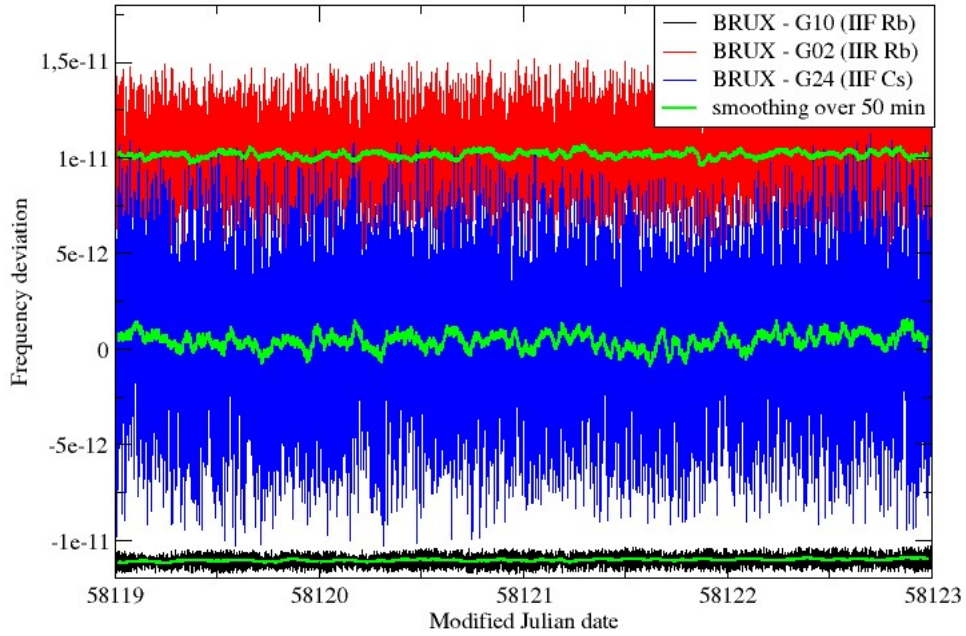

Figure 3- 10. Real-time frequency measurements on the three types of GPS clocks and the corresponding 50 min averaging results

In addition, it was tested if the measurement stability of the satellite clock could be improved by increasing the number of stations in the network. In Figure 3-11, the ADEVs of the satellite clock measurements by using 40 stations and 68 stations are plotted. As shown in the figure, only a slight improvement of the stability is observed for the IIF Rb clock within 3 hours interval, which means a slightly quicker detection of the jumps in the clock; meanwhile, the time for the least square computation in the software is also largely increased. During this work, only the network of 40 stations is chosen, the adequate number of stations will be studied in future work considering the computational efficiency and the measurement precision.

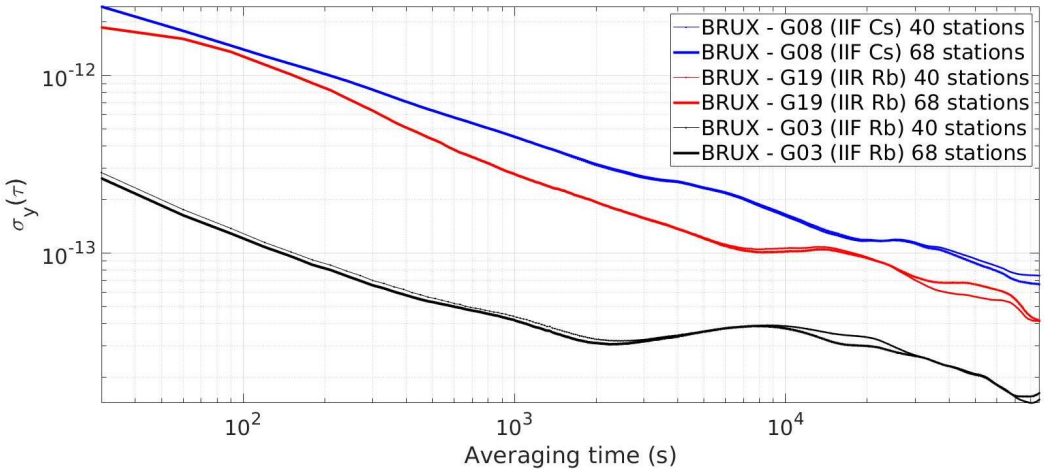

Figure 3- 11. The performance of the satellite clock measurements by increasing the number of stations from 40 to 68

In order to test the performance of this real-time method in the frequency jump detection, all the frequency jumps in the GPS satellite clock that have been detected using the IGS post-processed measurements at INRIM in the recent years have been re-measured using the new real-time method. Since the very small jumps (smaller than 5×10^{-13}) are very difficult to be affirmed due to the measurements noise even they have been detected by the detector, they are not included in the following tests. The sizes of the jumps that can be confirmed are typically from 5×10^{-13} to some 10^{-12}, and they have been all successfully detected in the jump detector taking the measurements from this real-time method.

Figures 3-12 to 3-16 give some examples of the GPS satellite clock frequency measurements by IGS product and real-time method during the jumps. The real-time method estimates the frequency deviation at 30 s interval, so it looks much noisier than the IGS measurements which are based on 5 min products. The 50 min averaging results (green lines) of the measurements from the real-time method (black lines) are plotted accordingly for a clearer view of the jumps.

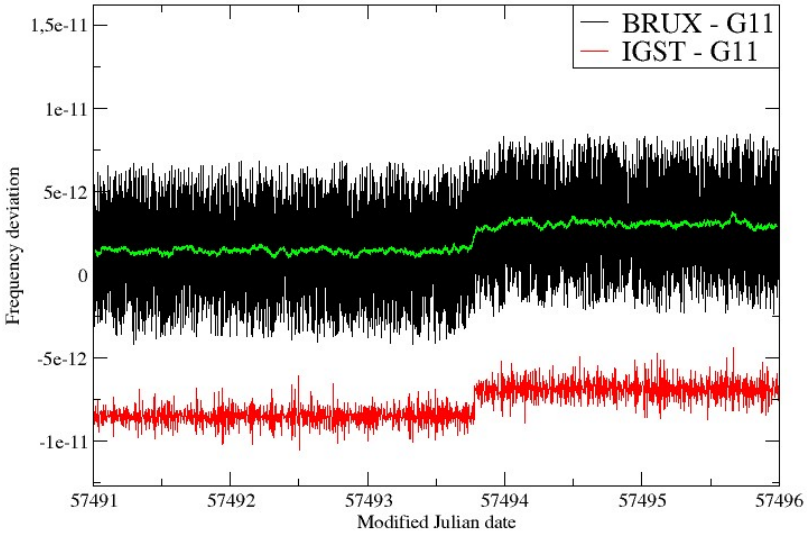

Figure 3- 12. A jump with the size around 2×10^{-12} in GPS11 clock (IIR Rb)

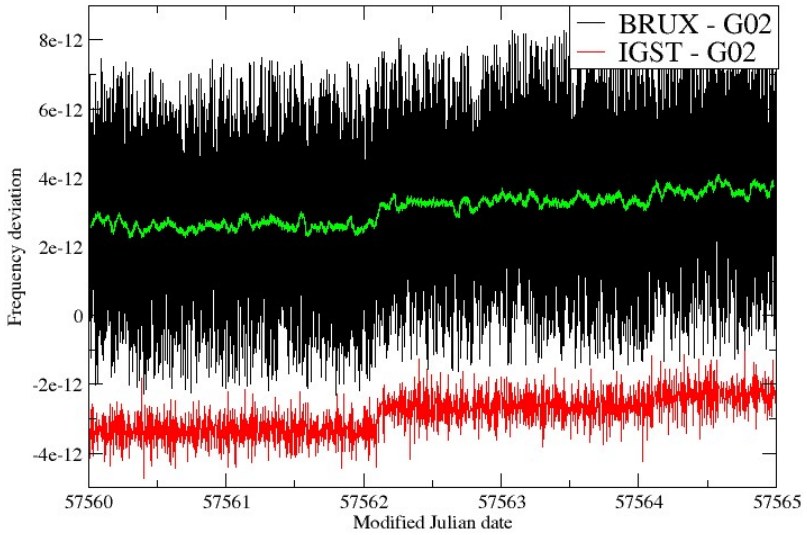

Figure 3- 13. A jump with the size around 7×10^{-13} in GPS02 clock (IIR Rb)

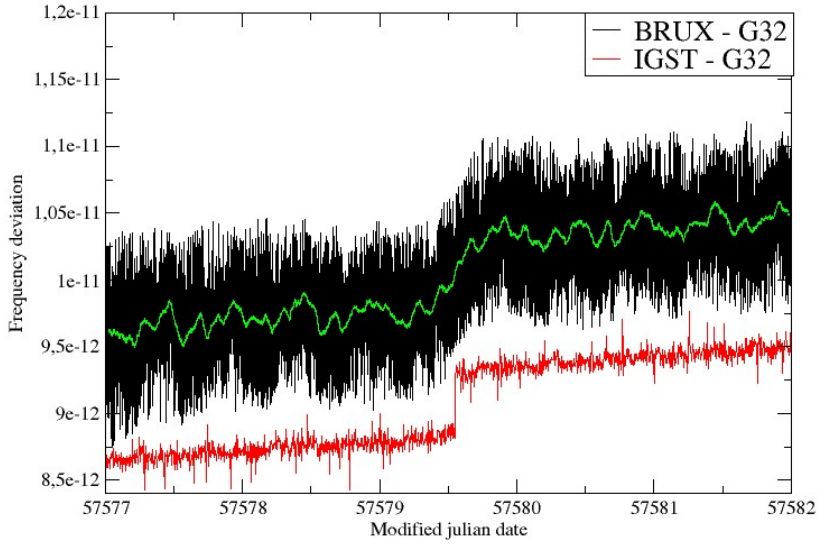

Figure 3- 14. A jump with the size around 5×10^{-13} in GPS32 clock (IIF Rb)

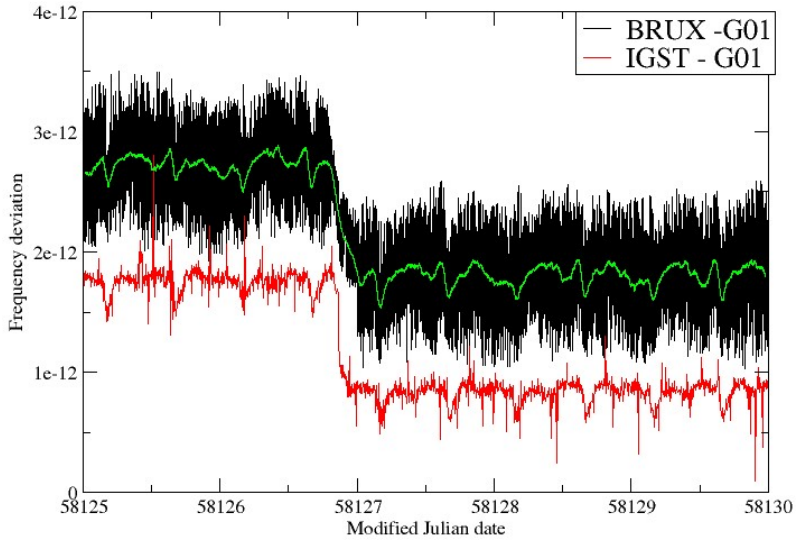

Figure 3- 15. A jump with the size around 1×10^{-12} in GPS01 clock (IIF Rb)

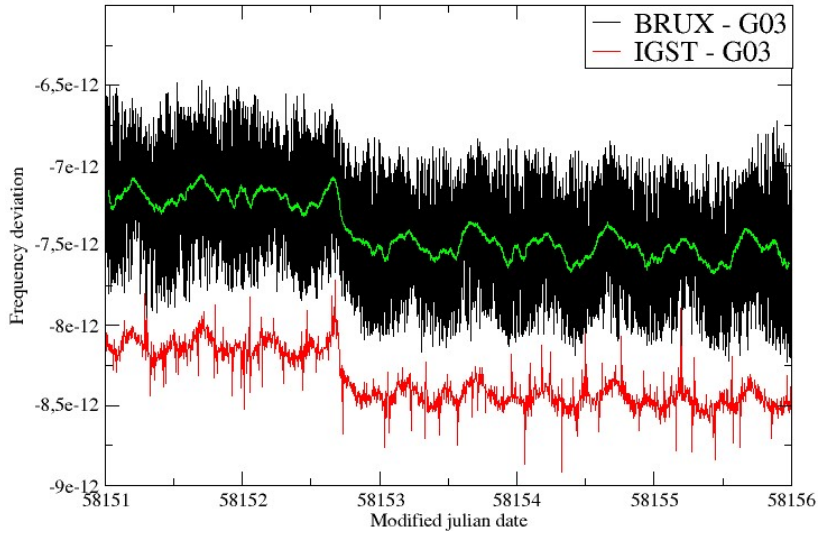

Figure 3- 16. A jump with the size around 5×10^{-13} in GPS03 clock (IIF Rb)

In addition to the GPS satellites, the real-time method was also applied to the Galileo satellite clock frequency monitoring. The related frequency measurements (called real-time measurements in the figures) are compared with the MGEX measurements in Figure 3-17 and 3-18, and they show the similar noise level (both are 30 second measurements). The exact time when the jumps happened, and the related Galileo satellite numbers are hidden in the figures.

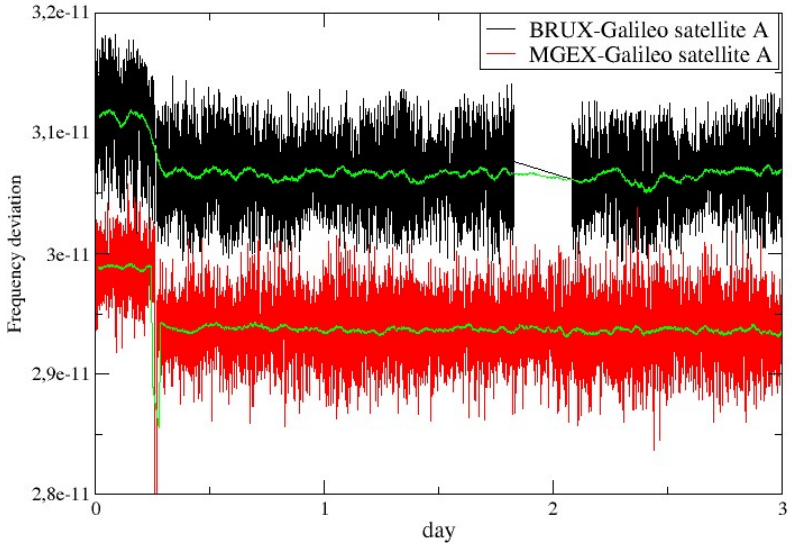

Figure 3- 17. comparison between MGEX and the “real-time” measurements

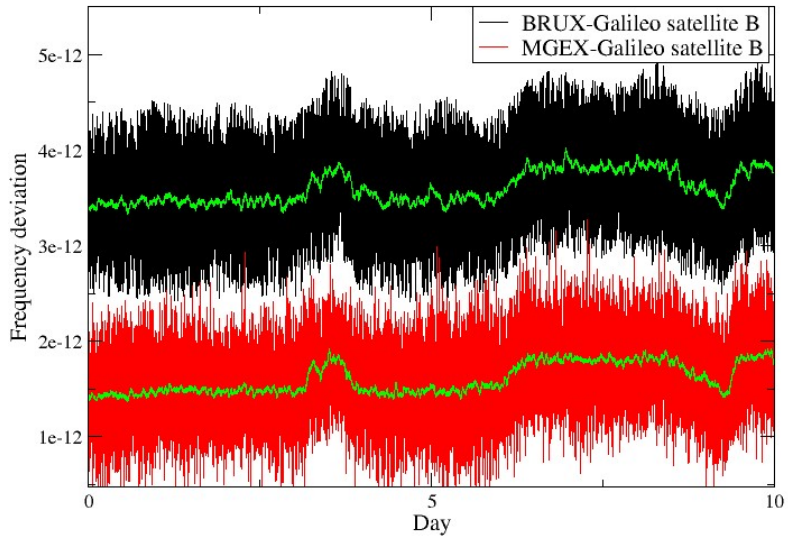

Figure 3- 18. comparison between MGEX and the “real-time” measurements

3.4 Alternative methods

Another method to measure the satellite clock frequency deviation in real-time was also studied in this work. Instead of a ground reference, it chose a

satellite clock as the reference. The IGS real-time service (RTS) products were used for this purpose. As can be seen in Figure 3-19, the reference time of the IGS RTS clock products varies at every epoch, so it can't be used directly as a reference for the satellite clock frequency measurement. However, the RTS clock reference is the same for all the measured satellite at each epoch. Therefore, by making a difference of the RTS clock measurements of two GPS satellites (for example, between the GPS02 and the GPS03 in Figure 3-19), the RTS reference will be cancelled out, and the GPS02 clock can be measured then using the GPS03 clock as a reference. Like the previous method, the RTS clock products are also generated in real-time from a network of GNSS station. Meanwhile, these RTS products are computed from a much larger number of stations, which guarantees a higher quality of the clock measurements.

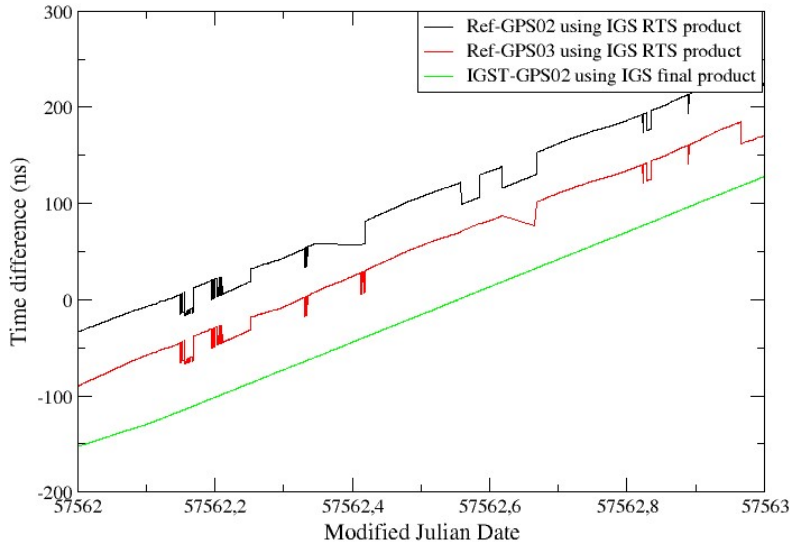

Figure 3- 19. Clock measurements using IGS final and RTS products.

Since the current IGS RTS product only includes the GPS and GLONASS measurements, only the GPS jump detection using the RTS products is studied here. The frequency measurements (filtered) of the GPS02 referring the GPS03 clock are plotted in Figure 3-20. It shows that the measurements from this alternative method (in black) have similar noise level as the IGS measurements (in red), and the jump in the GPS02 clock could be clearly discovered from the 25 min averaging results (in green) in both cases.

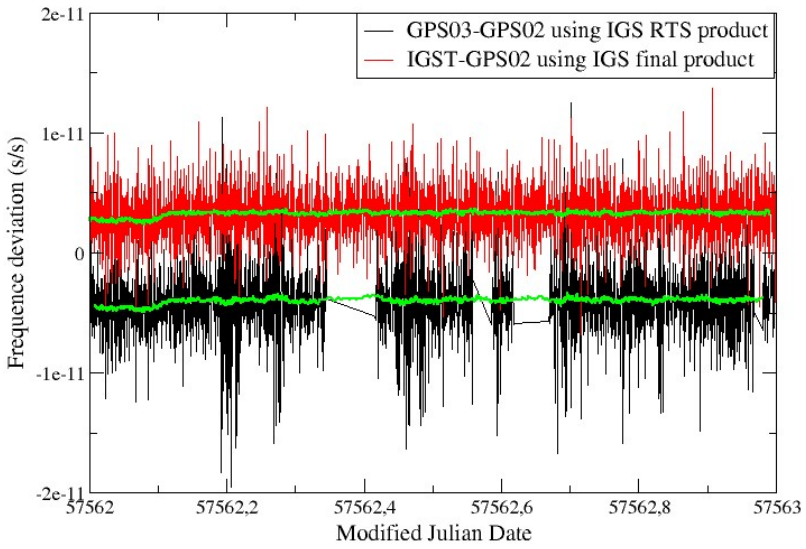

Figure 3- 20. Frequency jump on GPS02 measured by the GPS03 clock and IGS reference (both with 30 s interval). The corresponding 25 min averaging results are in green colour.

The frequency measurements of the satellite clock referring to another satellite clock using the RTS products may include a lot of missing data (see Figure 3-20), which depend on the availability of both satellite clock measurements in the RTS products. In order to reduce the data gaps, another method using the RTS products is proposed. First, the real-time PPP is carried out using the RTS clock products and the IGS ultra-rapid predicted orbit products to compute the differences between the RTS clock reference and the BRUX clock (BRUX – RTS reference). Meanwhile the phase measurements of one GPS clock (GPS n) are taken directly from the RTS clock products (GPS n – RTS reference). Then the clock differences "BRUX – GPS n" are computed from "BRUX – RTS reference" – "GPS n – RTS reference". Finally, the frequency measurements of GPS n clock referring to the BRUX clock are obtained.

Figure 3-21 demonstrates the frequency measurements of the GPS10 clock which were generated from the three methods as introduced above. The black lines stand for the results from the network method described in section 3.3. The results referring to the GPS03 clock using the RTS products are shown in red lines. And the results from the real-time PPP using the RTS products are plotted in green lines. The offset between the red lines and the other two lines are due to the different frequency references that were used. In general, the first method that were described in section 3.3 provide the most precise frequency measurements of the satellite clocks, and the performance of the method using satellite clock reference is slightly worse. Changing the reference from the satellite clock to the BRUX clock using the real-time PPP will increase the availability of the frequency measurements but will also bring in more noises.

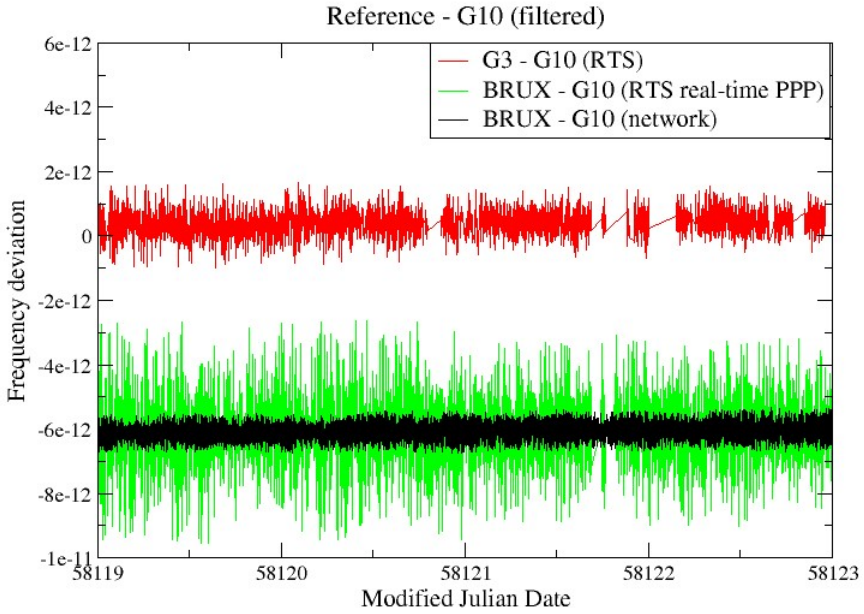

Figure 3- 21.Frequency measurements of the GPS10 clock referring to the BRUX and GPS32 clock

3.5 Discussions

Three methods that can be used for the real-time detection of the GNSS satellite clock frequency jump have been proposed and tested in this chapter. The first method, which uses the ground reference UTC(ORB) at BRUX, showed comparable measurement precision to the IGS/MGEX post-processed measurements, and a small frequency jump with size 5×10^{-13} on the satellite clock of good quality (GPS IIF Rb and GPS IIR Rb) could be detected normally within 30 min according to practice experience. The Cs clock measurement of the GPS satellite has more noise, therefore only large size frequency jump (over 1×10^{-12}) in the clock could be detected with acceptable delay (1 hour). In addition, the optimal number of stations used in the tracking network needs to be studied in the future, considering both the measurement precision and the computational efficiency.

Two alternative methods are also proposed based on the IGS RTS products. The implementation of these two methods are relatively easy, however, the corresponding results are less precise and may include some data gaps.

In this PhD work, only the related methods for the real-time satellite clock frequency jump detection are developed. While a more comprehensive study about the frequency jump will be carried out in future work, including the range of the sizes, the occurrence rate and so on. Meanwhile, the configuration of the frequency jump detector and the corresponding possibility of false alarm and false detection when using the real-time measurements as input will be investigated.

3.6 Real-time frequency detection algorithm Application: upgrade of DEMETRA time integrity service

The DEMETRA “time integrity service” keeps monitoring the time information provided by the satellite navigation message, such as the Galileo GPS Timing Offset (GGTO) and the broadcasted time scales (the predicted UTC and the GNSS system time), by receiving the GPS/Galileo satellite signals.

Additionally, this service offers GNSS satellites clock monitoring, including detection of possible non-stationarities [61], in order to improve user positioning and timing accuracy. For this purpose, the service uses the IGS/MGEX post-processing measurements for the detection of satellite clock anomalies. Due to the huge delay of the related products, the current service doesn’t provide any real-time alert for the satellite clock anomaly.

In order to benefit the real-time GNSS users, the methods that have been introduced in this chapter will be adopted by the DEMETRA time integrity service. When the related software programs are ready, they will be integrated to the DEMETRA server for the real-time detection of the GNSS satellite clock frequency anomalies, using the real-time stream of the GNSS observation data and the real-time clock products from the IGS RTS product distribution centers [42].

Chapter 4

Conclusions

In this dissertation, the improved Atomium PPP software for time and frequency transfer and the methods for real-time detection of the GNSS satellite clock frequency anomalies were introduced.

Two improved versions of Atomium PPP, including three main updates, have been developed. The first update was to combine GPS and Galileo signals in the PPP computation. Though the full capacity of Galileo time transfer hasn't be exploited yet (such as： the full constellation is not ready, the Galileo phase centers in the receiver antennas are not calibrated), using the GPS + Galileo PPP has already shown an improvement of about 20% - 10% to the short-term stability of the time transfer solution comparing to the GPS-only one. However, the long-term stability over one day is still contaminated by the daily boundary jump.

The second update of the Atomium PPP was adding the function to constrain the receiver clock in order to restrict the white frequency noise in the receiver clock measurements. The results indicated that the constrained PPP can largely improve the short-term stability of the PPP time solution if the receiver clock is a H-maser. In addition, the extra tests showed the potential of constrained PPP for obtaining continuous time solution and retrieving clock solution in the extremely noisy environment.

The last update was integer PPP, which fixes carrier phase ambiguities as integer values. There are mainly two advantages of using the integer PPP instead of the former float ambiguity PPP for time transfer: the mid to long term frequency stability can be improved by using integer PPP (reaches 10^{-16} within 3 to 10 days averaging); and integer PPP avoids the random walk noise in the clock solution produced by the float ambiguity estimation and increases the frequency accuracy in the monthly time transfer solution ($\pm 2 \cdot 10^{-16}$ peak to peak), it indicates that integer PPP can also be used for accurate time transfer with occasional calibration.

These improved versions of Atomium PPP have been integrated to DEMETRA servers to provide improved daily solutions using the post-processed

IGS/MGEX products. The GPS + Galileo PPP will be used to substitute the original GPS-only PPP to provide the near real-time (hourly) solution. Meanwhile, there are still some problems encountered during the tests (reported in the discussions of section 2.3 to 2.5), more future studies must be done to keep the software up to date.

The new method, that was proposed for measuring GNSS satellite clock frequency deviations by a ground reference in real-time, makes it possible for the detection of frequency jump in GNSS satellite clock in quasi real-time, and benefiting the users who perform the real-time positioning or timing. The frequency measurements of the satellite clocks using the new method showed similar precision to the post-processed measurements (from IGS products) that are currently used for the frequency jump detection. Any frequency jump of typical size from 5×10^{-13} to some 10^{-12} in the GPS satellite clock can be detected by the frequency jump detector using either the post-processed frequency measurements of that satellite clock or the measurements from the real-time method. Though the tests in this dissertation were based on the observation data in the past days to detect the jumps already happened, the results have shown that a frequency jump as small as 5×10^{-13} can be detected from these "real-time" measurements with 30 min delay. Two versions of the software have been already developed separately for the frequency measurements of GPS and Galileo clocks. The future work will include adding BeiDou and GLONASS related measurements and integrating the software into DEMETRA server for the real-time detections. In addition, two alternative methods have also been proposed based on the IGS RTS products, the measurements from these methods will be produced in parallel in this service.

References

[1] BIPM, CGPM: Compte rendus de la 11e reunion, Paris, 1960.

[2] BIPM, The 9th edition of the SI Brochure, 2019.

[3] CCTF, *Mise en pratique* for the definition of the second in the SI, SI brochure, 9th edition, 2019, Appendix 2.

[4] F. Levi, D. Calonico, C. Calosso, A. Godone, S. Micalizio, G. Costanzo, Accuracy evaluation of ITCsF2: a nitrogen cooled caesium fountain, Metrologia 2014, Volume 51, Number 3.

[5] CCTF, Recommendation CCTF 1 (2001), *Report of the 15th Meeting (June 2001) to the International Committee for Weights and Measures* (S`evres: BIPM) p. 132.

[6] J Guéna et al, Contributing to TAI with a secondary representation of the SI second, Metrologia 2014, Volume 51, Number 108.

[7] Recommended values of standard frequencies from the BIPM, URL: https://www.bipm.org/en/publications/mises-en-pratique/standard-frequencies.html.

[8] F. Riehle, On Secondary Representations of the Second, Proceedings of the 20th European Frequency and Time Forum, Germany, 2006.

[9] BIPM, Time metrology at the BIPM: Towards a new definition of the SI second, 26th meeting of the CGPM, 2018.

[10] CCDS, Report of the 12th meeting, 1993.

[11] The circular-T distributed by the BIPM, URL: https://www.bipm.org/en/bipm-services/timescales/time-ftp/Circular-T.html.

[12] J. R. Vig, QUARTZ CRYSTAL RESONATORS AND OSCILLATORS: For Frequency Control and Timing Applications - A TUTORIAL, 2004.

[13] M. A. Lombardi, Fundamentals of Time and Frequency, In book: The Mechatronics Handbook, Chapter17, Publisher: CRC Press, 2002.

[14] D. W. Allan, Statistics of atomic frequency standards, Proc. IEEE, volume 54, issue 2, pp. 221-230, 1966.

[15] Quasi-Zenith Satellite System (QZSS) homepage, URL: https://qzss.go.jp/en/.

[16] S. Kogure, A.S. Ganeshan, O. Montenbruck (2017) Regional systems. In: P. J. Teunissen, O. Montenbruck (eds) Springer Handbook of Global Navigation Satellite Systems. Springer Handbooks. Springer, Cham.

[17] J. Sanz Subirana, J.M. Juan Zornoza and M. Hernández-Pajares, GNSS DATA PROCESSING Volume I: Fundamentals and Algorithms, ESA, 2013.

[18] BeiDou ICD, URL: http://en.beidou.gov.cn/SYSTEMS/ICD/.

[19] Newly released GLONASS interface control documents, URL: https://www.gpsworld.com/new-glonass-interface-control-documents-released/.
[20] The status of the GPS satellite clocks , URL: https://www.navcen.uscg.gov/?Do=constellationStatus.
[21] Introduction to the Galileo satellite clocks, URL: http://www.esa.int/Applications/Navigation/Galileo/Galileo_s_clocks.
[22] G. Blewitt (1997), Basics of the GPS Technique: Observation Equations, In: Geodetic Applications of GPS, Swedish Land Survey.
[23] P. J. Teunissen (2017) Carrier Phase Integer Ambiguity Resolution. In: P. J. Teunissen, O. Montenbruck (eds) Springer Handbook of Global Navigation Satellite Systems. Springer Handbooks. Springer, Cham.
[24] P. Dabove, M. G. Petovello, What are the actual performances of GNSS positioning using smartphone technology?, Inside GNSS, 2014, pp. 34-37
[25] G. Lachapelle, M. G. Petovello, Y. Gao, L. Garin, Precise point positioning and its challenges, aided-gnss and signal tracking. *InsideGNSS*, November/December 2006, pp. 16-21.
[26] C. J. Hegarty, the Global Positioning System (GPS), In: P. J. Teunissen, O. Montenbruck (eds) Springer Handbook of Global Navigation Satellite Systems. Springer Handbooks. Springer, Cham, 2017, pp. 197-218.
[27] D. Engeler, Performance analysis and receiver architectures of DCF77 radio-controlled clocks, IEEE transactions on ultrasonics, ferroelectrics, and frequency control 59(5):869-84, 2012.
[28] EndRun Technologies ,White paper Introduction to NTP, URL: https://endruntechnologies.com/pdf/NTP-Intro.pdf.
[29] F. Arias, The Metrology of Time, Philosophical Transactions of The Royal Society A Mathematical Physical and Engineering Sciences 363(1834):2289-305, 2005.
[30] W. Wu, S. Dong, H. Li, H. Zhang, Two-way satellite time and frequency transfer: Overview, recent developments and application, Proceedings of the European Frequency and Time Forum, 2014.
[31] D. Matsakis, P. Defraigne, P. Banerjee, Precise Time and Frequency Transfer, The radio science bulletin, No. 351, 2014, pp. 29-44.
[32] C. Lisdat et al., A clock network for geodesy and fundamental science, Nature Communications, volume 7, No. 12443, 2016.
[33] CCTF, *Report of the 21st meeting (8-9 June 2017) to the International Committee for Weights and Measures*, (S`evres: BIPM) p. 23.
[34] L. Kun et al., Preliminary time transfer through optical fiber at NIM, Proceedings of the IEEE IFCS and EFTF joint conference, 2015.
[35] F. Arias, Z. Jiang, W. Lewandowski, G. Petit, BIPM comparison of time transfer techniques, Proceedings of the 2005 IEEE International Frequency Control Symposium and Exposition, 2005.
[36] BIPM, BIPM Annual Report on Time Activities, Volume 4, 2019.

[37] D. W. Allan and M. Weiss, Accurate Time and Frequency Transfer During Common-View of a GPS Satellite, Proceedings of IEEE Frequency Control Symposium, Philadelphia, PA, 1980, pp. 334-356.
[38] D. W. Allan, C. Thomas, Technical Directives for Standardization of GPS Time Receiver Software: to be implemented for improving the accuracy of GPS common-view time transfer, Metrologia, Volume 31, No.1, 1991, pp.69-79.
[39] J.Azoubiband, W. Lewandowski, CGGTTS GPS/GLONASS Data Format Version, 27th CGGTTS meeting, 1998.
[40] P. Defraigne, G. Petit, CGTTS-V2E: an upgraded standard for GNSS Time Transfer, Metrologia, Volume 52, No. 6, 2015.
[41] List of IGS products, URL: https://www.igs.org/products.
[42] IGS real-time services introduction, URL: http://www.igs.org/rts.
[43] P. Defraigne, G. Petit, Time Transfer to TAI Using Geodetic Receivers, Metrologia, Volume 40, No. 4, 2003.
[44] P. Defraigne, K. Verhasselt, Multi-GNSS Time Transfer with CGGTTS-V2E, Proceedings of EFTF, Torino, April 2018, pp.270-275.
[45] T. Schildknecht, G. Beutler, W. Gurtner, M. Rothacher, Towards sub-nanosecond GPS time transfer using geodetic processing technique, Proceedings of 4th European Frequency and Time Forum, 1990, pp.335-346.
[46] BIPM, BIPM guidelines for GNSS calibration V3.2, 2016.
[47] Radiocommunication Bureau. ITU Handbook: satellite time and frequency transfer and dissemination, Edition 2010, Chapter 12-13.
[48] P. Defraigne, GNSS Time and Frequency Transfer, In: P. J. Teunissen, O. Montenbruck (eds) Springer Handbook of Global Navigation Satellite Systems. Springer Handbooks. Springer, Cham, 2017, pp. 1187-1206.
[49] P. Defraigne, C. Bruyninx, A. Moudrak, F. Roosbeek, Time and Frequency Transfer Using GNSS, proceedings of IGS Workshop and Symposium, Bern, 2004.
[50] J. Kouba, P. Héroux, Precise Point Positioning using IGS Orbit and Clock Products, GPS Solutions, 2001, Volume 5, No. 2, p. 12.
[51] P. Defraigne, N. Guyennon, Atomium: a new tool for time and frequency transfer in PPP mode, TAI working group, Paris, September 2006.
[52] P. Defraigne, C. Bruyninx, N. Guyennon, PPP and Phase-only GPS Time and Frequency transfer, Proceedings of 21st EFTF, Geneva, May 2007, pp 904–908.
[53] ANTEX format description, September 2010, URL: https://kb.igs.org/hc/en-us/articles/216104678-ANTEX-format-description
[54] GSA, GNSS market report, 2017, issue 5, P82-89.
[55] K. F. Hasan, Y. Feng, Y. Tian, GNSS Time Synchronization in Vehicular Ad-Hoc Networks: Benefits and Feasibility. IEEE Transactions on Intelligent Transportation Systems 2018, Volume 19, Issue 12, pp. 3915-3924.

[56] T. Grelier et al., GNSS in Space Part 1: Formation Flying Radio Frequency Missions, Techniques, and Technology. InsideGNSS, November 2008, pp. 40–46.
[57] O. Pallares, S. Shariat-Panahi, J. del Rio, A. Manuel, Time synchronization of a commercial seismometer through IEEE-1588. Fourth International Workshop on Marine Technology, 2011, Cádiz, Spain, pp.22–23.
[58] P. A. Clements, Global Positioning System Timing Receivers in the DSN. TDA progress report, 1981, pp.42-67.
[59] B. Caccianiga et al., GPS-based CERN-LNGS time link for Borexino. Journal of Instrumentation 2012, Volume 7.
[60] European horizion2020 project webpage, URL: https://ec.europa.eu/programmes/horizon2020/en.
[61] P. Tavella et al., The Horizon 2020 DEMETRA project: DEMonstrator of EGNSS services based on Time Reference Architecture, proceedings of 2015 IEEE Metrology for Aerospace, pp.98-102.
[62] P. Defraigne et al., Demonstrator of Time Services based on European GNSS Signals: The H2020 DEMETRA Project, ION PTTI, Monterey, January 2017, pp.127-137.
[63] D. Calonico, C. Clivati, A. Mura, A. Tampellini, M. Gertosio, F. Levi, Time and Frequency Distribution over fibre for Geodesy, Seismology and Industry, Proceedings of ISPCS, Geneva, Sept. 2018.
[64] BIPM, BIPM Annual Report on Time Activities, Volume 6, 2011.
[65] W. Huang, P. Defraigne, G. Signorile, I. Sesia, improved multi-GNSS PPP Software for Upgrading the DEMETRA Project Time Monitoring Service, Sensors 2019, 19(20).
[66] J. Ray, K. Senior, Geodetic techniques for time and frequency comparisons using GPS phase and code measurements, Metrologia, 2005, 42(4):215.
[67] P. Defraigne, GNSS Time Transfer, Tutorial at BIPM, 2012. URL: https://www.bipm.org/ws/CCTF/TAI_TRAINING/Allowed/Fundamentals/Training-2012-GNSS-Defraigne.pdf.
[68] G. Petit, The TAIPPP pilot experiment, Proceedings of the IEEE IFCS and EFTF joint conference, Besancon, 2009, pp.116-119.
[69] G. Petit et al. 1 × 10−16 frequency transfer by GPS PPP with integer ambiguity resolution. Metrologia, 2015, Volume 52, pp.301-309.
[70] P. Defraigne, C. Bruyninx, On the link between GPS pseudorange noise and day-boundary discontinuities in geodetic time transfer solutions, GPS solutions, 2007, 11:239–249.
[71] J. Delporte, F. Mercier, D. Laurichesse, O. Galy, GPS Carrier-Phase Time Transfer Using Single-Difference Integer Ambiguity Resolution, International Journal of Navigation and Observation, Volume 2008 Article ID 273785, 7 pages.

[72] Ł. Śliwczyński, P. Krehlik, A. Czubla, Ł. Buczek, M Lipiński, Dissemination of time and RF frequency via a stabilized fibre optic link over a distance of 420 km, Metrologia, 2013, 50(2):133.
[73] F. Xia et al., Assessing the latest performance of Galileo-only PPP and the contribution of Galileo to Multi-GNSS PPP, Advances in Space Research, Volume 63, No. 9, May 2019, pp.2784-2795.
[74] K. Verhasselt, P. Defraigne, Multi-GNSS time transfer based on the CGGTTS, Metrologia, Volume 56, No. 6, 2019
[75] The IGS MGEX products introductions, URL: http://mgex.igs.org/IGS_MGEX_Products.php.
[76] F. Zhou, D. Dong, P. Li, X. Li, H. Schuh, Influence of stochastic modelling for inter-system biases on multi-GNSS undifferenced and uncombined precise point positioning, GPS solutions, July 2019, 23:59.
[77] IGS ANTEX file, URL: ftp://www.igs.org/pub/station/general//igs14.atx.
[78] K. Wang, M. Rothacher, Stochastic modeling of high-stability ground clocks in GPS analysis, J Geodesy, 2013, 87(5):427–437.
[79] Y. Ge et al., Enhancing real-time precise point positioning time and frequency transfer with receiver clock modeling, GPS Solutions, 2019, 23: 20.
[80] G. Cerretto, F. Lahaye, P. Tavella, S. Vitrano, Precise Point Positioning: Implementation of the constrained clock model and analysis of its effects in T/F transfer, Proc. 24th EFTF, Noordwijk, Netherlands, April 2010.
[81] L. Galleani, L. Sacerdote, P. Tavella, C. Zucca, A mathematical model for the atomic clock error, Metrologia 40 (2003), pp.257-264.
[82] L. Galleani, P. Tavella, Robust Detection of Fast and Slow Frequency Jumps of Atomic Clocks, IEEE Transactions on UFFC, volume 62, No. 2, pp.475-485.
[83] CH1-75 active hydrogen maser specification, URL: http://ptfinc.com/ch1-75-active-hydrogen/.
[84] 5071A primary frequency standard specification, URL: https://www.microsemi.com/document-portal/doc_download/133269-5071a-datasheet.
[85] J. Leute, G. Petit, P. Exertier, High accuracy continuous time transfer with GPS IPPP and T2L2, Proc. EFTF, Torino, April 2018, pp.249-252.
[86] D. Laurichesse, F. Mercier, Integer ambiguity resolution on undifferenced GPS phase measurements and its application to PPP, ION GNSS 2007 20th international technical meeting of the satellite division, 25–28 Sept 2007, Fort Worth, TX, pp 839–848.
[87] S. Loyer, F. Perosanz, Zero-difference GPS ambiguity resolution at CNES–CLS IGS Analysis Center, Journal of Geodesy, November 2012, Volume 86, Issue 11, pp 991–1003.
[88] P. J. G. Teunissen, GNSS Ambiguity Bootstrapping: Theory and Application, Proc. KIS, Banff, Canada, 2001, pp.246–254.

[89] P. Defraigne, J. M. Sleewaegen, Code-Phase Clock Bias and Frequency Offset in PPP Clock Solutions, IEEE transactions on UFFC, Volume 63, Issue 7, 2016, pp. 986-992.
[90] R. B. Langley, Dilution of Precision, GPS world, May 1999, pp. 52-59.
[91] M. Caissy, L. Agrotis, G. Weber, M. Hernandez-Pajares, U. Hugentobler, Coming Soon: The IGS Real-time Service, GPS World, June 2012, pp.52-58.
[92] P. Defraigne et al., EGNOS Time and UTC Disseminated by EGNOS, Proceedings of the 48th PTTI, 2017, pp.235-242.
[93] I. Sesia, G. Signorile, G. Cerretto, E. Cantoni, P. Tavella, A. Cernigliaro, A. Samperi, Time metrology in the Galileo navigation system: The experience of the Italian National Metrology Institute, proceedings of IEEE Metrology for Aerospace, Benevento, Italy, May 2014.
[94] IGS tracking network, URL: http://www.igs.org/network.